SEISMIC EVALUATION
OF
BOLU VIADUCT 1

by

B. Tolga CANDAN

Submitted to
Kandilli Observatory and Earthquake Research Institute
in partial fulfillment of the requirements for the degree of

Master of Science in Earthquake Engineering

Boğaziçi University

2006

Time is for free, though still it’s priceless
The more struggles spent, the more memorable life is.

Come what come may,
Time and the hour runs through the roughest day

This study is dedicated to my mentor my father, my beloved mother, my promising brother Sinan and my fiancé İpek, Without their endless support, patience and devotion, this achievement could never be possible.

ACKNOWLEDGEMENTS

I would like to express my esteem and gratitude to Professor Doctor Nuray Aydınoğlu for his assistance and guidance during my Master of Science education and the preparation of this thesis. It has been so impressive and influential to work with such an exceptional academician and engineer. I would also like to thank sincerely to all the academicians in the Department of KOERI for their warm, respectful and instructive attitude.

I wish to offer my sincerest thank you to Research Assistant Göktürk Önem for sharing his invaluable time and knowledge.

I would also like to thank Mr. Doğan Demir, the project manager of Anatolia Motorway ~ Gümüşova-Gerede Section Project and other engineers of the project; Mr. Serhat Yalçın, Chief of The Bridges and Viaducts Department of Emay Engineering, for providing me documentation. I also wish to express my thanks to Mr. Özgür Özçıtak for providing me documentation and sharing his knowledge.

I am most grateful to the members of Anadoluray Project (Yapı Merkezi, Doğuş, Yüksel, Yenigün Joint Venture) and especially to Mr. Ramih Muştu, Mr. İlter Tutkavul and Mr. Ertan Gültekin for their support and tolerance during this academic research.

ABSTRACT

A thesis is presented on the seismic evaluation of a viaduct using non-linear analysis techniques. The Bolu viaduct is a 2-3 km long seismically isolated structure with two parallel bridges each with a span length of 39.2 m and pier height of maximum 49 m that was nearly complete when it was struck by the 1999 Duzce earthquake in Turkey. With the design based on AASHTO standards, it suffered complete failure of the seismic isolation system and narrowly avoided total collapse due to excessive superstructure moment. After investigations the retrofit of the viaduct had been decided due to the study carried out by Michele Calvi and J. Nigel Priestley.

This thesis concentrates on the retrofitted structure of Viaduct 1 by non-linear time history analysis.

Keywords: seismic performance; isolation, Bolu Viaduct; Duzce Earthquake, bridge

ÖZET

Bu tezin konusu bir viyadük yapısının ‘nonlinear’ analiz yöntemiyle incelenmesidir. Türkiye’deki 1999 Düzce depremine maruz kaldığında neredeyse bitmiş durumda olan Bolu Viyadüğü, 2-3 km uzunluğunda, her açıklığı 39.2 m ve ayak yükseklikleri en fazla 49 m olan iki paralel sismik izolasyonlu köprüden oluşmaktadır. AASHTO standartlarına dayanan dizaynıyla; sismik izolasyon cihazlarının kapasitelerinin aşılmış, yüklü yapısal momentlere karşın tam göçmenin sınırlarında dayanmıştır. Yapılan araştırmalardan sonra Michele Calvi ve J. Nigel Priestley’in çalışmalarına dayanarak viyadüğün güçlendirilmesine karar verilmiştir.

Bu tez Viyadük 1’in güçlendirilmiş durumunun ‘nonlinear’ zaman tanımlı analizleri ile incelenmesine yoğunlaşmıştır.

Anahtar Kelimeler: sismik performans; izolasyon; Bolu Viyadüğü; Düzce Depremi; köprü

TABLE OF CONTENTS

LIST OF FIGURES

LIST OF TABLES

1. INTRODUCTION

Bridges are one of the essential elements in transportation projects since the beginning of modern ages. With the evolution of engineering approaches, the design and construction criteria's have changed considerably. As the importance of the parameters 'travel time between two points' and 'continual operation' increased in transportation, it became necessary to design the bridges appropriate to the site characteristics by means of challenging geometries, seismic durability, aesthetic considerations. The simplicity of the bridges has become a challenge in constructional engineering not allowing any design and detailing mistakes.

The deficiencies of the bridge design criteria's appeared in the 1971 San Fernando earthquake with many highway bridges severely damaged. The answer to the demand of a new design concept rose from New Zealand emphasizing the importance of avoiding brittle modes of failure and showing the lacks of strength based design.

Until recent years, analyses of engineering structures were generally being performed by linear analysis techniques. Nonlinear behavior of the structural system was taken into account by reducing the design forces by certain factors, depending on the characteristics of the structure. Nonlinear procedures could only be applied to important structures. Because these procedures took much time and effort, it was impractical to perform, for instance, nonlinear time history analysis to an ordinary bridge. However, the introduction of new nonlinear analysis methods, combined with the advances in computers, allowed engineers to perform more detailed analyses of structures in a small amount of time. For the seismic evaluation of Bolu Viaduct #1, second segment consisting of 20 spans is subjected to 7 different strong ground motions both in longitudinal and transversal directions; which is named as 'time history analysis'.

2. DESCRIPTION OF THE BRIDGE

2.1. General Information

Bolu Mountain Passage includes four viaducts and one tunnel. The alignment of the Anatolian Motorway in Turkey is eastbound from İstanbul until Ankara and then southbound towards Adana. Most sections of this motorway have 3 lanes in both carriageways. Regarding physical and geometric characteristics, AASHTO standards are observed. This motorway is being realized in numerous consecutive sections. Each section is constructed as an independent project by different contractors. Contracts are awarded by the Turkish state highway authority connected to the Ministry of Public Works, namely "General Directorate of Highways" that is referred as 'employer'. Gümüşova-Gerede Motorway is one of such sections (starting at about 220 km east of İstanbul, and having a length of approximately 114 km.) The construction of this section of the motorway was undertaken by Astaldi SpA in 1990. For convenience, the section is subdivided into 3 consecutive main stretches as

Stretch 1	Gümüşova-Kaynaşlı Connection	about 29 km
Stretch 2	Bolu Mountain Crossing	about 24 km
Stretch 3	Abant Interchange-Gerede	about 61 km

Table 2.1 Stretches of Gümüşova-Gerede Motorway

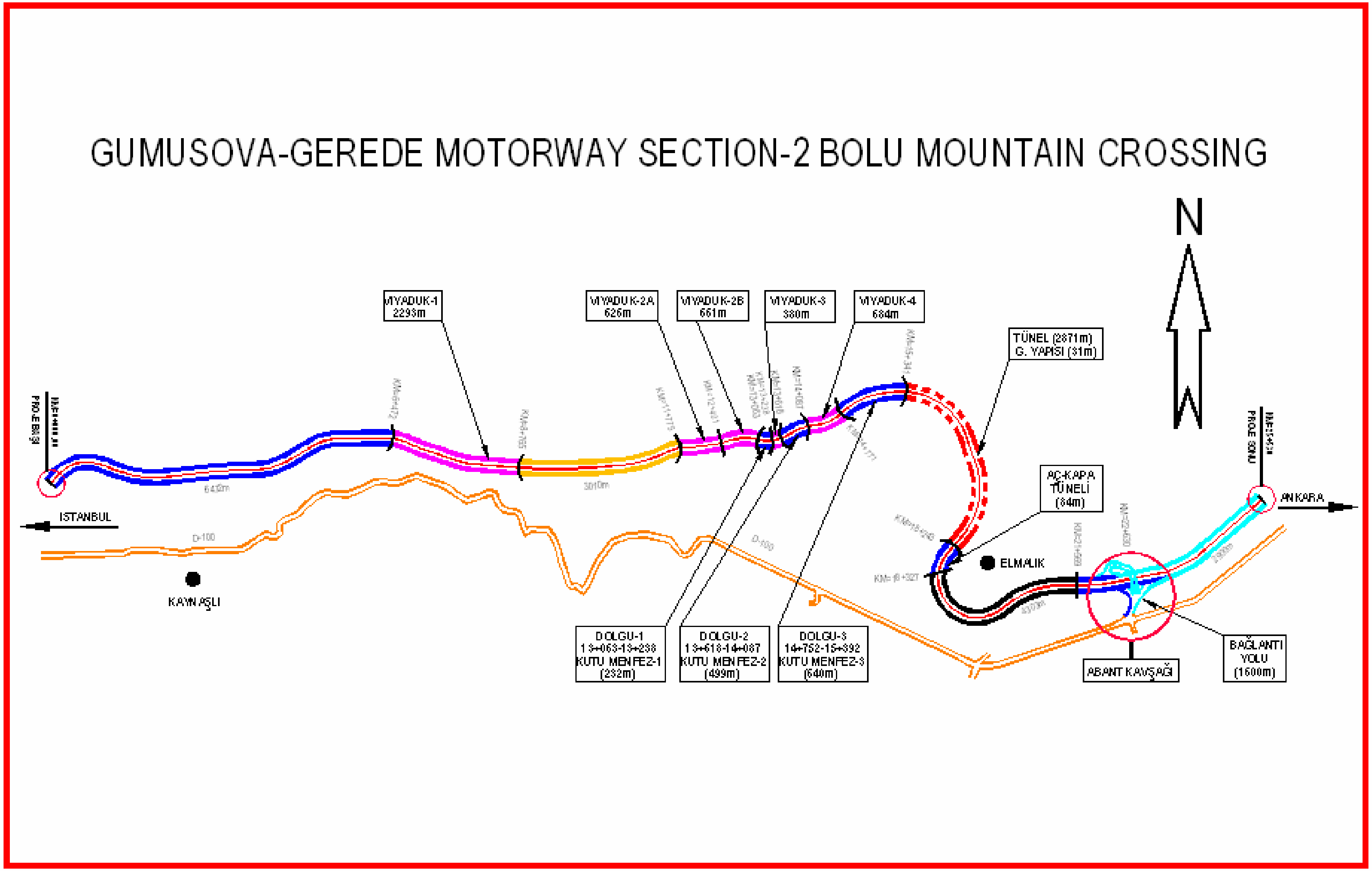

Figure 2.1 Gümüşova-Gerede Motorway Stretch-2 Bolu Mountain Crossing

After commissioning of Stretches 1 & 3, the remaining part (Stretch 2) could not be realized for quite a long period of time due to numerous difficulties that arose in the progress works, those regarding to tunnel drilling in particular. Physical difficulties were encountered in passing the Asarsuyu Valley which is indicated as Viaduct #2.

Viaduct #1, the first viaduct of Istanbul-Ankara Line, is the subject of this project. The structure consists of 2 parallel viaducts for converse directions. Both 17.50m wide directions contain three lane highways in Anadolu Highway Standard. The right side vehicle road is a bridge in Ankara direction that consists of 58 spans, 57 piers, and 2 abutments of each have a span length of 39.2 m. The Istanbul direction, the left side one way vehicle road, has 59 spans, 58 piers, and 2 abutments. Total length is 2313m. There are 115(58+57) piers, the shortest of has a height of 10m and others mostly have 40-49m heights. The piers have 4,5m x 8m rectangular empty box sections. The foundations consist of massive concrete footing, resting on 12 uniformly placed 1.80 m diameter cast-in-drilled-hole piles. They are on the 3m wide pile headings. Each foundation has a friction pile group that consists of 12 piles of 180m diameter. The lengths of piles change in 14m to 37m.

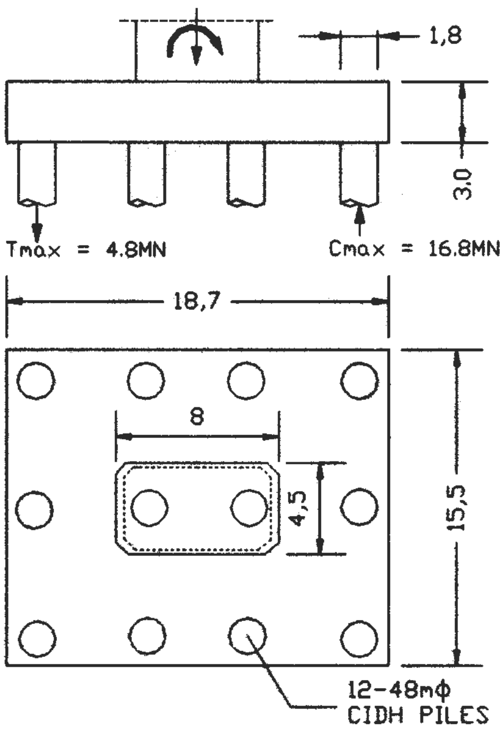

Figure 2.2 General dimensions of column section and pile cap (plan and elevation).

(a) Early Construction of Viaduct #1

(b) Recent view of Viaduct #1

(c) Early Construction of a pier

Figure 2.3 Three photos showing general views of the viaduct.

2.2. The Condition before 12 November Earthquake

Except the installation of dilation joints and approach plaques in the abutment Viaduct #1 was completed. In the visual examination after the earthquake dated 17^{th} August 1999, no damage and no modification in its geometry were observed.

- Each Span was supported on seven beams on independent bearings
- Continuity was partly provided by the upper deck.
- Bearings had a displacement capacity equal to 200 mm.
- EDU had a total displacements capacity equal to 480 mm.
- The mass of a pier was in the order of 36 t/m
- The mass of a pier head was in the order of 400 t.
- The mass of the superstructure was in the order of 1400 t per span
- The force capacity of the isolation system was in the order of 1800 kN
- The design flexural capacity of the typical pier was in the order of 500 MN and the shear capacity in the order of 15 MN; it should be noted that the force due to the deck mass was absorbing less than %20 of the capacity [**Ref. 8**]

2.3. The Damage of Viaduct 1 Caused by 12 November Earthquake

On November 12, 1999 an earthquake of moment magnitude 7.2 occurred on the Duzce fault. This followed three months after the Kocaeli earthquake of August 17th, 1999, which caused extensive damage and loss of life. As well as causing damage to buildings, with the loss of about 1000 lives, the Duzce earthquake caused severe damage to tunnels and bridges under construction on the Great Anatolian Highway.

Figure 2.4 Failure of an EDU

Peak ground accelerations in the vicinity of 0.8g, based on accelerograms recorded nearby (records were available in Bolu, 8 km from the viaduct site, and in Duzce, 7 km from the site) were estimated at the viaduct site. More important to the bridge performance, right lateral fault slip of approximately 1.6 m occurred on a fault scarp traversing the bridge alignment, at an acute angle (approximately 15° to the bridge longitudinal axis), resulting in shortening of the bridge length by about 1.5 m, concentrated over two spans of the bridge.

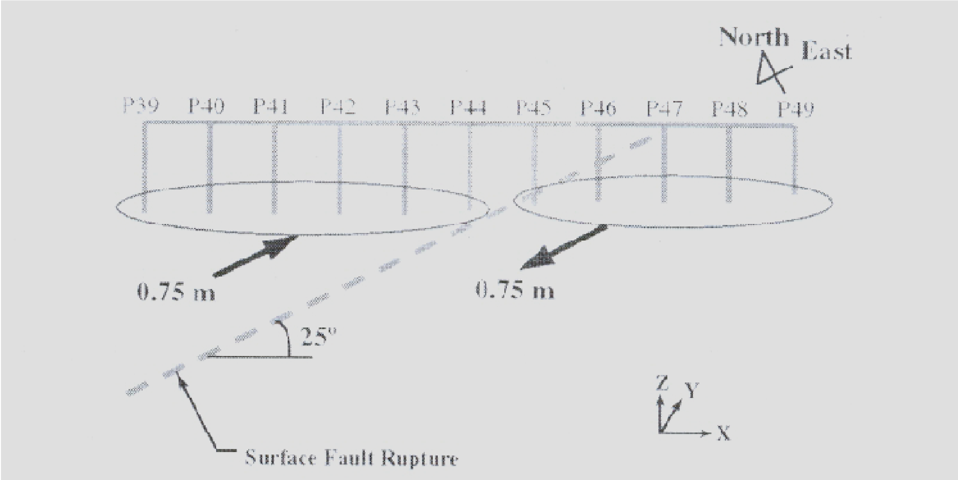

Figure 2.5 Orientation of the surface fault rupture and direction of static ground displacement

The earthquake incident that happened on 12 November 1999 with an epicenter near Düzce (about 15 km away from the starting point of the project), created an enormous effect on the contract works. Damages occurred in various parts of the project. Those in the tunnels and on Viaduct #1 were substantial. Upon this catastrophe, all contract works ceased, and solutions for recovering the damages were sought for months after the event. It was even quite difficult to determine the precise nature of damages, because some of these were not visible, and detailed surveys had to be conducted.

Figure 2.6 The shortening of bridge

Near-fault motions usually contain both intense dynamic motions and large static displacements. The intense, coherent dynamic motions are caused by forward rupture directivity which is commonly characterized by a long-period velocity pulse acting normal to the fault. Static ground displacements in near-fault ground motions are caused by the differential movement of the two sides of the fault on which the earthquake takes place, and the magnitude of the displacement decreases with distance from the fault. If ther is faulting at the ground surface, the ground displacement is discontinuous across the surface fault rupture and can subject a bridge crossing the fault to significant differential movements, posing a primary seismic hazard. Coherent dynamic motions in the fault normal direction and permanent static displacements in the fault-parallel direction occur almost simultaneously and thus these two effects are treated as coincident loads.

(a) A general photo of Surface fault rupture of taken on Viaduct #1

(b) A closer photo of surface fault rupture of taken on Viaduct #1

(c) A closer photo of surface fault rupture of taken on the ground

Figure 2.7 Three photos showing the surface fault rupture and direction of static ground displacement

There were no ground motions during the Duzce earthquake at or in the immediate vicinity of the Bolu Viaduct site. The recording stations closest to the site included the Bolu and Duzce stations, which are also used as input ground motion in the time-history analyses in this paper.

Numerous meetings were held among the relevant executives of the insured parties, the contractor, the engineer and the employer. Several experts that are well known throughout the world by their know-how and experience in their profession in different but related disciplines were consulted.

Relatively smaller damages that occurred by the earthquake event have already been repaired or reinstated. Some constructional items such as a number of pre-cast girders stored in the stockyard for the future use that could not be repaired were simply got rid of by having treated as thrash. The repair of damages that occurred on Viaduct #1 and the reinstatement of the damages in the tunnels were the major items remained. As a result of the detailed study named “Strategies for Repair and Seismic Upgrading of Bolu Viaduct 1, Turkey” by M. J. N. Priestley and G. M. Calvi; the authors were contracted by the Italian firm Astaldi SpA to develop the conceptual design for reinstatement of the bridge.

2.4. The Retrofit Criteria by Calvi and Priestley

- The last earthquake imposed permanent relative displacement demands, due to fault slip, in excess of 1 m. A relative displacement equal to 600 mm should be assumed in the fault effected are, considering a 100 years period.
- The design peak ground acceleration has been set to 0.81 g in a return period of 2000 years.
- A displacement demand in the order of 0.6 m, for periods of vibration between 2 and 6 seconds.
- At bearing level, demand level between 0.7 and 0.9 m
- The displacement capacity excludes the possibility of supporting each single beams; the only viable solution is then to make the beams continuous over the support, allowing large permanent displacements without significant effects on the bearing capacity of the bridge
- As a consequence it can be assumed that, independently of the choice of the bearing/EDU system, it will be necessary to lift up each span, to strengthen the deck system and to insert two or more new devices in the central area of the pier cap.
- The whole soil-foundation-pier systems should be verified considering the strength demand deriving from the combination of the possibly increased force coming from the isolation system (due to a larger displacement capacity) and the increased force coming from the pier response (due to the larger design acceleration)

[**Ref. 8**]

Figure 2.8 During ‘recentering’

3. SITE INVESTIGATION

3.1. Current Situation of the Viaduct 1

The Bolu Viaduct 1 is visited twice in winter and summer respectively. The retrofitted bridge is particularly in good condition, and about to finish in 1-2 years with all the phases including the tunnel completed. The piers

The Anatolia Fault goes under the Viaduct 1,

- 12 November Earthquake caused damage at the viaduct but it wasn't collapsed.
- The viaduct is supported and restored with special methods

3.2. Piers

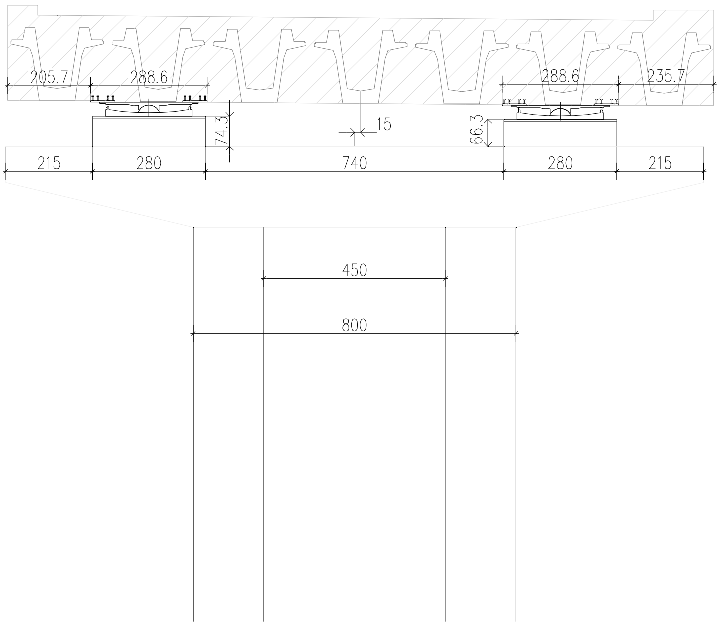

(a) View

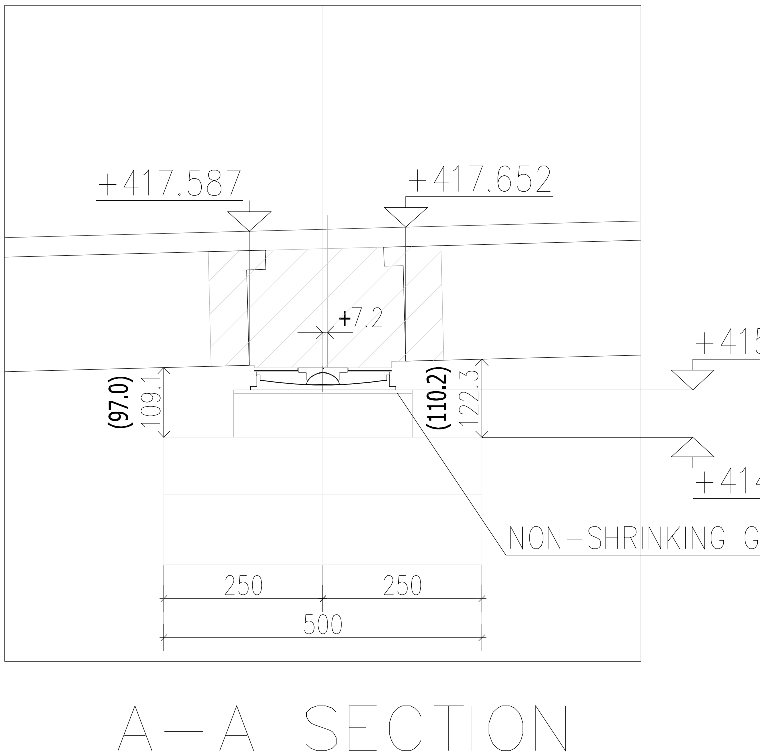

(b) A-A Section

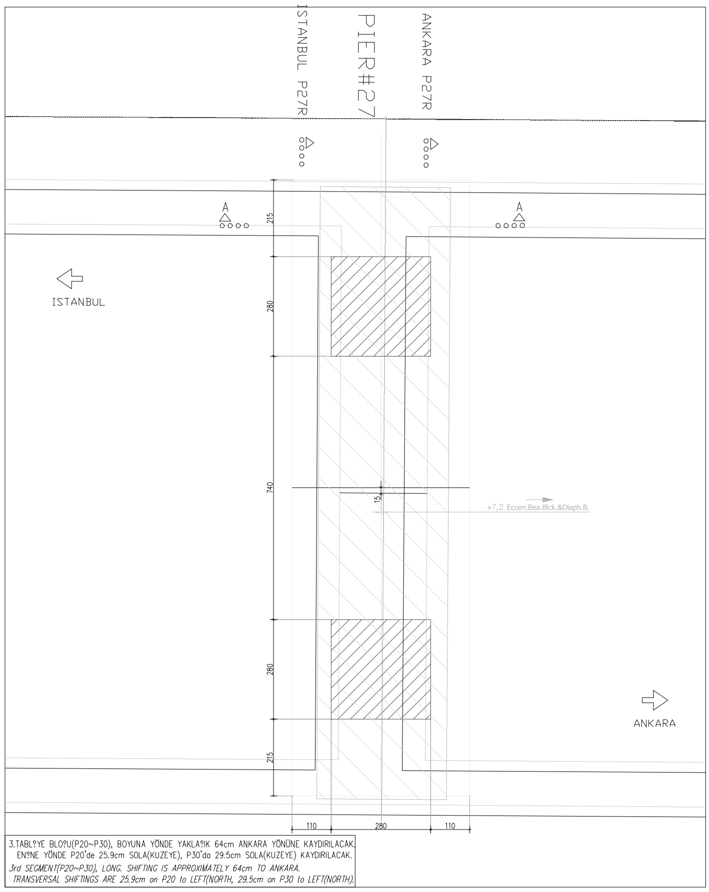

(c) Plan View

Figure 3.1 Pier Section of the retrofitted structure (Pier #21)

3.3. Diaphragm Beam

Considering the large residual displacement that resulted from the November earthquake and the large displacement demand, it is assumed to make each 10-span segment fully continuous by adding a diaphragm beam over each support to allow reducing bearing/isolators to two per support except at movement joints.

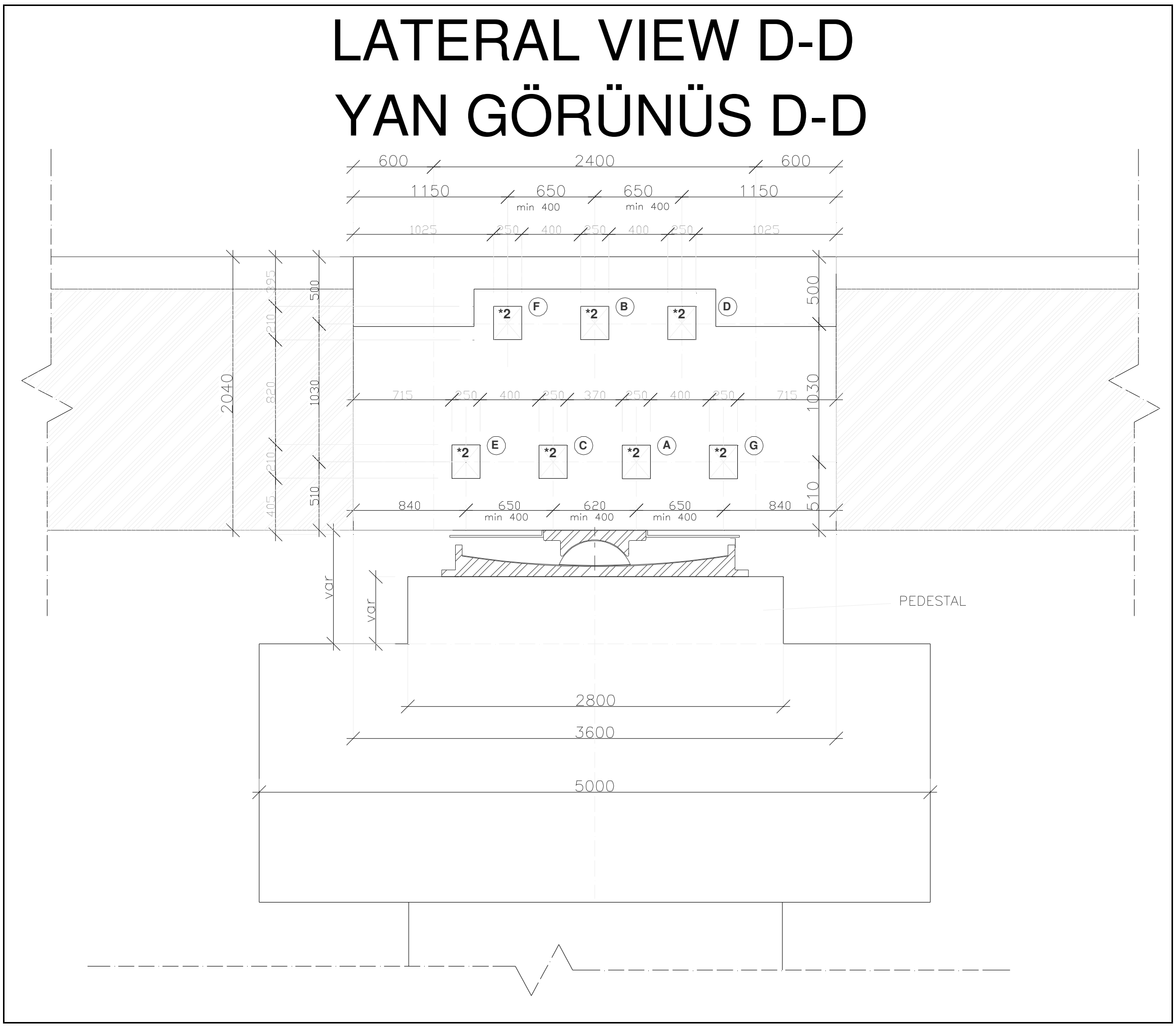

(a) Lateral View

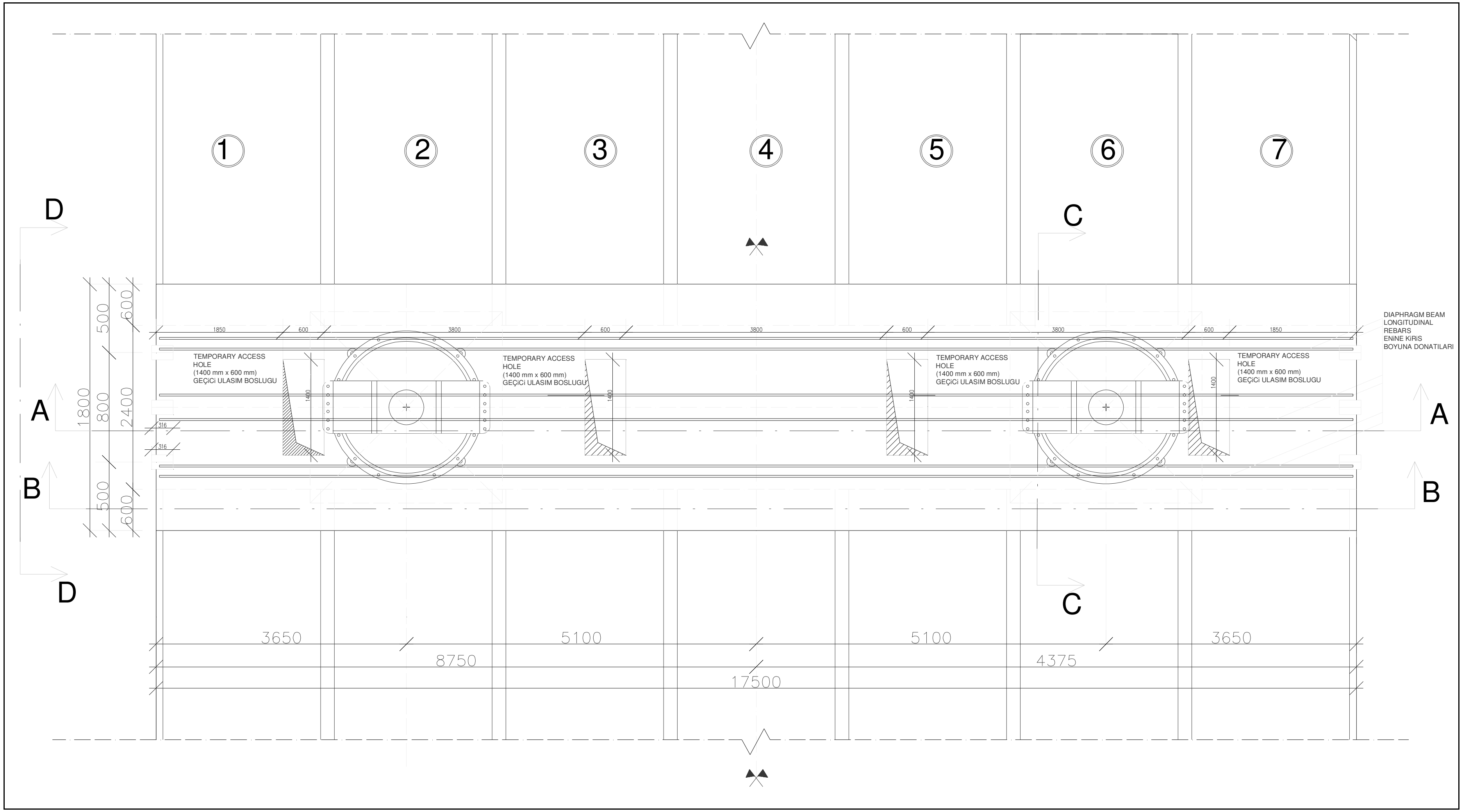

1
2
3
4
5
6
7
D
C
A
B
TEMPORARY ACCESS HOLE (1400 mm x 600 mm) GEÇiCi ULASIM BOSLUGU
DIAPHRAGM BEAM LONGITUDINAL REBARS ENINE KiRiS BOYUNA DONATILARI
1850
600
3800
500
600
1800
800
2400
3650
5100
8750
4375
17500

(b) Plan View

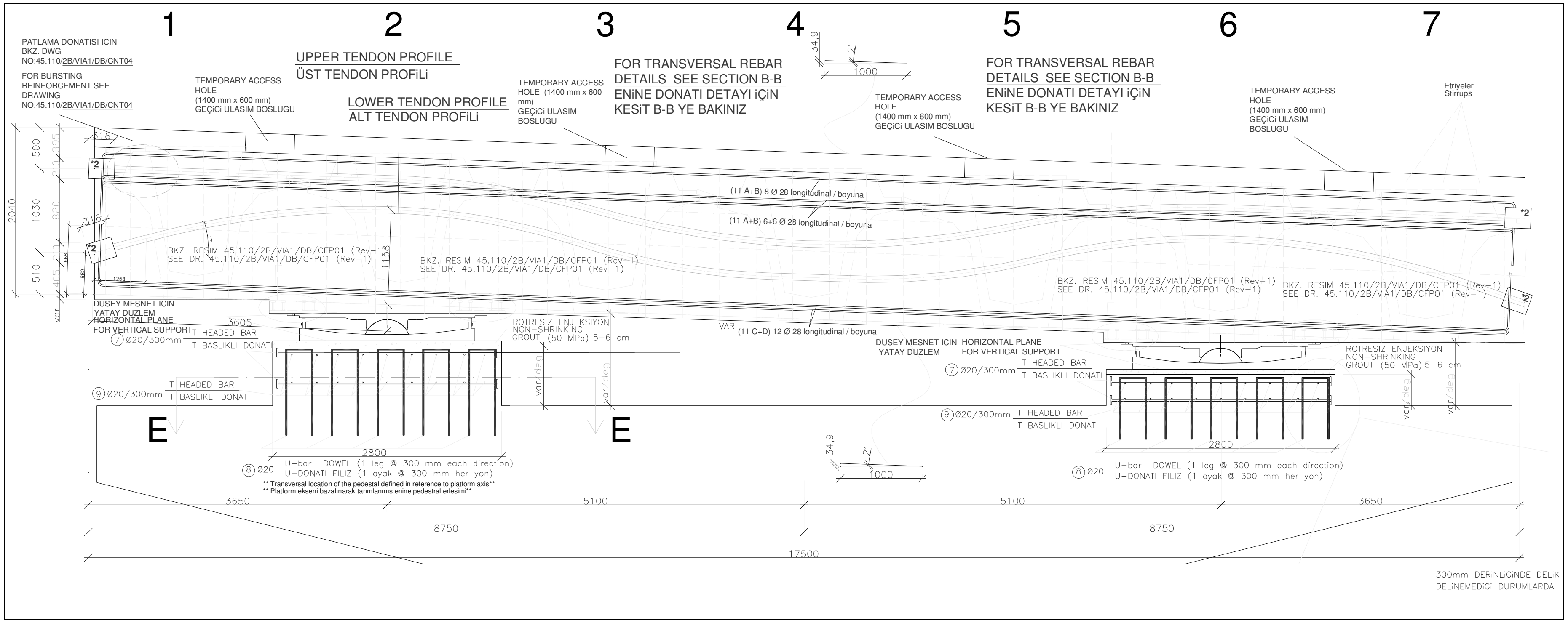

(c) Tendon Profile

Figure 3.2 The design plans for the diaphragm beam

(a) Section View

(b) Perspective View

(c) Before Post Tension

(d) Post Tension Process

Figure 3.3 Photos during the implementation of the post tension diaphragm beam

3.4. Expansion Joints

In the report of Calvi and Priestley it's suggested that the increased potential displacement demand would require movement joints with total displacement capacities of the order of 1.5 m. Joints of this kind would be movement joints would be extremely expensive and would imply difficult design problems for pier caps and super structure. By a more convenient solution assuming to create transversal shear key between the two parts of the deck interlocking the two new diaphragm beams, to allow longitudinal relative displacements considering thermal and creep deformations only and to add at the sides of diaphragm beams two shock absorbers acting in the longitudinal direction. This solution will imply total displacement capacities of the order of 400 mm and a global response of the whole viaduct in case of earthquake. [**Ref. 8**]

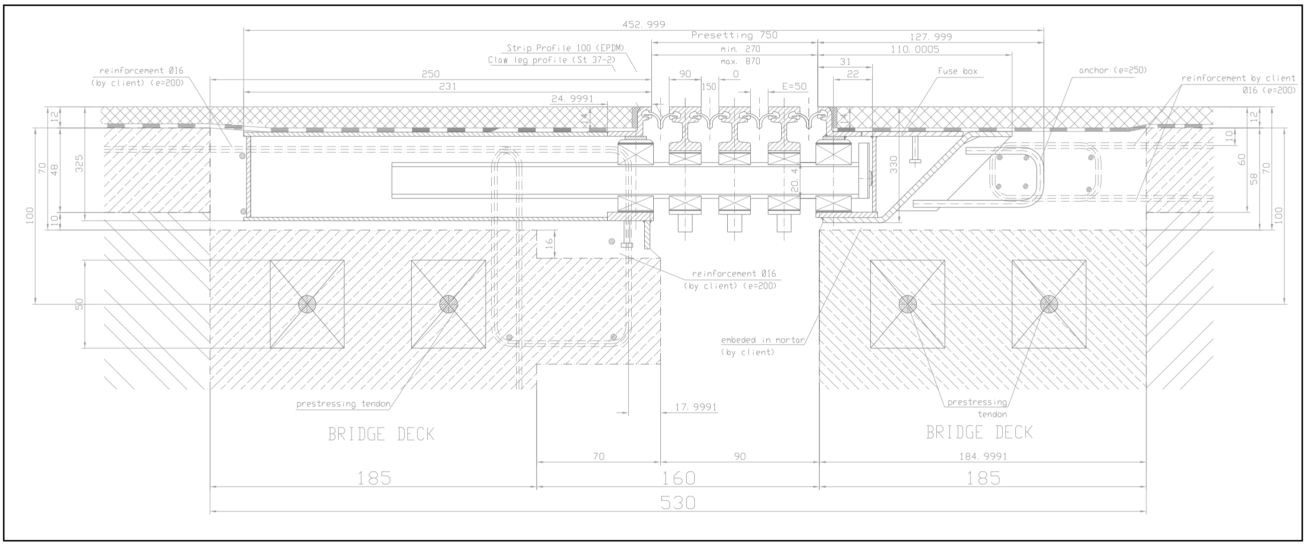

(a) DS 320 / 400 F

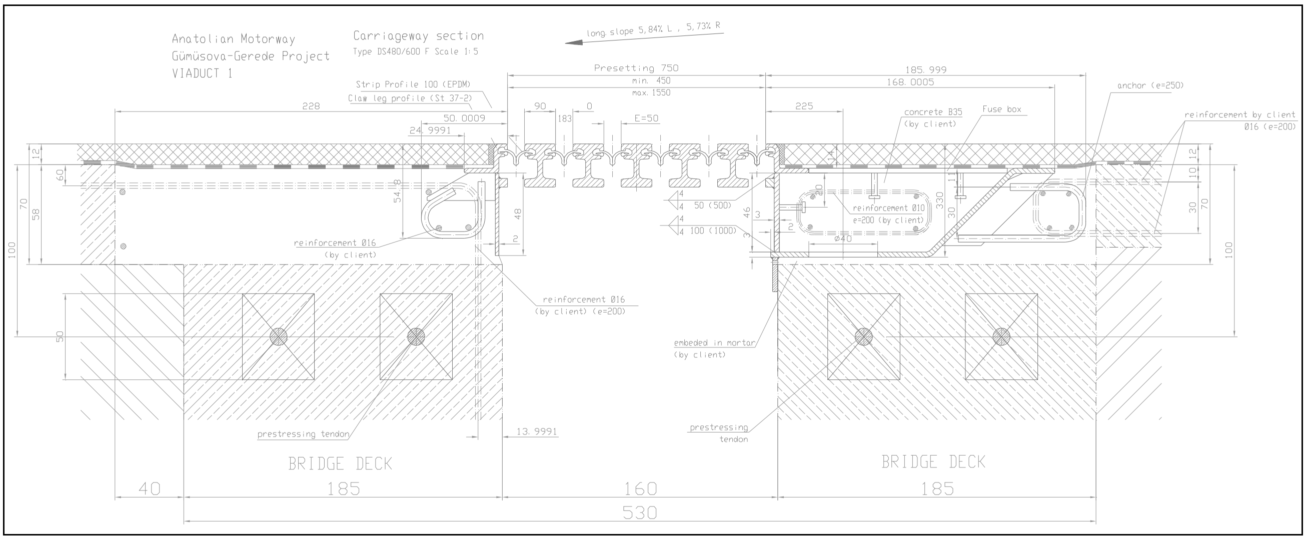

(b) DS 480 / 600 F

Figure 3.4 Plans of Maurer Expansion Joints

In the scope of these criteria, expansion joints produced by Maurer Söhne with displacement capacities of 800 mm are implemented. (Maurer Expansion Joints DS 480 / 600 F)

(a) Section View

(b) Upper View

Figure 3.5 Photos of Maurer Expansion Joints

Expansion joints for viaduct#1 are designed with 10 spans (approximately 390m). The number of joints is 6 for each right and left vehicle roads. To solve the shrinkage problem of the viaduct because of earthquake, cutting 3 of the connection deck upon the pier of the deck were decided. Otherwise this caused to shrinkage of the widths of the diaphragm beams. Hence, this action was not sufficient so that 2 expansion joints were cancelled by the way 2 segments were connected. Expansion joints are made at the 20th, 40th, and 50th piers and also at the abutments. Moreover, back walls of the abutments have been moved 80 cm. The negative moment that arose after change of deck static state is covered by the intensive thermal expansion reinforcement inside the deck at the connections.

The restoration and strengthen works are finished on July 2005 and next works are started.

3.5. Alignment

Both slabs consist of 6 segments and each segment has 10 spans except second segment with 20 spans. The curves are designed 1000m right and 3500m left in horizontal, and 30000m in vertical. The vertical slopes are % 2.68 and % 3.08

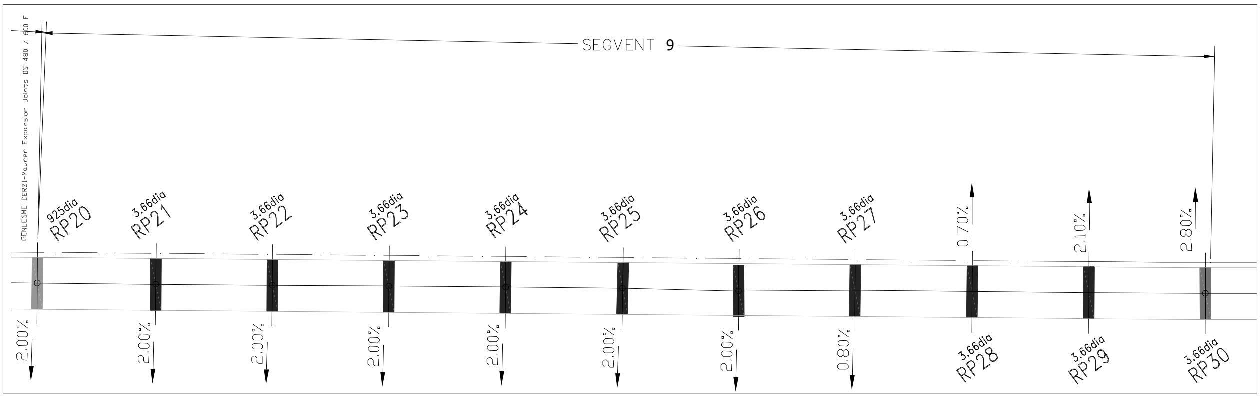

(a) Piers 20-30

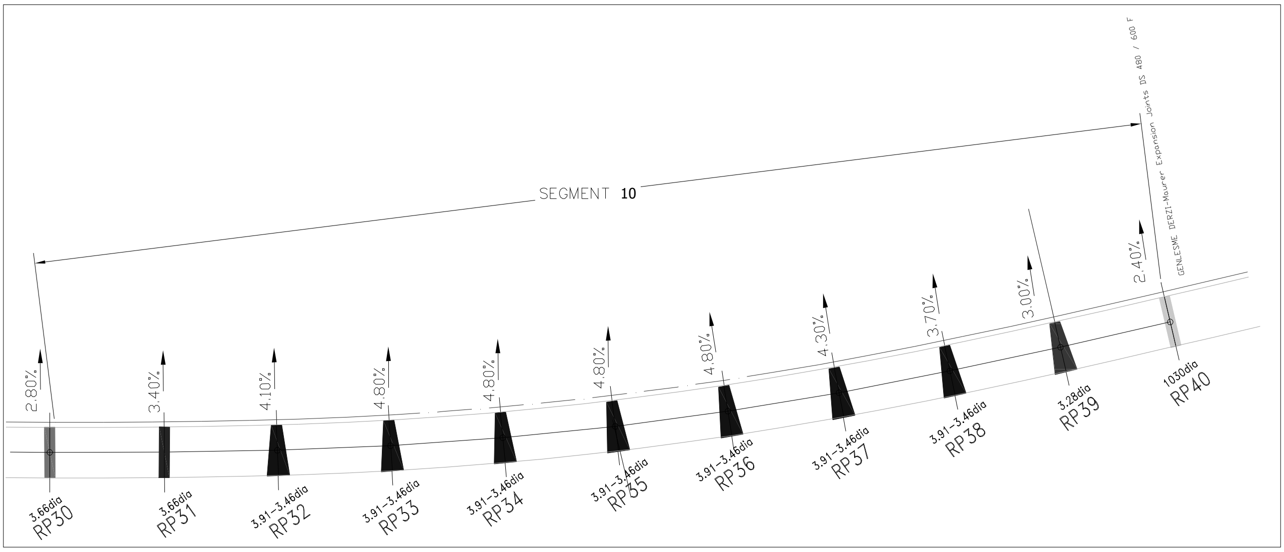

(b) Piers 30-40

Figure 3.6 Alignment of Piers 20-40

3.6. Foundations

In the 'Preliminary Report on Repair and Retrofit of Viaduct 1' it shown that the structural capacity greatly exceeds the soil capacity and some damage to the piles will not reduce axial load capacity.

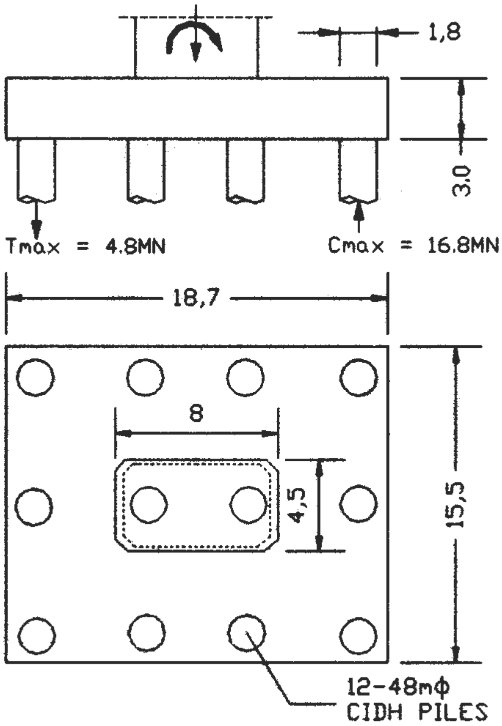

Figure 3.7 General dimensions of column section and pile cap (plan and elevation).

Pile cap:

A pile cap extension has been carried out.

(a) General View

(b) Closer View

Figure 3.8 Photos during the extension of pile caps

4. MODELING OF THE BRIDGE

4.1. Modeling objectives

The purpose of the mathematical modeling of any system is to quantify the response of the structure under earthquake loading based on the specified geometric and material properties. It is generally more preferable to create a simple model to capture meaningful seismic demand, rather than a complex model. In the mathematical model of the Bolu Viaduct #1 the segments between piers 20 and 40 are used assuming that the segments behave independently from the first and last segments. In the model of the bridge, force deformation behavior of subsystems, such as piers were developed. Other components, such as superstructure, intended to remain elastic, are modeled by elements, which have linear elastic behavior. As a final stage, deformation, force and displacement demands estimated by analysis of three-dimensional mathematical model of the viaduct were compared with the capacities of the components.

For the analysis of the bridge, SAP2000 v10.0.1 Nonlinear Dynamic Analysis Program and Xtract Cross Sectional Analysis Program v. 3.0.5 is used. The coordinate system used in the capacity and demand analysis is shown in Table 4.1 Coordinate Key. The X and Y axes are referred to as the global longitudinal and transverse directions, respectively.

	Global Axes	
X	Parallel To Bridge Direction	U1
Y	Perpendicular To Bridge Direction	U2
Z	Elevation	U3
	Frame Local Axes	
X	Parallel To Bridge Direction	U2
Y	Perpendicular To Bridge Direction	U3
Z	Elevation	U1
	Joint Local Axes	
X	Parallel To Bridge Direction	U1
Y	Perpendicular To Bridge Direction	U2
Z	Elevation	U3
	FPB Link Local Axes	
X	Parallel To Bridge Direction	U2
Y	Perpendicular To Bridge Direction	U3
Z	Elevation	U1

Table 4.1 Coordinate Key

The model doesn’t include soil structure interaction effect. Ground motion was assumed to be uniform for the supports, so asynchronous motion effect was neglected.

4.2. Material Modeling

To completely reflect the behavior of the piers, detailed modeling has been done by complete geometry and reinforcement plan. For the analyses of piers cross section analysis program Xtract v3.05 is used. Because of the complex geometry of the pier section three components are defined with three different confinement ratios. For longitudinal reinforcement St 50 type III construction steel by the German Norm 17100 is used in the project. For transverse reinforcement with diameters less than 20 mm, St 37 type construction steel by the German Norm 17100 is used in the project.

The concrete model given by J.B. Mander, M.J.N. Priestley, and R. Park [**Ref. 3**] is used. For the reinforcement steel, a steel model with parabolic strain-hardening is used.

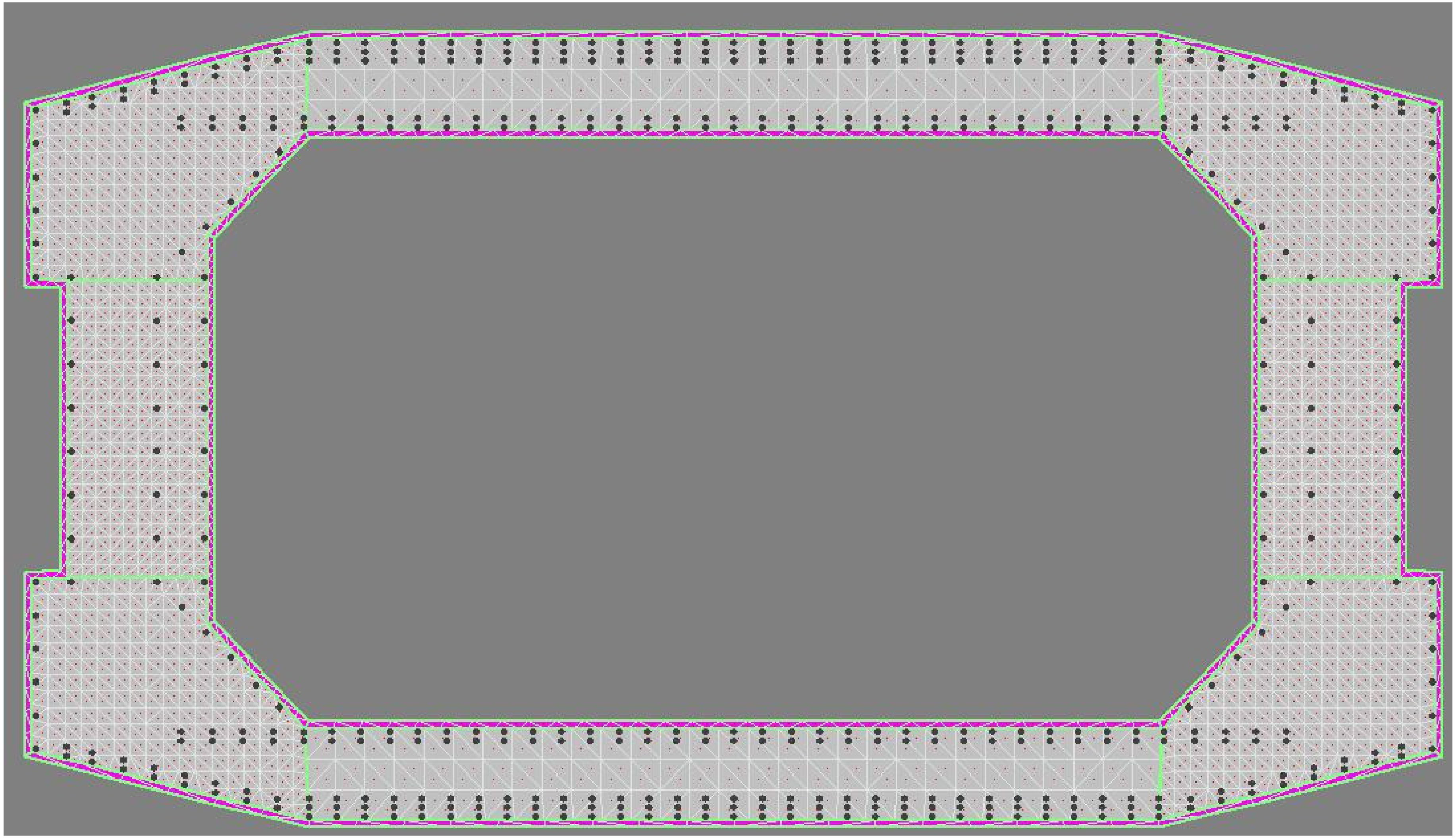

Figure 4.1 Xtract Model Geometry

4.2.1. Unconfined Concrete

The cover concrete C30 with minimum 4 cm width is modeled with unconfined concrete properties.

28-Day Compressive Strength:	$f'_c = 30$ MPa
Modulus of elasticity:	$E_c = 25\ 900$ MPa
Yield strain:	$\varepsilon_y = 0.0014$
Crushing strain:	$\varepsilon_{cu} = 0.004$
Spalling strain:	$\varepsilon_{sp} = 0.005$

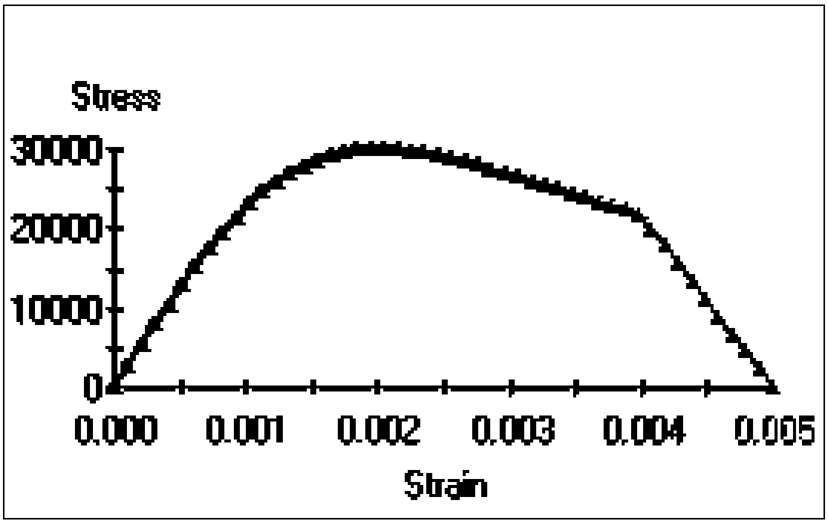

Figure 4.2 Stress-strain curve for unconfined concrete

4.2.2. Confined Concrete

The concrete model given by J.B. Mander, M.J.N. Priestley, and R. Park [**Ref. 3**] is used. Since the model parameters are affected by various parameters, such as reinforcement configuration; three different subsections are used in the model. The shared properties are :

28-Day Compressive strength:	f'_c = 30 Mpa
Tension strength:	f_t = 0 MPa
Modulus of elasticity:	E_c = 25 900 Mpa
Crushing strain:	ε_{cu} = 0.020

The reinforcement ratio calculations are shown in detail in Figure 4.4

<u>Confined 1 (Vertical Section)</u>

Confined Concrete Strength :	f'_c =	42.91	Mpa
Yield strain:	ε_y =	0.00441	

<u>Confined 2 (Horizontal Section)</u>

Confined Concrete Strength :	f'_c =	44.40	Mpa
Yield strain:	ε_y =	0.00476	

<u>Confined 3 (Corner Section)</u>

Confined Concrete Strength :	f'_c =	43.90	Mpa
Yield strain:	ε_y =	0.00464	

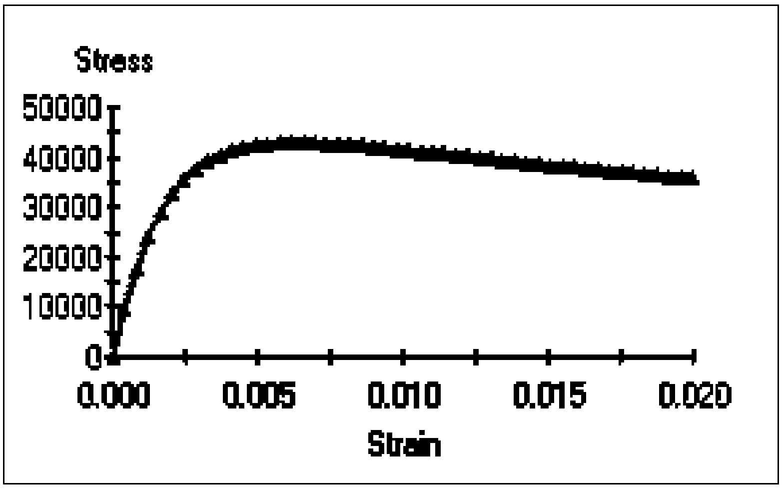

Figure 4.3 Xtract Confined Concrete Model

Bolu Viaduct 1 Confined Concrete Model For Piers 20-40

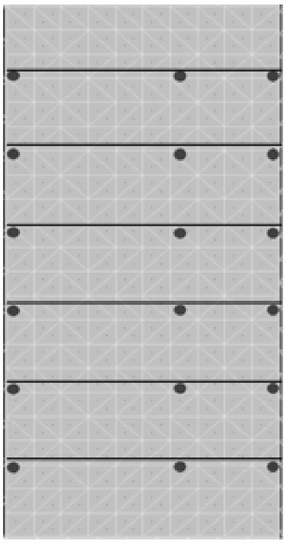

	Type	Length
Section Subpart Name :	Confined 1	
Section Dimensions & Area :	1.68*0.79	1.3272
Longitudinal Bars :	3*6Ø32	
Transversal Bars :	6Ø12/0.10*0.25	(0.79)
	2Ø20/0.10	(1.68)

ρ_x = (2*3.14)/(79*10) = 0.00795

ρ_y = (6*1.13)/(168*10) = 0.00404

ρ_v = 0.0795+0.00404 = 0.01199

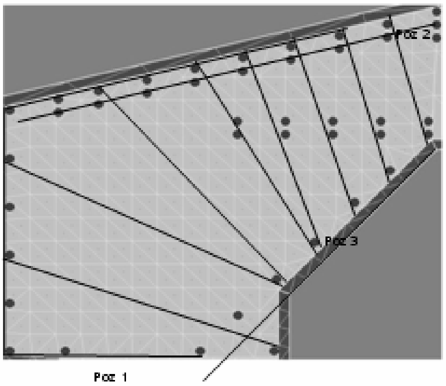

	Type	Length
Section Subpart Name :	Confined 2	
Section Dimensions & Area :	variable	1.5066
Longitudinal Bars :	35Ø32	
Transversal Bars :	8Ø12/0.10*var	variable
Poz 1	1Ø16/0.10	(.70+.96+1.2)
Poz 2	1Ø20/0.10	(1.61)
Poz 3	1Ø20/0.10	(1.19)

ρ_v = (8*1.13*73.38 + 1*2.01*286 + 3.14*(1.61+1.19)) / (15066*10) = 1.405E-02

$\rho_x = \rho_y$ = 7.025E-03

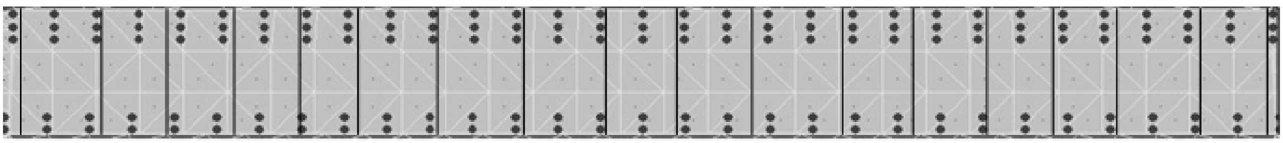

	Type	Length
Section Subpart Name :	Confined 3	
Section Dimensions & Area :	0.52*4.82	2.5064
Longitudinal Bars :	5*31Ø32	
Transversal Bars :	18Ø12/0.10*0.25	0.52
	2Ø20/0.10	(4.82)

ρ_x = (18*1.13)/(482*10) = 4.220E-03

ρ_y = (2*3.14)/(52*10) = 1.207E-02

ρ_v = (4.22+12.07)/1000 = 1.629E-02

Figure 4.4 Xtract Confined Concrete Model - Reinforcement Ratios

4.2.3. Steel Reinforcement

For longitudinal reinforcement St 50 type III construction steel by the German Norm 17100 modeled with parabolic strain-hardening is used in the project.

Yield stress:	f_y = 490 MPa
Fracture stress:	f_{su} = 660 MPa
Modulus of elasticity:	E_s = 200 000 MPa
Strain at onset of strain hardening:	ε_{sh} = 0.008
Failure strain:	ε_{su} = 0.090

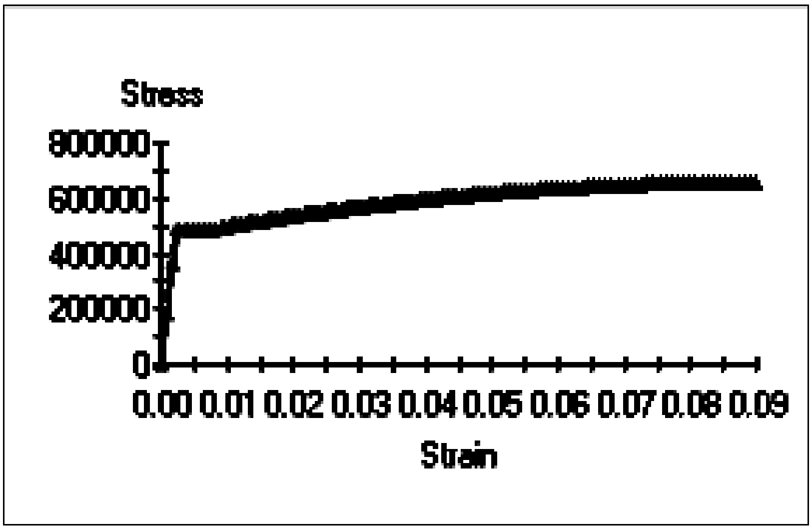

Figure 4.5 Stress-strain curve for steel

4.2.4. Results of Section Analysis (Longitudinal Direction)

XTRACT Analysis Report - Educational

For use only in an academic or research setting.

Imbsen & Associates, Inc. (in-hous
KOERI
9/4/2006
Via1
Section A-A
Page __ of __

Section Name:	A-A
Loading Name:	1
Analysis Type:	Moment Curvature

Section Details:

X Centroid:	.2947E-15 m
Y Centroid:	-.9526E-16 m
Section Area:	15.33 m^2

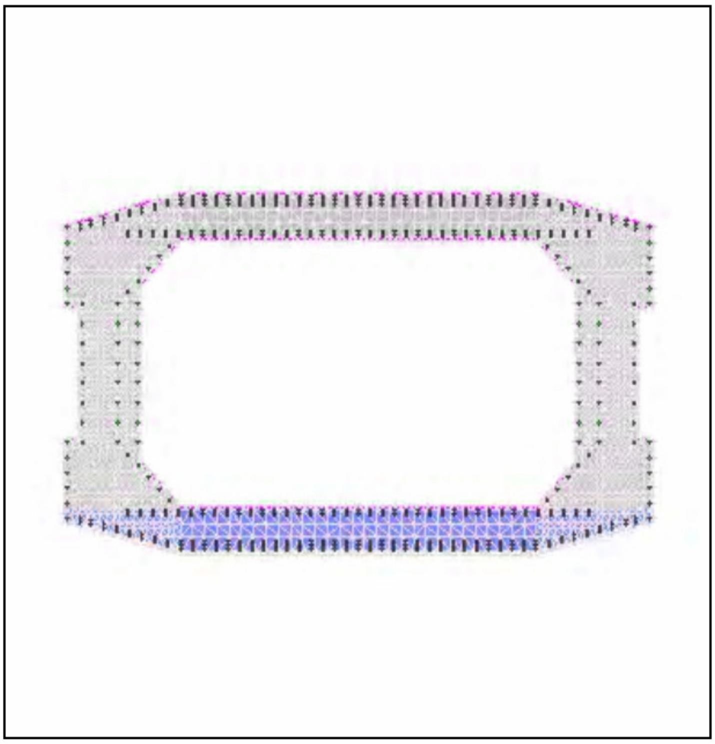

Loading Details:

Constant Load - P:	35.00E+3 kN
Incrementing Loads:	Mxx Only
Number of Points:	30
Analysis Strategy:	Displacement Control

Analysis Results:

Failing Material:	Steel1
Failure Strain:	90.00E-3 Tension
Curvature at Initial Load:	-.1509E-19 1/m
Curvature at First Yield:	.8018E-3 1/m
Ultimate Curvature:	23.11E-3 1/m
Moment at First Yield:	381.9E+3 kN-m
Ultimate Moment:	582.3E+3 kN-m
Centroid Strain at Yield:	.6940E-3 Ten
Centroid Strain at Ultimate:	39.39E-3 Ten
N.A. at First Yield:	.8655 m
N.A. at Ultimate:	1.704 m
Energy per Length:	11.98E+3 kN
Effective Yield Curvature:	1.007E-3 1/m
Effective Yield Moment:	479.5E+3 kN-m
Over Strength Factor:	1.215
EI Effective:	4.76E+11 N-m^2
Yield EI Effective:	4.65E+9 N-m^2
Bilinear Harding Slope:	.9771 %
Curvature Ductility:	22.95

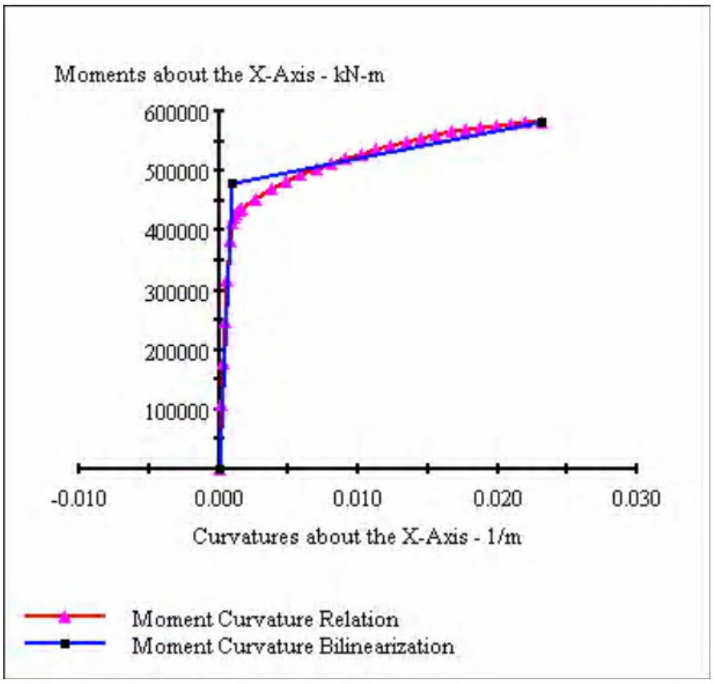

Comments:

User Comments

	Curvatures About the X axis	Moments About the X axis
	Kxx	Mxx
Section	A-A	A-A
Loading	1	1
Units	1/m	kN-m
0	-1.51E-20	0.00
1	1.60E-04	108,700.00
2	3.21E-04	178,700.00
3	4.81E-04	247,400.00
4	6.42E-04	315,200.00
5	8.02E-04	381,900.00
6	9.62E-04	413,900.00
7	1.12E-03	422,700.00
8	1.28E-03	428,900.00
9	1.44E-03	433,300.00
10	1.60E-03	436,900.00
11	2.68E-03	452,300.00
12	3.75E-03	469,000.00
13	4.83E-03	482,500.00
14	5.91E-03	494,000.00
15	6.98E-03	504,300.00
16	8.06E-03	512,900.00
17	9.13E-03	520,900.00
18	1.02E-02	529,100.00
19	1.13E-02	536,700.00
20	1.24E-02	543,700.00
21	1.34E-02	550,100.00
22	1.45E-02	555,900.00
23	1.56E-02	561,100.00
24	1.67E-02	565,800.00
25	1.77E-02	569,900.00
26	1.88E-02	573,500.00
27	1.99E-02	576,500.00
28	2.10E-02	579,000.00
29	2.20E-02	580,900.00
30	2.31E-02	582,300.00

Initial	0.000E+00	0.00
Yield	1.007E-03	479,500.00
Ultimate	2.311E-02	582,300.00

$\kappa_{plastic} = \kappa_{ultimate} - \kappa_{yield}$ = 2.210E-02

$\theta_{\mathrm{plastic}} = \kappa_{plastic} * \ell_{\mathrm{p}}$ = 9.283E-02

Table 4.2 Moment Curvature Analysis Results for U1 Direction

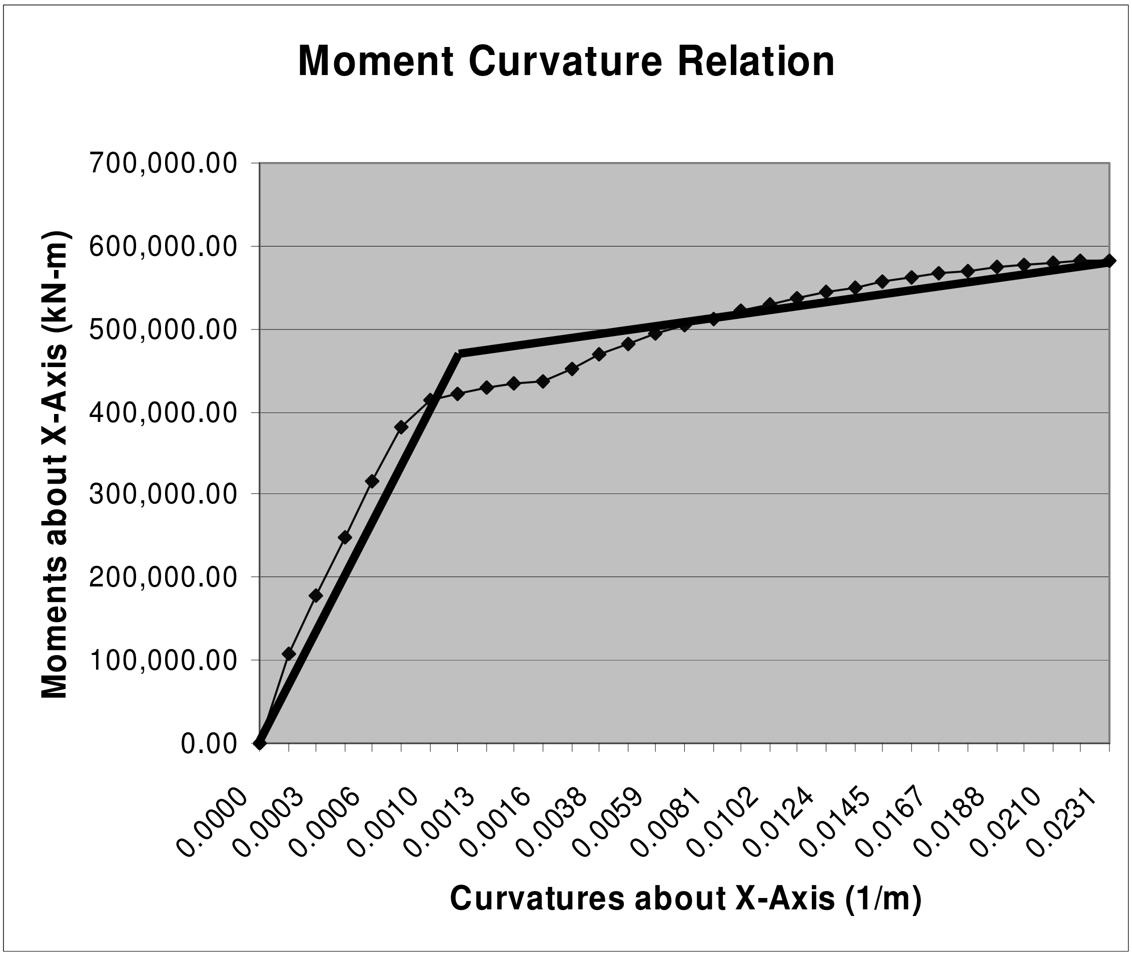

Figure 4.6 Moment Curvature Bilinearization for Longitudinal Direction

		Moment (kNm)	Rotation (rad)
U1 - Direction	Inital	0.00	0.000E+00
	Yield	479,500.00	4.229E-03
	Ultimate	582,300.00	9.706E-02

Table 4.3 Moment Hinge Coefficients for SAP2000 Model

4.2.5. Results of Section Analysis (Transversal Direction)

XTRACT Analysis Report - Educational

For use only in an academic or research setting.

Imbsen & Associates, Inc. (in-ho
KOERI
9/3/2006
Via1
Section A-A
Page __ of __

Section Name:	A-A
Loading Name:	2
Analysis Type:	Moment Curvature

Section Details:

X Centroid:	.2947E-15 m
Y Centroid:	-.9526E-16 m
Section Area:	15.33 m^2

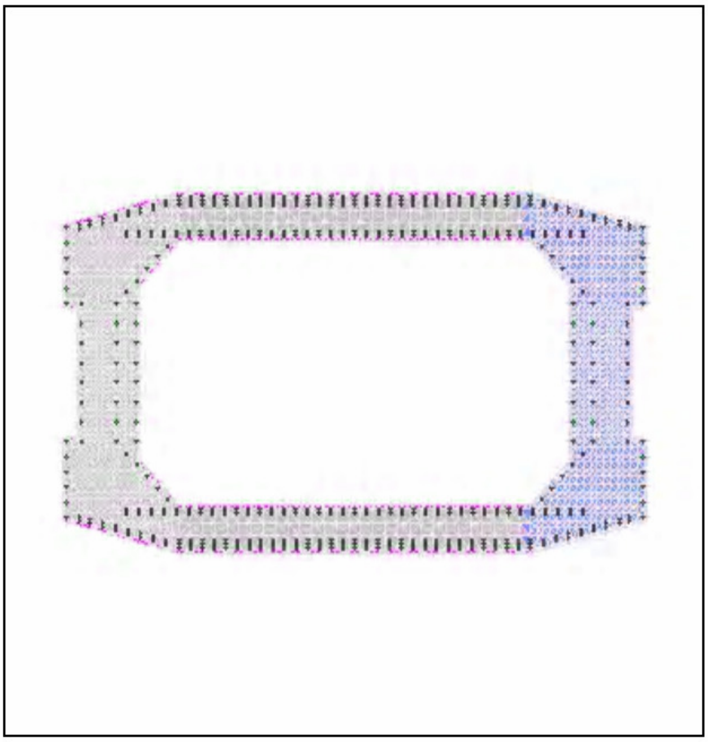

Loading Details:

Constant Load - P:	35.00E+3 kN
Incrementing Loads:	Myy Only
Number of Points:	30
Analysis Strategy:	Displacement Control

Analysis Results:

Failing Material:	Confined2
Failure Strain:	20.00E-3 Compression
Curvature at Initial Load:	-.2017E-19 1/m
Curvature at First Yield:	.4505E-3 1/m
Ultimate Curvature:	12.32E-3 1/m
Moment at First Yield:	482.9E+3 kN-m
Ultimate Moment:	896.5E+3 kN-m
Centroid Strain at Yield:	.6741E-3 Ten
Centroid Strain at Ultimate:	28.43E-3 Ten
N.A. at First Yield:	1.496 m
N.A. at Ultimate:	2.307 m
Energy per Length:	9925 kN
Effective Yield Curvature:	.7148E-3 1/m
Effective Yield Moment:	766.3E+3 kN-m
Over Strength Factor:	1.170
EI Effective:	1.07E+12 N-m^2
Yield EI Effective:	1.12E+10 N-m^2
Bilinear Harding Slope:	1.046 %
Curvature Ductility:	17.24

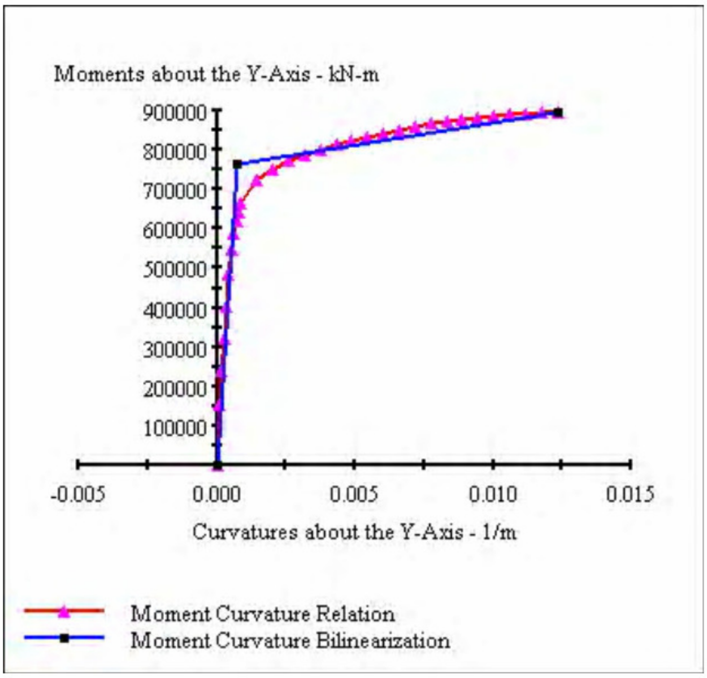

Comments:

User Comments

	Curvatures About the Y axis	Moments About the Y axis
	Kyy	Myy
Section	A-A	A-A
Loading	2	2
Units	1/m	kN-m
0	-2.02E-20	0.00
1	9.01E-05	153,000.00
2	1.80E-04	238,800.00
3	2.70E-04	322,000.00
4	3.60E-04	403,400.00
5	4.51E-04	482,900.00
6	5.41E-04	546,600.00
7	6.31E-04	589,500.00
8	7.21E-04	620,700.00
9	8.11E-04	644,300.00
10	9.01E-04	662,600.00
11	1.47E-03	722,900.00
12	2.04E-03	751,300.00
13	2.61E-03	771,400.00
14	3.19E-03	785,700.00
15	3.76E-03	799,100.00
16	4.33E-03	811,900.00
17	4.90E-03	823,500.00
18	5.47E-03	833,900.00
19	6.04E-03	843,300.00
20	6.61E-03	851,800.00
21	7.18E-03	859,600.00
22	7.75E-03	866,500.00
23	8.33E-03	872,700.00
24	8.90E-03	877,600.00
25	9.47E-03	881,700.00
26	1.00E-02	885,900.00
27	1.06E-02	889,400.00
28	1.12E-02	892,300.00
29	1.18E-02	894,600.00
30	1.23E-02	896,500.00

Initial	0.000E+00	0.00
Yield	7.148E-04	766,300.00
Ultimate	1.232E-02	896,500.00

$\kappa_{plastic} = \kappa_{ultimate} - \kappa_{yield} =$ 1.161E-02

$\theta_{plastic} = \kappa_{plastic} * \ell_p =$ 4.874E-02

Table 4.4 Moment Curvature Analysis Results for U2 Direction

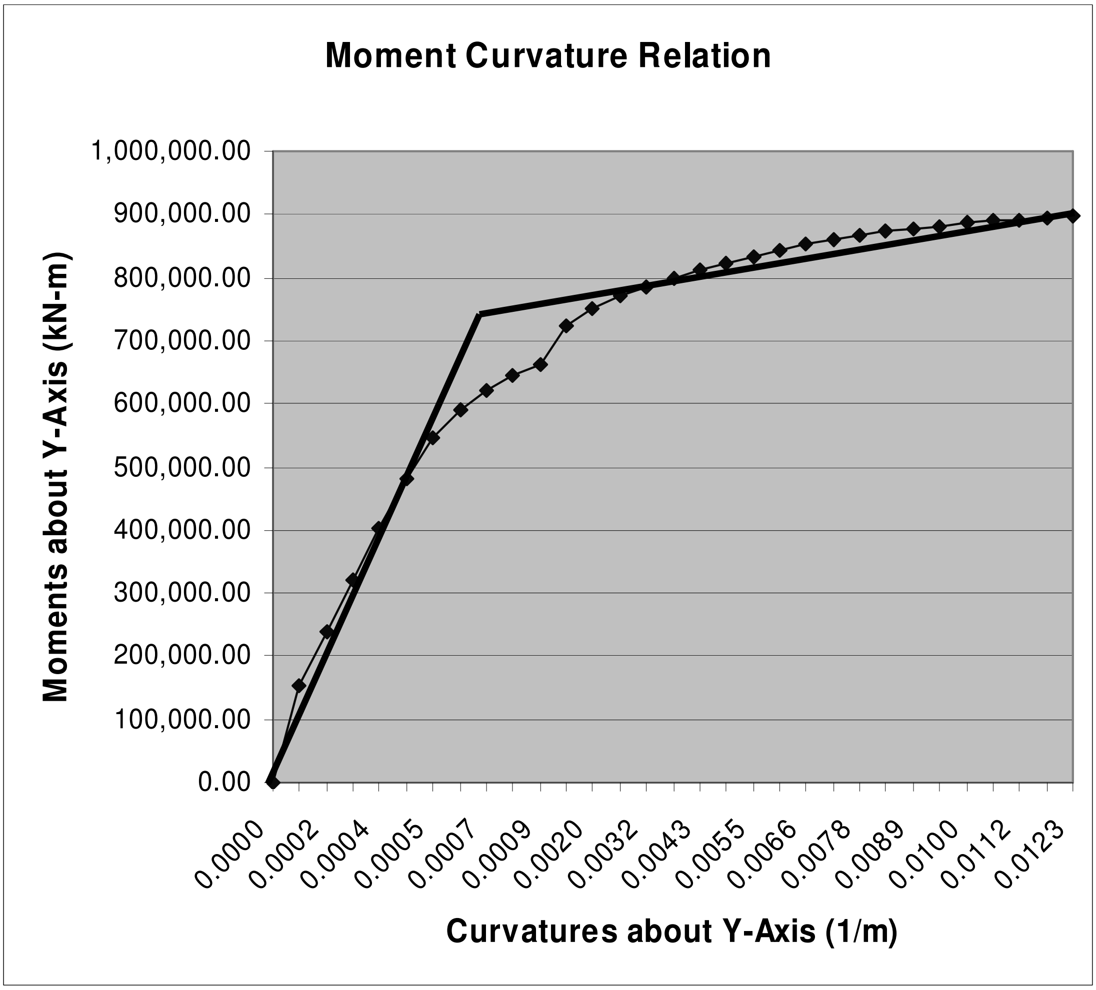

Figure 4.7 Moment Curvature Bilinearization for U2 Direction

	Moment	Rotation
Initial	0.00	0.000E+00
Yield	766,300.00	3.002E-03
Ultimate	896,500.00	5.174E-02

Table 4.5 Moment Hinge Coefficients for SAP2000 Model

4.2.6. Cracked Section Modification Factor

Using the data from section analysis, plastic moment hinges are defined for plastic hinge lengths of approximately 4 m. Also, cracked section modification factor is calculated as

$E = 25{,}907{,}000 \text{ kN/m}^2$
$I_{xx} = 71.4364 \text{ m}^4$
$I_{yy} = 226.976 \text{ m}^4$
$EI_{xx} = 0.0185E11 \text{ kN-m}^2$
$EI_{yy} = 0.0588E11 \text{ kN-m}^2$

From the section analysis (4.2.4 and 4.2.5) :
$EI_{xx \cdot effective} = 4.76E+11 \text{ N-m}^2$
$EI_{yy \cdot effective} = 10.7E+11 \text{ N-m}^2$

Modification $Factor_{yy} = EI_{yy} / EI_{yy\ effective} = 0.182$ for longitudinal direction,
Modification $Factor_{xx} = EI_{xx} / EI_{xx\ effective} = 0.257$ for transversal direction.

4.3. Superstructure

For the earthquake analysis of the bridges, it is common to use three-dimensional beam-column element (line element) to represent the behavior of the superstructure. The curvature in the alignment after pier 30 is reflected in the model. For the first 8 m of the pier the section is a little larger, and after 8 m the section shrinks from the inside. The foundation of the piers is modeled as a joint restrained in all six degrees of freedom.

Primary structural elements idealized as frame elements. Frame elements are placed at the geometric center of the elements they represent. Continuity is provided with rigid, fictitious elements connecting the structural elements. Beams and the cast-inplace deck are modeled as a single frame element with section properties calculated to represent the whole superstructure. Bending stiffness of columns is modified to take into account the cracked-section properties.

4.3.1. Piers

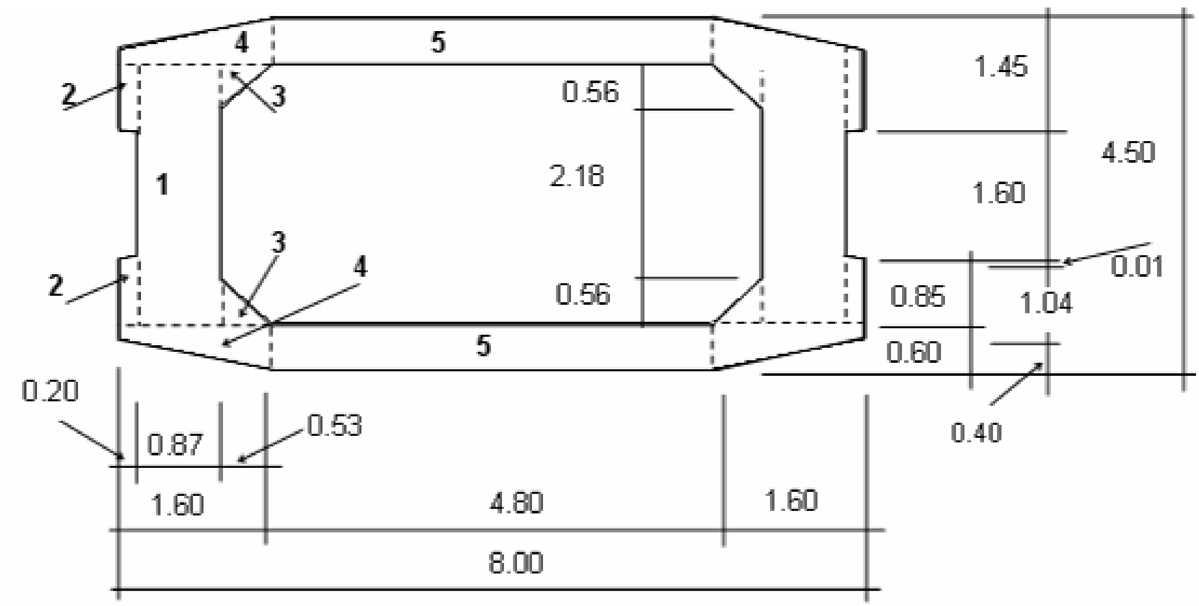

❶ ➔ 2 x [3.30 x 0.87] = 5.742 m²

❷ ➔ 4 x [0.85 x 0.20] = 0.680 m²

❸ ➔ 4 x [0.50 x 0.53 x 0.56] = 0.594 m²

❹ ➔ 4x [(0.20 +0.60) / 2 x 1.60] = 2.560 m²

❺ ➔ 2 x [0.60x4.80] = 5.760 m²

15.336 m² - 0.004 = **15.332 m².**

Figure 4.8 Pier elevation cross-section area for the first 8m height

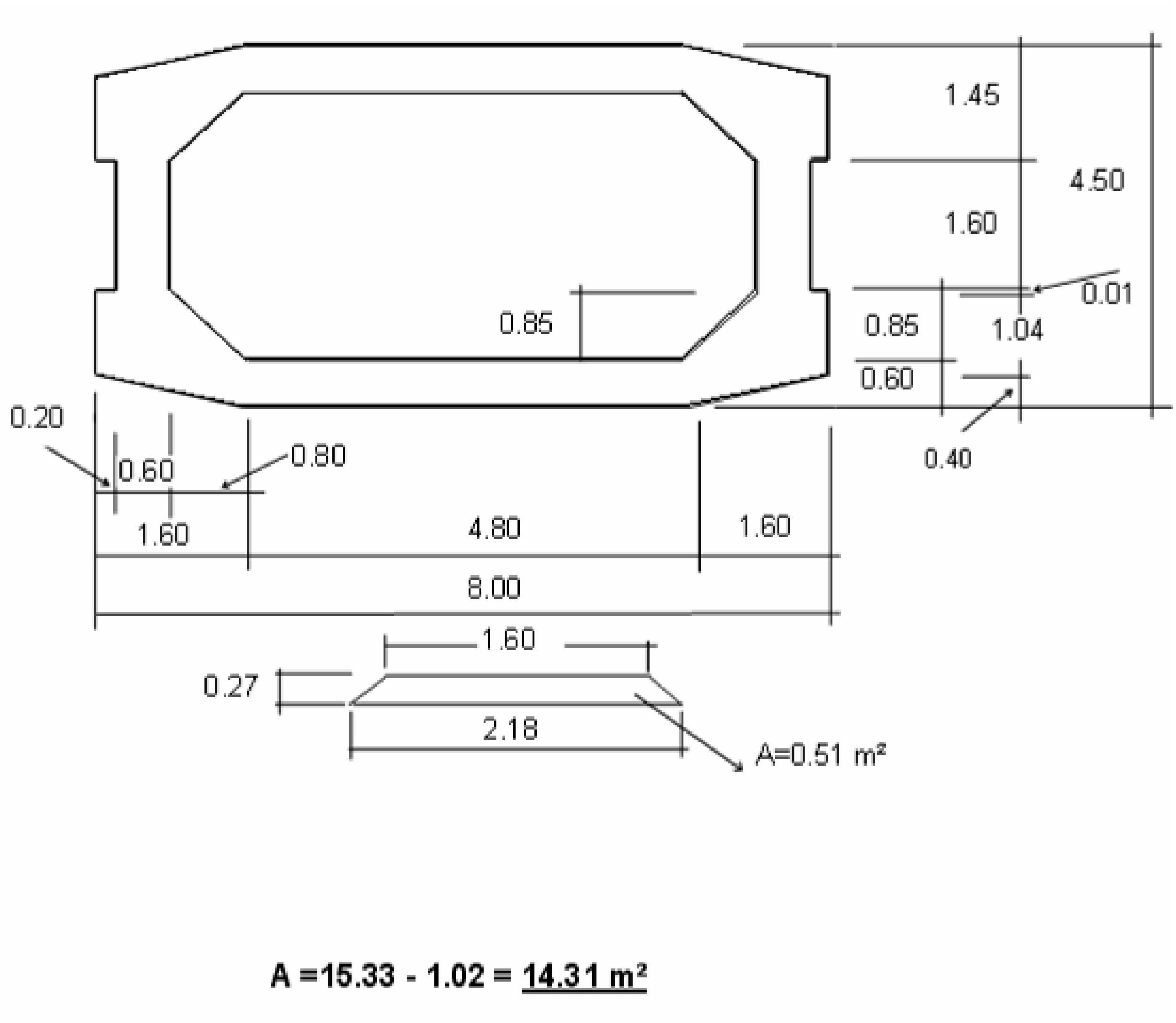

Figure 4.9 Pier elevation cross-section area after the first 8m height

4.3.2. Geometrical and Mathematical Modeling

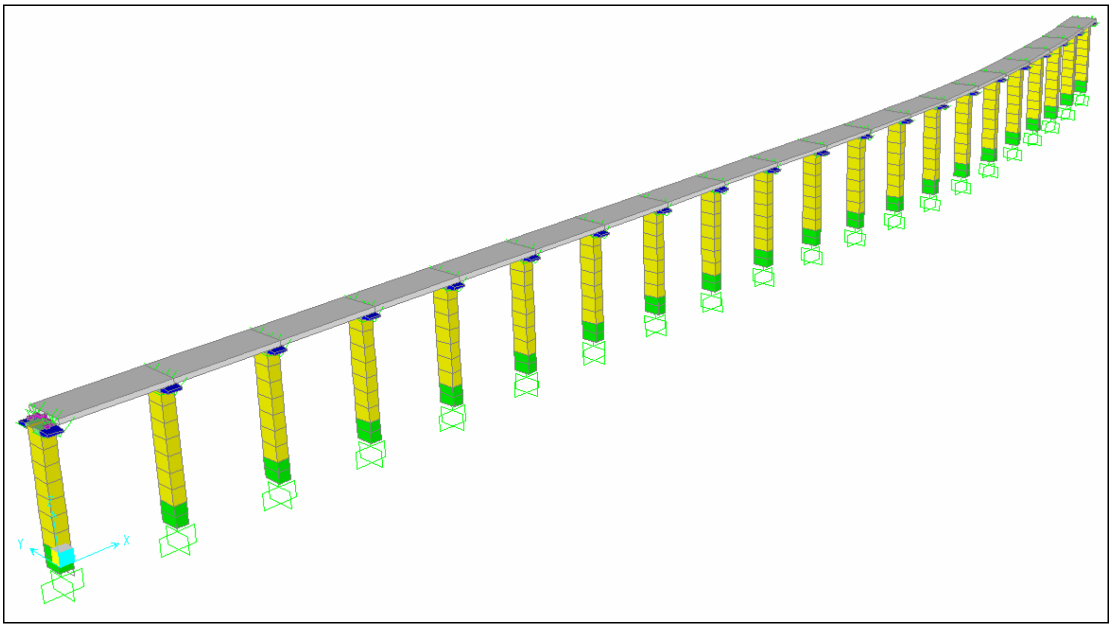

(a) General 3D View

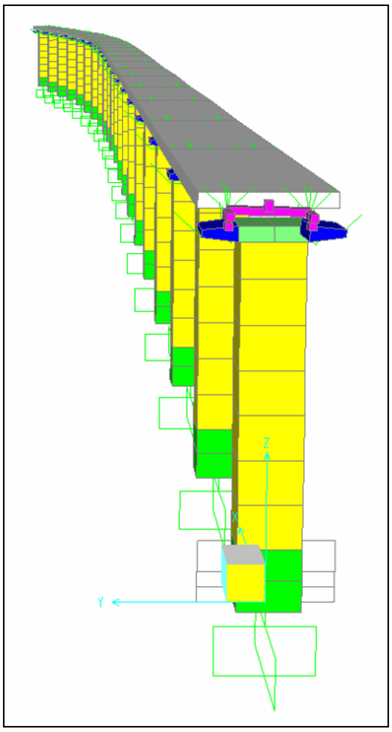

(b) Curvature and Elevation

Figure 4.10 SAP2000 Geometrical Model

To connect the basic elements of the pier and deck at center of masses; very stiff fictive elements are used. After the pier cap frame element a fictive element is used to connect the bearing and the FPB. Another fictive element connecting FPB's in transverse direction is used. The deck is modeled using a single frame element with corresponding stiffness and mass values. All the mass in the system is defined through mass properties of section properties in SAP 2000; no joint masses are defined.

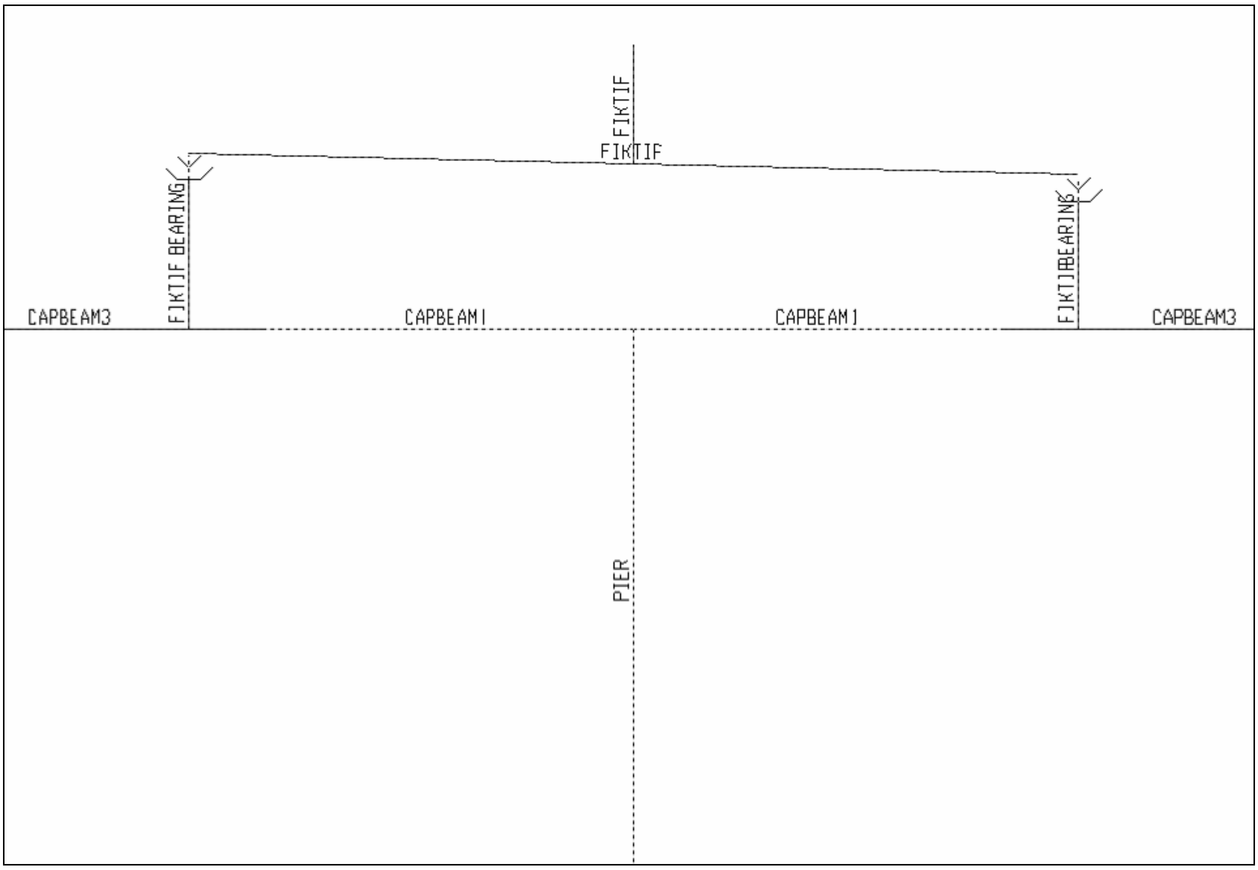

(a) Pier and Superstructure Connection

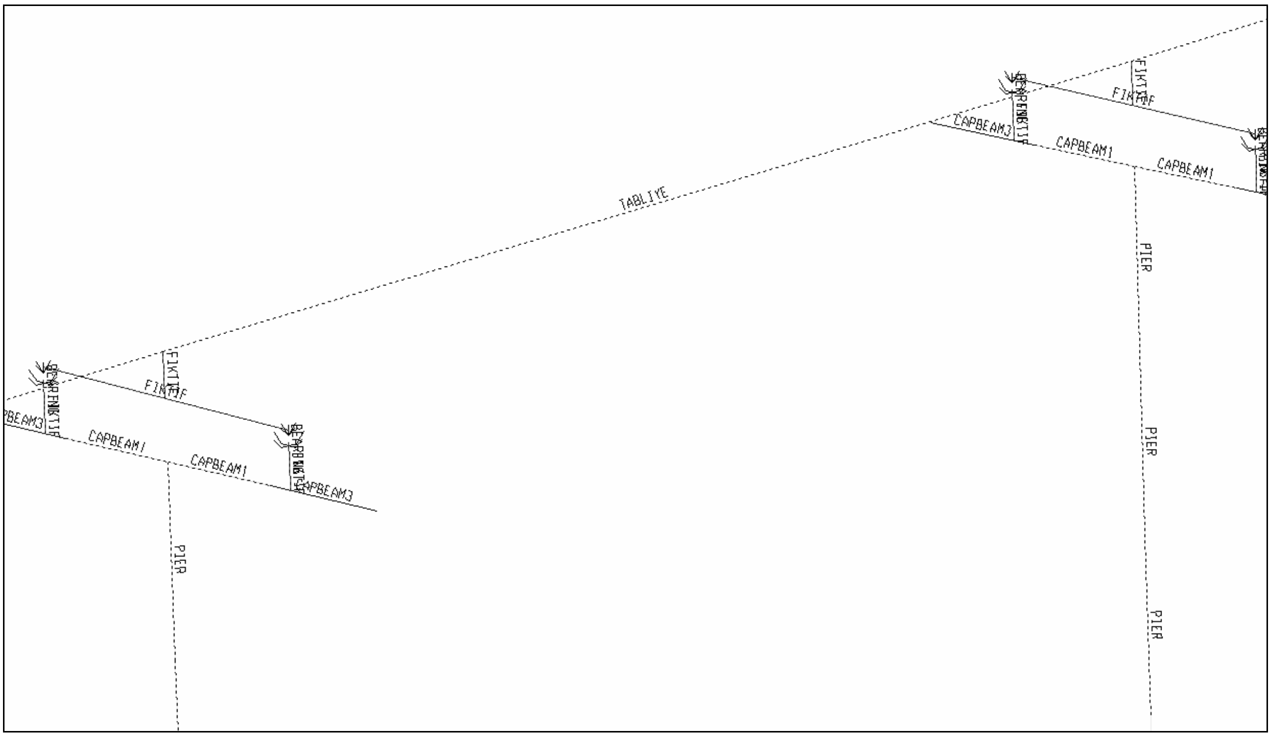

(b) Connection of Piers

Figure 4.11 SAP2000 Mathematical Model

4.3.3. Mass and Inertia Calculations

4.3.3.1. Beams

Pre-Stressed V Beams	:	7.0938 m² * 25.00 kN/m³ =	177.345	kN/m
Concrete Slab	:	(0.24 m * 17.50 m) * 25.00 kN/m³ =	105.000	kN/m
Asphalt	:	(0.06 m * 15.25 m) * 24.00 kN/m³ =	21.960	kN/m
Border	:	(0.30 m * 2.25 m) * 25.00 kN/m³ =	16.875	kN/m
			321.180	**kN/m**
Deck Section Area	:	7.0938 m² + (0.24 m * 17.50 m) =	11.29	m²
Deck Section Weight	:	(321.180 kN/m) / (11.29 m²) =	28.448	kN/m³

Table 4.6 Mass Calculations

• Single Beam

Area	A	:	1.0134	m^2
Moment of inertia	I_{xx}	:	0.3484	m^4
Moment of inertia	I_{yy}	:	0.3182	m^4
Center of mass	ΔX	:	0.895	M
Center of mass	ΔY	:	0.000	M

• For 7 beams

Area	A	:	7.0938	m^2
Moment of inertia	I_{xx}	:	2.4388	m^4
Moment of inertia	I_{yy}	:	180.6890	m^4
Center of mass	ΔX	:	0.895	M
Center of mass	ΔY	:	0.000	M

• Concrete Slab

Area	A	:	4.20	m^2
Moment of inertia	I_{xx}	:	0.0202	m^4
Moment of inertia	I_{yy}	:	107.1875	m^4
Center of mass	ΔX	:	1.920	M
Center of mass	ΔY	:	0.000	M

• The whole system

Area	A	:	11.29	m^2
Moment of inertia	I_{xx}	:	5.2577	m^4
Moment of inertia	I_{yy}	:	287.8765	m^4
Center of mass	ΔX	:	1.273	M
Center of mass	ΔY	:	0.000	M

Table 4.7 Moments of inertia calculations

4.3.3.2. Piers

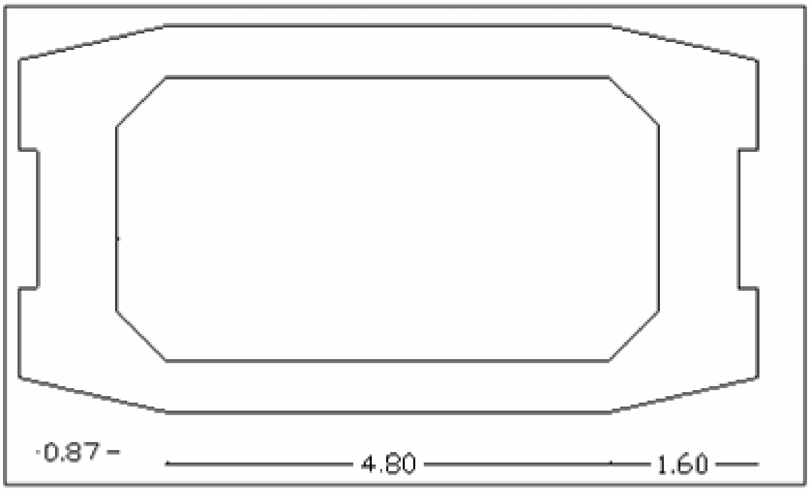

Area	A :	15.3349 m^2
Moment Of Inertia	I_{xx} :	71.1271 m^4
Moment Of Inertia	I_{yy} :	217.441 m^4
Radius of Gyration	x :	1.1605 m
Radius of Gyration	y :	2.029 m
Center of Mass	ΔX :	0.000 m
Center of Mass	ΔY :	0.000 m
Shear Area	x :	8.320 m^2
Shear Area	y :	6.990 m^2

Figure 4.12 Pier elevation moment of inertia for the first 8m height

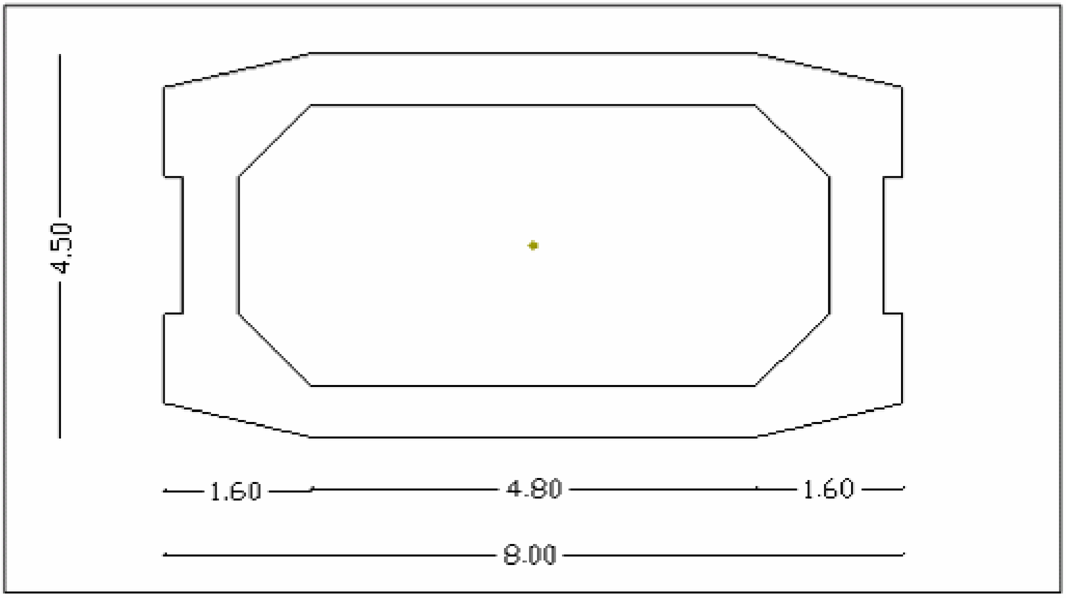

Area	A :	14.316	m^2
Moment Of Inertia	I_{xx} :	71.4364	m^4
Moment Of Inertia	I_{yy} :	226.976	m^4
Radius of Gyration	x :	1.1519	m
Radius of Gyration	y :	2.0533	m
Center of Mass	ΔX :	0.000	m
Center of Mass	ΔY :	0.000	m
Shear Area	x :	8.320	m^2
Shear Area	y :	4.740	m^2

Figure 4.13 Pier elevation moment of inertia after the first 8m height

4.3.4. Plastic Hinge Calculations

$$\ell_p = 0.08*\ell + 0.022*d_b*f_y$$

- d_b= 32 Mm
- f_y= 490 Mpa

ℓ (m)	ℓ_p (m)	$\ell_p/2$ (m)
46	4.00	2.00
47	4.10	2.05
48	4.20	2.10
49	4.30	2.15

Table 4.8 Plastic hinge location for different pier lengths

A plastic hinge by itself represents the force-deformation characteristics of the section it belongs to. When applied to the structural model, plastic hinges provide an insight into the nonlinear behavior of the system. Although plastic action can be defined for each degree of freedom of a particular element, only bending degrees of freedom are allowed plastic deformations in concrete moment frames. Shear, axial and torsion degrees of freedom are assumed to be elastic, since these degrees of freedom exhibit very little ductile behavior. It is common practice to assume that the plastic deformation is concentrated at a single point, namely the plastic hinge.

In the SAP2000 model moment hinges are appointed to the middle point of the plastic hinge zones. The reason moment hinges are used is there is always pressure axial forces at the piers and these forces remain at about the same level during the time history analyses. Plastic hinge properties are obtained from the moment-curvature analysis of the column section as described in 4.2.4 and 4.2.5.

4.4. Friction Pendulum Bearing (FPB) Modeling

4.4.1. General

Base isolation is a design technique for reducing the effects of earthquake motions on structures. This technique is becoming widely accepted. Sliding isolation systems utilize sliding interfaces (usually Teflon-steel interfaces) to support the weight of the structure. These interfaces provide little resistance to lateral loading by virtue of their low friction. Recentering capability is provided by a separate mechanism. One isolation system with spherical surface carries the name Friction Pendulum System (or FPS). In the Friction Pendulum System, the isolated structure is supported by bearings. Each bearing consists of an articulated slider on a spherical concave chrome surface. The slider is faced with a bearing material which, when in contact with the polished chrome surface, results in a maximum sliding friction coefficient of the order of 0.1 or less at high velocity of sliding and a minimum friction coefficient of the order of 0.05 or less at very slow velocity of sliding. This dependency of the coefficient of friction on velocity is a characteristic of Teflon type materials as described by Mokha et al, 1988 and 1990. The FPS bearing acts like a fuse which is activated only when the earthquake forces overcome the static value of friction. When set in motion, the bearing develops as a result of the induced rising of the structure along the spherical surface. This restoring force is proportional to the displacement and the weight carried by the bearing and is inversely proportional to the radius of curvature of the spherical surface.

a) Rigidity for forces up to the static value of coefficient of friction times the weight
b) Lateral force which is proportional to the weight carried by the bearing. As a result of this significant property the resultant lateral force develops at the center of mass, thus eliminating eccentricities. This property has been confirmed in shake table tests by Zayas et al, 1987
c) Period of vibration is the sliding mode which is independent of the mass of the structure and related only to the radius of curvature of the spherical surface.

In addition to above mentioned properties, the Friction Pendulum System has other properties common to sliding isolation systems, like low sensitivity to the other frequency content of excitation and high degree of stability (Mokha et al 1988, Constantinou et al 1990, Su et al 1989, Mostaghel and Khodaverdian 1987). [**Ref. 12**]

4.4.2. Nonlinear Modeling of FPB Elements

FPB is a biaxial friction-pendulum isolator that has coupled friction properties for the two shear deformations, post-slip stiffness in the shear directions due the pendulum radii of the slipping surfaces, gap behavior in the axial direction, and linear effective-stiffness properties for the three moment deformations. (See Figure 4.14)

This element can also be used to model gap and friction behavior between contacting surfaces.

The friction model is based on the hysteretic behavior proposed by Wen (1976), and Park, Wen and Ang (1986), and recommended for base-isolation analysis by Nagarajaiah, Reinhorn and Constantinou (1991). The pendulum behavior is as recommended by Zayas and Low (1990).

The friction forces and pendulum forces are directly proportional to the compressive axial force in the element. The element can not carry axial tension. The axial force, P, is always nonlinear, and is given by:

$$P \equiv f_{u1} = \begin{cases} \mathbf{k1}\ d_{u1} & \text{if } d_{u1} < 0 \\ 0 & \text{otherwise} \end{cases}$$

Stiffness **k1** must be positive in order to generate nonlinear shear force in the element. For each shear deformation degree of freedom you may independently specify either linear or nonlinear behavior:

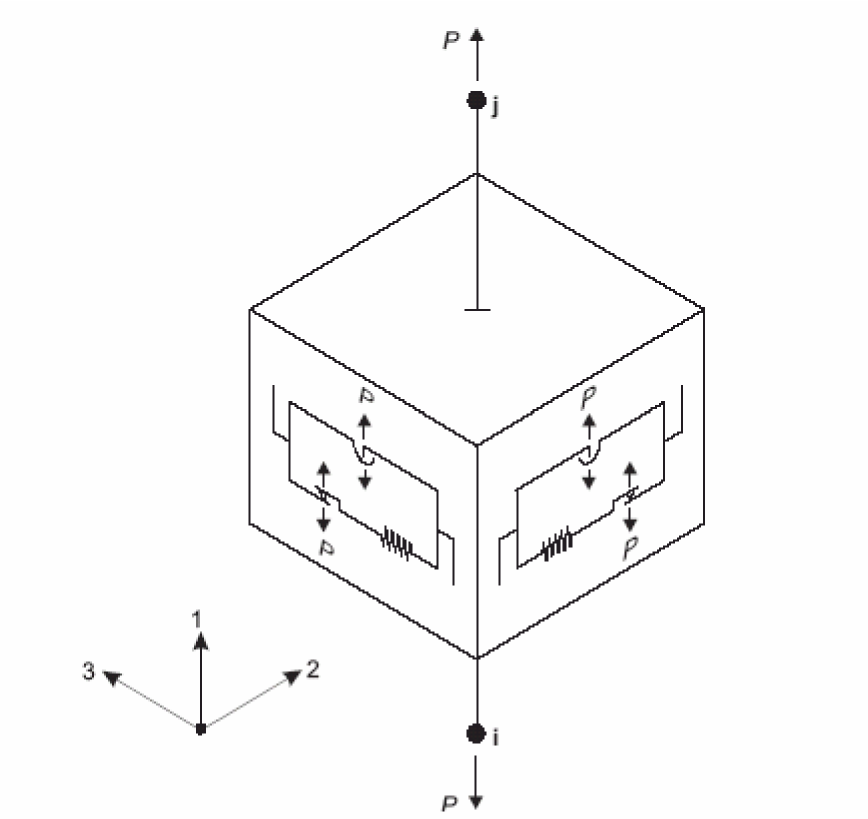

Figure 4.14 Friction-Pendulum Isolator Property for Biaxial Shear Behavior

• If both shear degrees of freedom are nonlinear, the friction and pendulum effects for each shear deformation act in parallel:

$$f_{u2} = f_{u2f} + f_{u2p}$$
$$f_{u3} = f_{u3f} + f_{u3p}$$

The frictional force-deformation relationships are given by:

$$f_{u2f} = -P\,\mu_2\, z_2$$
$$f_{u3f} = -P\,\mu_3\, z_3$$

where μ_2 and μ_3 are friction coefficients, and z_2 and z_3 are internal hysteretic variables. The friction coefficients are velocity-dependent according to:

$$\mu_2 = \mathbf{fast2} - (\mathbf{fast2} - \mathbf{slow2})\, e^{-r v}$$
$$\mu_3 = \mathbf{fast3} - (\mathbf{fast3} - \mathbf{slow3})\, e^{-r v}$$

where **slow2** and **slow3** are the friction coefficients at zero velocity, **fast2** and **fast3** are the friction coefficients at fast velocities, *v* is the resultant velocity of sliding:

$$v = \sqrt{\dot{d}_{u2}^{\ 2} + \dot{d}_{u3}^{\ 2}}$$

r is an effective inverse velocity given by:

$$r = \frac{\mathbf{rate2}\ \dot{d}_{u2}^{\ 2} + \mathbf{rate3}\ \dot{d}_{u3}^{\ 2}}{v^2}$$

and **rate2** and **rate3** are the inverses of characteristic sliding velocities. For a Teflon-steel interface the coefficient of friction normally increases with sliding velocity (Nagarajaiah, Reinhorn, and Constantinou, 1991).

The internal hysteretic variables have a range $\sqrt{z_2^2 + z_3^2} \leq 1$, with the yield surface represented by $\sqrt{z_2^2 + z_3^2} = 1$. The initial values of z_2 and z_3 are zero, and they evolve according to the differential equations:

$$\begin{Bmatrix} \dot{z}_2 \\ \dot{z}_3 \end{Bmatrix} = \begin{bmatrix} 1 - a_2\ z_2^{\ 2} & -a_3\ z_2\ z_3 \\ -a_2\ z_2\ z_3 & 1 - a_3\ z_3^{\ 2} \end{bmatrix} \begin{Bmatrix} \dfrac{\mathbf{k2}}{P\,\mu_2}\ \dot{d}_{u2} \\ \dfrac{\mathbf{k3}}{P\,\mu_3}\ \dot{d}_{u3} \end{Bmatrix}$$

where **k2** and **k3** are the elastic shear stiffnesses of the slider in the absence of sliding, and

$$a_2 = \begin{cases} 1 & \text{if } \dot{d}_{u2}\ z_2 > 0 \\ 0 & \text{otherwise} \end{cases}$$

$$a_3 = \begin{cases} 1 & \text{if } \dot{d}_{u3}\ z_3 > 0 \\ 0 & \text{otherwise} \end{cases}$$

These equations are equivalent to those of Park, Wen and Ang (1986) with A=1 and $\beta = \gamma = 0.5$.

This friction model permits some sliding at all non-zero levels of shear force; the amount of sliding becomes much larger as the shear force approaches the “yield” value of P μ. Sliding at lower values of shear force can be minimized by using larger values of the elastic shear stiffnesses.

The pendulum force-deformation relationships are given by:

$$f_{u2p} = -P \frac{d_{u2}}{\mathbf{radius2}}$$
$$f_{u3p} = -P \frac{d_{u3}}{\mathbf{radius3}}$$

A zero radius indicates a flat surface, and the corresponding shear force is zero. Normally the radii in the two shear directions will be equal (spherical surface), or one radius will be zero (cylindrical surface). However, it is permitted to specify unequal non-zero radii.

• If only one shear degree of freedom is nonlinear, the above frictional equations reduce to:

$$f_f = -P\, \mu\, z$$
$$\mu = \mathbf{fast} - (\mathbf{fast} - \mathbf{slow})\, e^{-\mathbf{rate}\, \dot{d}}$$
$$\dot{z} = \frac{\mathbf{k}}{P\,\mu} \begin{cases} \dot{d}\,(1 - z^2) & \text{if } \dot{d}\, z > 0 \\ \dot{d} & \text{otherwise} \end{cases}$$

The above pendulum equation is unchanged for the nonlinear degree of freedom.

A linear spring relationship applies to the three moment deformations, and to any shear deformation without nonlinear properties. All linear degrees of freedom use the corresponding effective stiffness, which may be zero. The axial degree of freedom is always nonlinear for nonlinear analyses. [**Ref. 6**]

4.4.3. Mechanical Characteristics of Friction Pendulum System

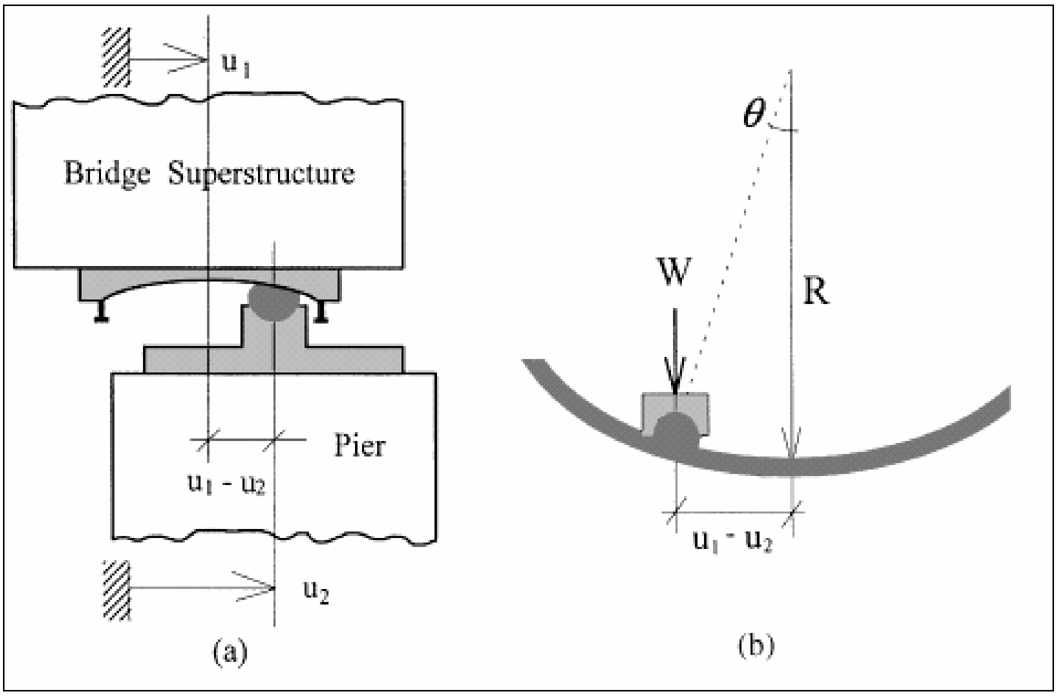

Figure 4.15 FPB illustrative diagram

The load on an FPB isolator is W, the horizontal displacement is D, and the friction coefficient is μ, then the resisting force F is given by

$$F = \frac{W}{R} D + \mu W (\operatorname{sgn} \dot{D})$$

Where R is the radius of curvature of the dish. The first term is the restoring force due to rise of the mass, providing a horizontal stiffness

$$K_H = \frac{W}{R}$$

Which produces an isolated structure period T given by

$$T = 2\pi \sqrt{R/g}$$

Which is independent of the carried mass. [**Ref. 7**]

4.4.4. Model

There are two types of FPB's in Viaduct #1,

- Type L : At expansion joints, with a displacement capacity of 900 mm,
- Type K : At the rest of the piers, with a displacement capacity of 700 mm.

One of the important parameter affecting the behavior of the model is the stiffness values of the FPB's, and calculated from the formula:

$$K_h = \frac{W}{R}$$

- Where K_h is the horizontal stiffness value, R is the radius of the curvature for the FPB, and W is the load on an FPB isolator. Stiffness value is calculated:
  6500kN / 6.2 m = 1049 kN/m.
- For friction coefficient values, contact with the technical manager of the producer of the bearings Mr. Mokha has been established and due to his advices taken as :
  0.04 for slow ,
  0.05 for fast.
  Which results in a yield force = μ*W = 260 kN
- And rate parameter is assumed 35.43.

Each type of isolator device has been simulated by means of a non-linear link placed between the superstructure and the piers.

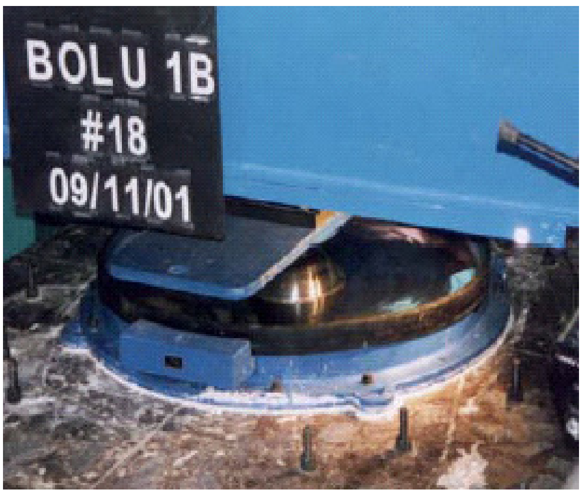

Figure 4.16 Friction Pendulum Isolation Bearings

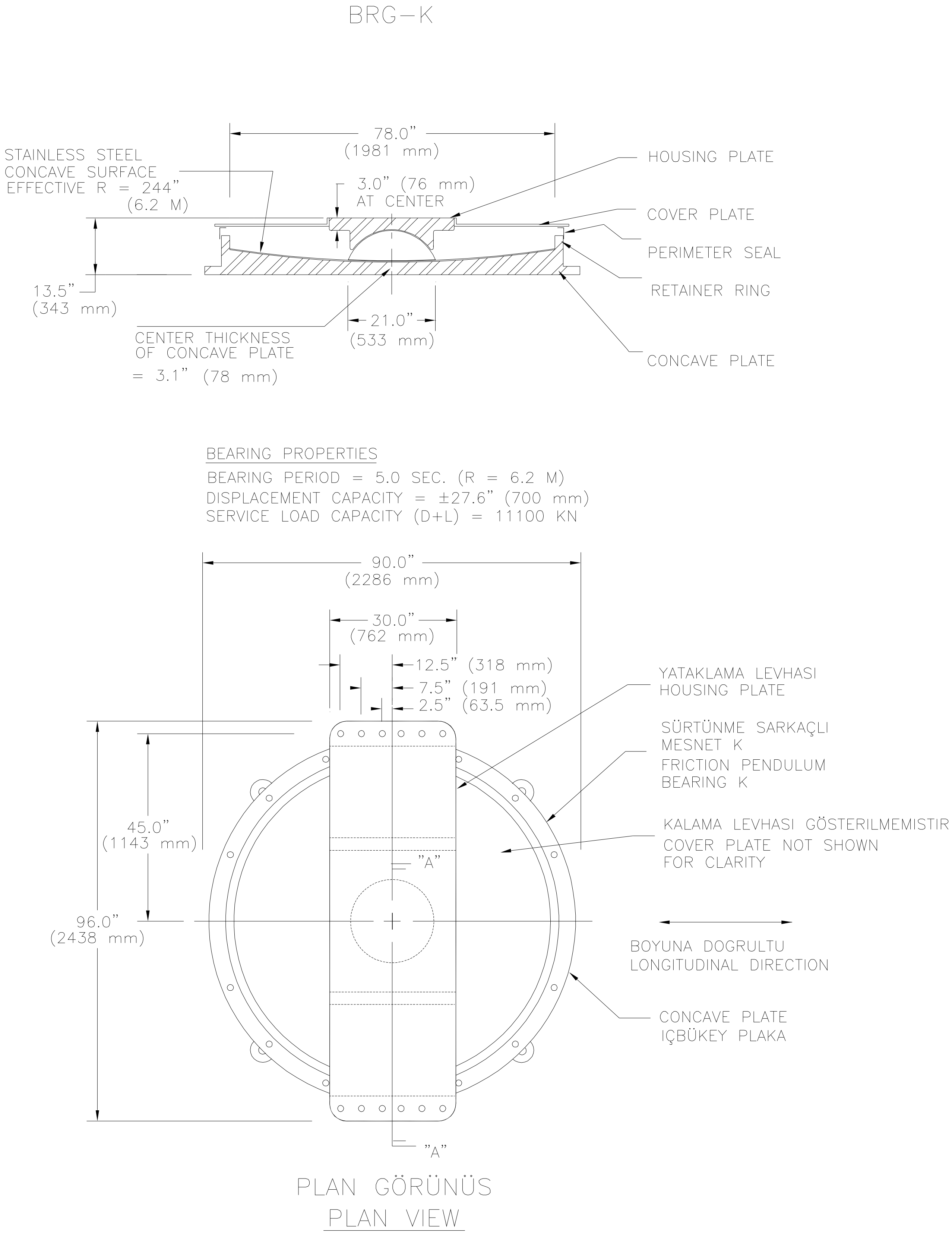

Figure 4.17 Friction Pendulum Bearing – Type K

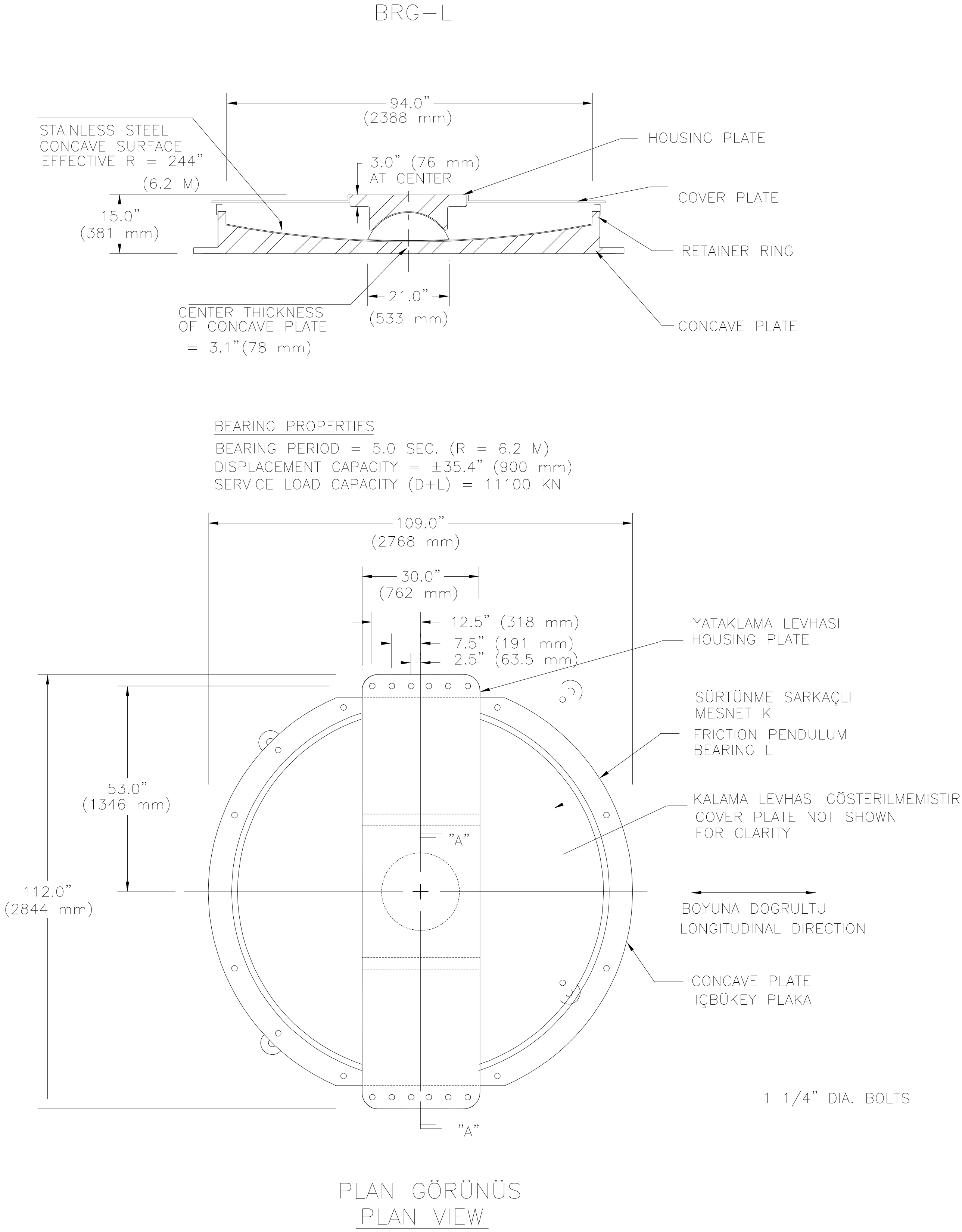

Figure 4.18 Friction Pendulum Bearing – Type L

4.5. Damping

Rayleigh Damping is assumed in the both models; using the data from the modal analysis, with the contribution of 25 modes calculated by Ritz Vectors in both transversal and longitudinal direction :

- For the isolated system model; modes 1 and 2 in the longitudinal direction; modes 2 and 6 in the transversal direction are selected with 0.01 damping due to modal participating mass ratios and mode shapes. The reason 0.01 damping is selected is that the friction pendulum bearings are dominant in the modal shape of the bridge with high participating mass ratios and the own mechanism of the FPB's would characterize the damping of the bridge.

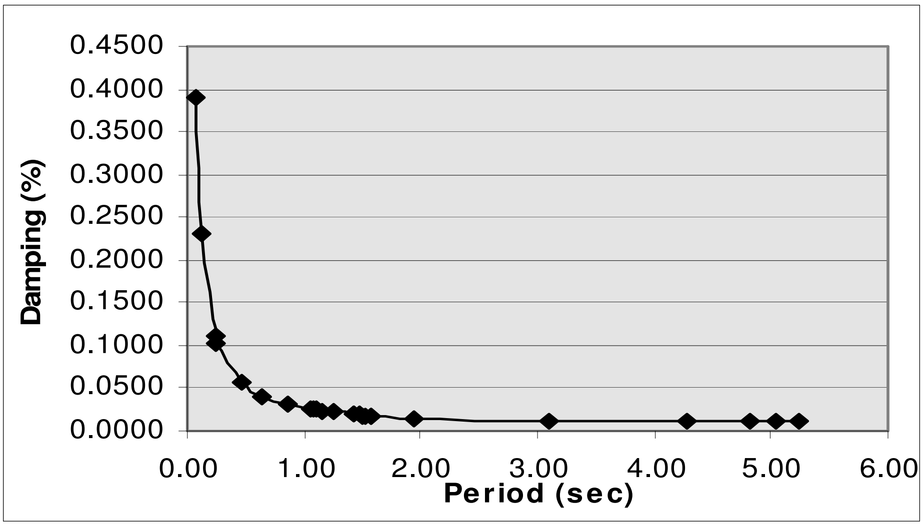

a) Longitidunal Direction

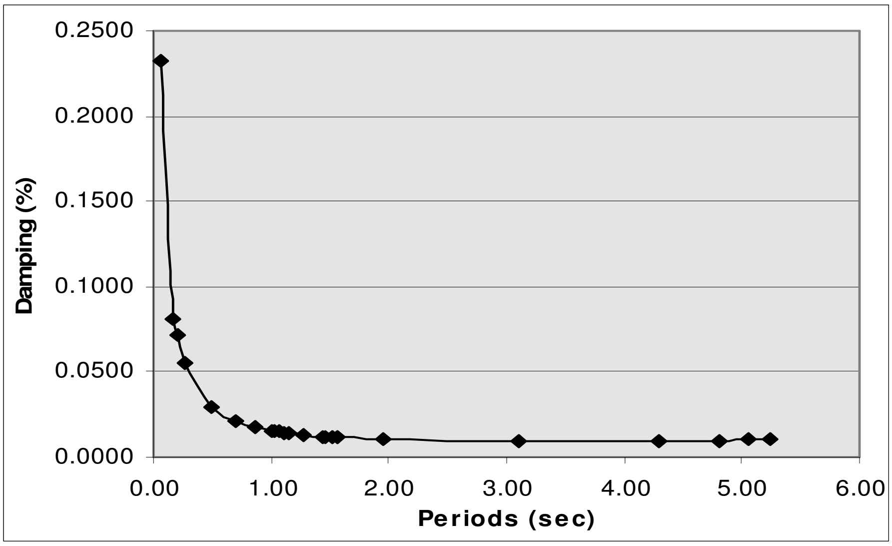

b) Transversal Direction

Figure 4.19 Rayleigh damping characteristics for the isolated system

- For the Unisolated system model; modes 1 and 18 in the longitudinal direction; modes 2 and 20 in the transversal direction are selected with 0.05 damping due to modal participating mass ratios and mode shapes.

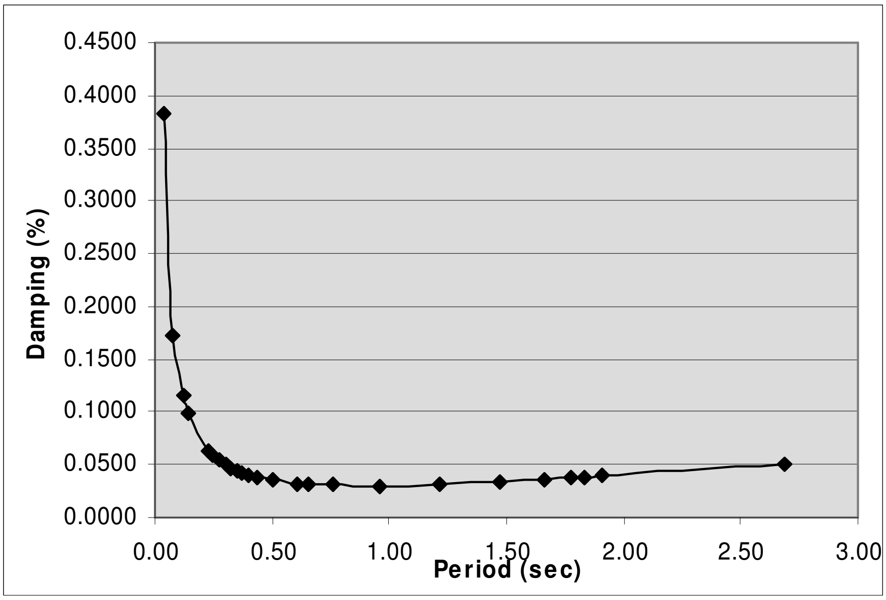

a) Longitidunal Direction

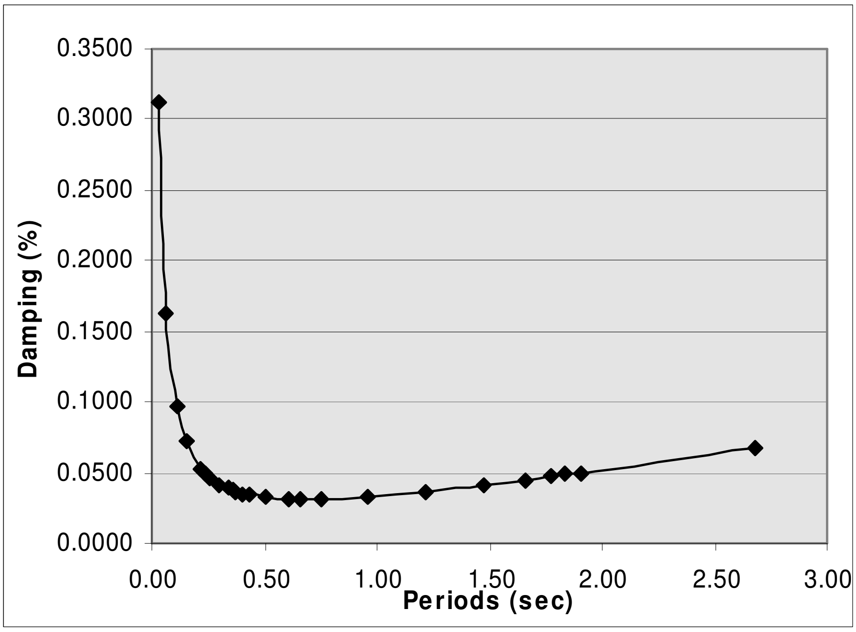

b) Transversal Direction

Figure 4.20 Rayleigh damping characteristics for the isolated system

5. ANALYSIS

5.1. Analysis Objectives

A dead load case, temperature change analysis, a modal analysis and time history analyses for 7 different cases in longitudinal and transversal directions have been carried out. For all cases two types of model is constructed one of which is isolated as the structure itself.

Another model which is named as “Unisolated System Model” in this thesis is created by holding the FPB isolators in three translational degrees of freedom but letting free in rotational degrees of freedom to see the response of the structure as if the bridge was not isolated with FPB devices, behaving “un-isolated”.

5.2. Analysis Cases

5.2.1. Dead Load Analysis

A dead load analysis is essential to determine the parameters for friction pendulum model and preliminary calculations. The axial load at the base of piers are around 32000-33000 kN while the load over the FPB's are around 6500 kN which matches the hand calculations.

5.2.2. Modal Analysis

A modal analysis was carried out to understand the dynamic behavior of the structural system and to determine the parameters required for defining Rayleigh Damping in the time history analyses.

Modal superposition is an elastic dynamic analysis approach that relies on the assumption that the dynamic response of a structure may be found by considering the independent response of each natural mode of vibration and then combining the responses in some way. Its advantage lies in the fact that generally only a few of the lowest modes of vibration have significance when calculating moments, shears, and deflections at different levels of the building. In its purest form, the response to a given accelerograms in each significant mode of vibration is calculated as a time history of forces and displacements. [**Ref. 5**]

5.2.3. Time History Analysis

Although it takes much time and much effort, the nonlinear time history analysis is the most feasible way for determining the seismic demands that provides more insight about the bridge behavior. But anyway, the bridge behavior under seismic attack should be understood well and a preliminary elastic analysis may be useful to have an idea about the seismic behavior to have a healthy comments on the results. Another but a major problem is the selection of the appropriate accelerograms for nonlinear time history analyses, which are affected by the source mechanism, travel path geology and the local soil conditions. This problem becomes more complicated if a scaling procedure is necessary since there is not an agreement on this subject (Elnashai-McClure, etc). Since there are very recent and strong near-fault records that would reflect the characteristics of the seismic behaviour of the area, no scaling has been done to the strong ground motion data for the analyses.

5.2.3.1. Selection of Motions for Time History Analysis

The Duzce and Kocaeli earthquakes imposed great permanent relative displacement demands, due to fault slip, in excess of 1 m. Another point is a very active fault line is crossing the alignment of the bridge. So, mainly near-fault ground motions records with large spectral displacements and high peak ground accelerations are selected. In order to have a comparison of results, the ground motion records used in the Preliminary Retrofit Report of Calvi and Priestley are noted.

In the Preliminary Report of Calvi and Priestley the records of Kobe JMA, Shin Kobe, Bolu, Fukiai, Motoyoma, Bonds Corner, Corralitos earthquakes are used for the retrofit design of the Viaduct 1. The characteristic properties of the design record are :

- Design peak ground acceleration (PGA) 0.81g
- Design peak spectral acceleration (%5 damping) 1.8-2.0g
- Design peak spectral displacement (%5 damping) 600 mm
- Consideration of near field directivity effects.
- The magnitude of the earthquake should be of the order 7-7.2, consistent with the characteristic earthquake on the Duzce fault
- The earthquake fault rupture should be strike slip;
- The recording site should be located with respect to the epicenter in such a way that the angle between the fault and the line connecting the epicenter and location is clockwise and small.

[**Ref. 8**]

Under the scope of these criteria, most significant records from the retrofit design and two additions, Duzce and Kocaeli records are used for the analysis of the Viaduct 1. Within 5 different earthquakes and 10 component records, 7 components are applied in orthogonal directions resulting as 14 set of time history analyses. A comparison to the Turkish Design code is shown in Figure 5.15 Acceleration response spectra

5.2.3.2. The Strong Ground Motion Data

Mostly near-field and large scale records are chosen to verify the limits of the capacities of the Viaduct#1

#	Earthquake Name	Analysis Case Name	EQ Data Component	Time Interval used in Analysis (s)	# of Points	Time Step (s)	PGA (g)	PGV (cm/s)	PGD (cm)
1	**Imperial Valley**	BONDS-U2	H-BCR140	0-22	4401	0.005	0.588	45.2	16.78
		BONDS-U1	H-BCR230	0-22			0.775	45.9	14.89
2	**Duzce**	DUZCE-BOLU-U2	BOL000	5-24	1901	0.010	0.728	56.4	23.07
		DUZCE-BOLU-U1	BOL090	5-24			0.822	62.1	13.55
3	**Duzce**	DUZCE-DZC-U2	DZC180	0-16	3201	0.005	0.348	60	42.09
		DUZCE-DZC-U1	DZC270	0-16			0.535	83.5	51.59
4	**Kobe**	KOBE-U2	TAZ000	0-18	1801	0.010	0.693	68.3	26.65
		KOBE-U1	TAZ090	0-18			0.694	85.3	16.75
5	**Kocaeli**	KOCAELI-U2	YTP060	6-24	3601	0.005	0.268	65.7	57.01
		KOCAELI-U1	YTP330	6-24			0.349	62.1	50.97

Table 5.1 Strong ground motion data

Imperial Valley 1979/10/15 23:16 Magnitude: M (6.5) Ml (6.6) Ms (6.9)	**Station: 5054 Bonds Corner** Data Source: USGS
Distance (km): Closest to fault rupture (2.5) Hypocentral ( ) Closest to surface projection of rupture (2.6)	Site conditions: Geomatrix or CWB (D) USGS (C)

Duzce, Turkey 1999/11/12 Magnitude: M (7.1) Ml (7.2) Ms (7.3)	**Station: Bolu** Data Source: ERD
Distance (km): Closest to fault rupture (17.6) Hypocentral ( ) Closest to surface projection of rupture (17.6)	Site conditions: Geomatrix or CWB (D) USGS (C)

Duzce, Turkey 1999/11/12 Magnitude: M (7.1) Ml (7.2) Ms (7.3)	**Station: Duzce** Data Source: ERD
Distance (km): Closest to fault rupture (8.2) Hypocentral ( ) Closest to surface projection of rupture (8.2)	Site conditions: Geomatrix or CWB (D) USGS (C)

Kobe 1995/01/16 20:46 Magnitude: M (6.9) Ml ( ) Ms ( )	**Station: 0 Takarazuka** Data Source: CUE
Distance (km): Closest to fault rupture (1.2) Hypocentral ( ) Closest to surface projection of rupture ( )	Site conditions: Geomatrix or CWB (E) USGS (D)

Kocaeli, Turkey 1999/08/17 Magnitude: M (7.4) Ml ( ) Ms (7.8)	**Station: Yarimca** Data Source: KOERI
Distance (km): Closest to fault rupture (2.6) Hypocentral ( ) Closest to surface projection of rupture (2.6)	Site conditions: Geomatrix or CWB (D) USGS (C)

Table 5.2 Strong ground motion data by station details

Graphs of Each EQ Data

Imperial Valley 1979/10/15 23:16	Station: 5054 Bonds Corner
BONDS-U1	IMPVALL/H-BCR230

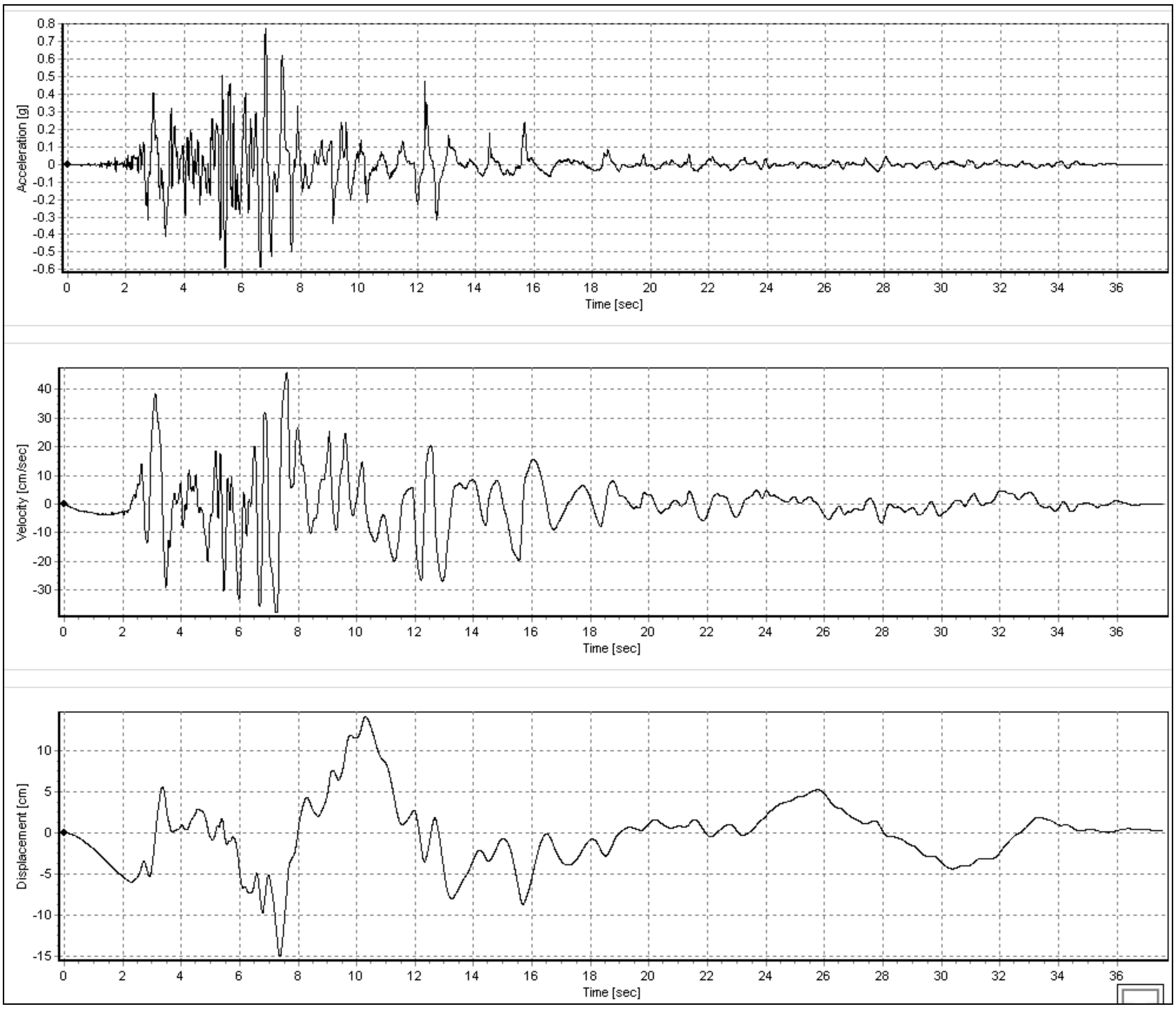

Figure 5.1 H-BCR230 record - acceleration, velocity and displacement time history graphs

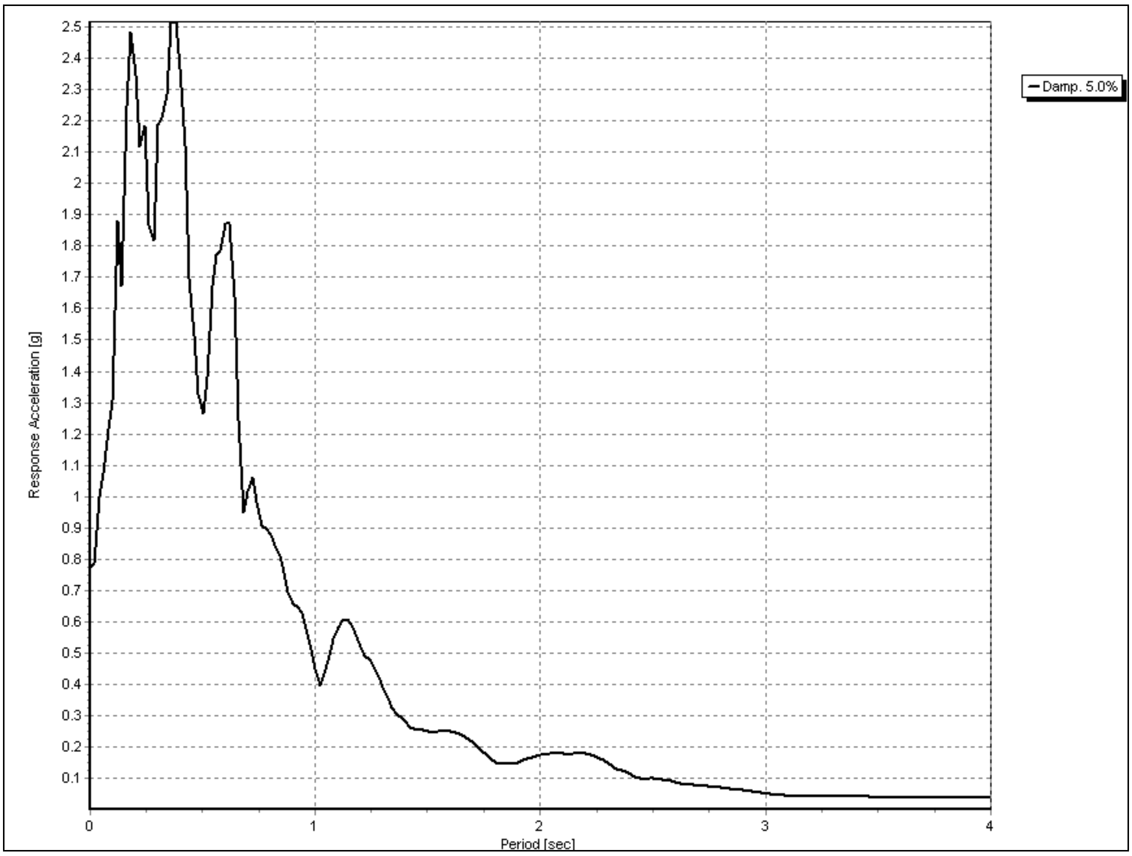

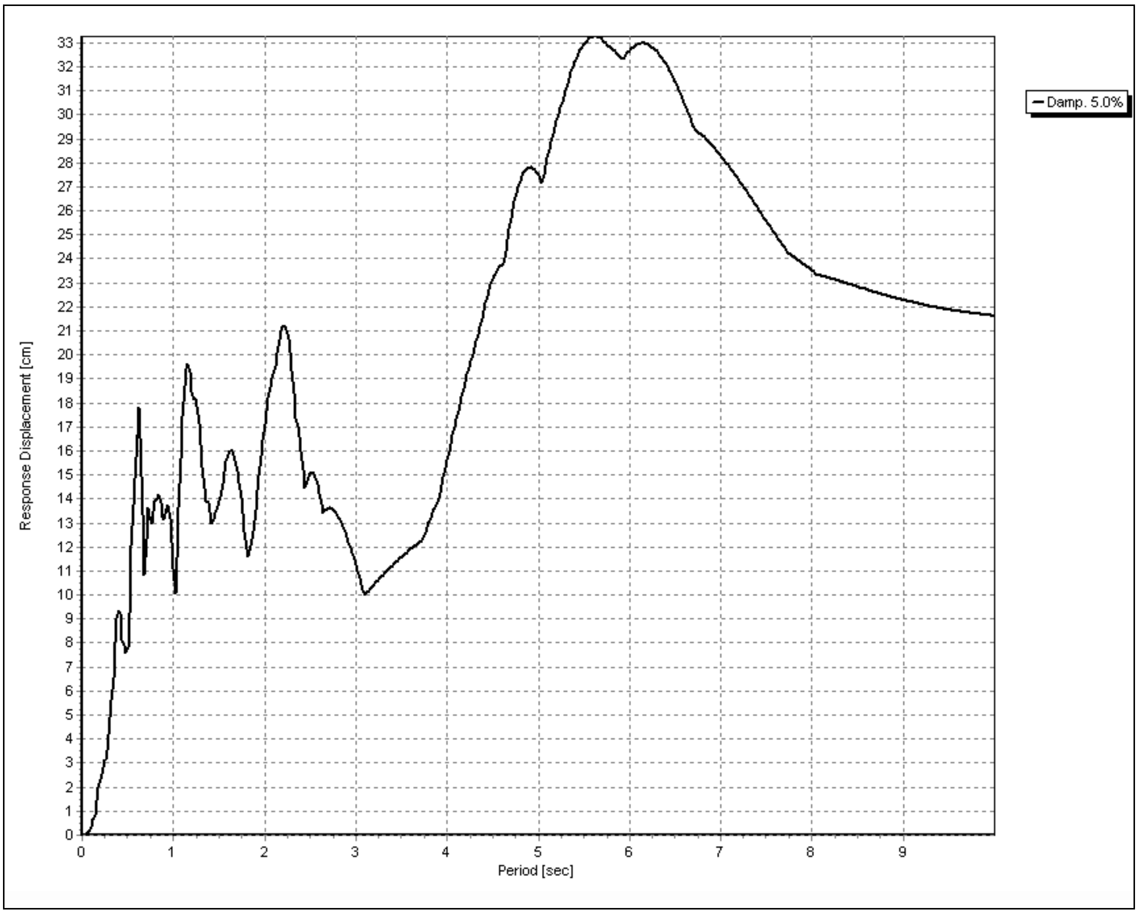

Figure 5.2 H-BCR230 record - response and displacement spectrum graphs

Duzce, Turkey 1999/11/12	**Station: Bolu**
DUZCE-BOLU-U1	DUZCE/BOL090

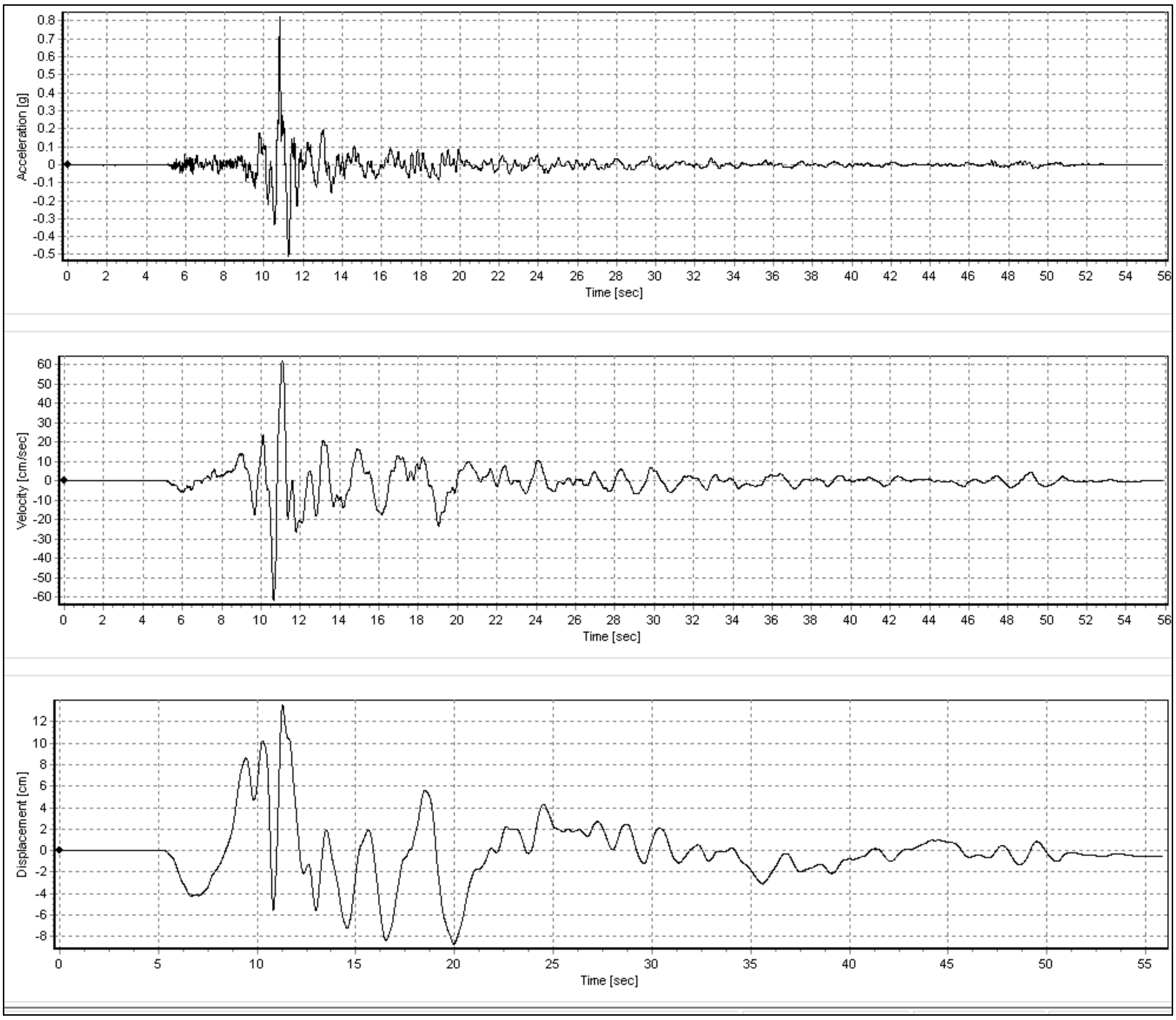

Figure 5.3 BOL090 record - acceleration, velocity and displacement time history graphs

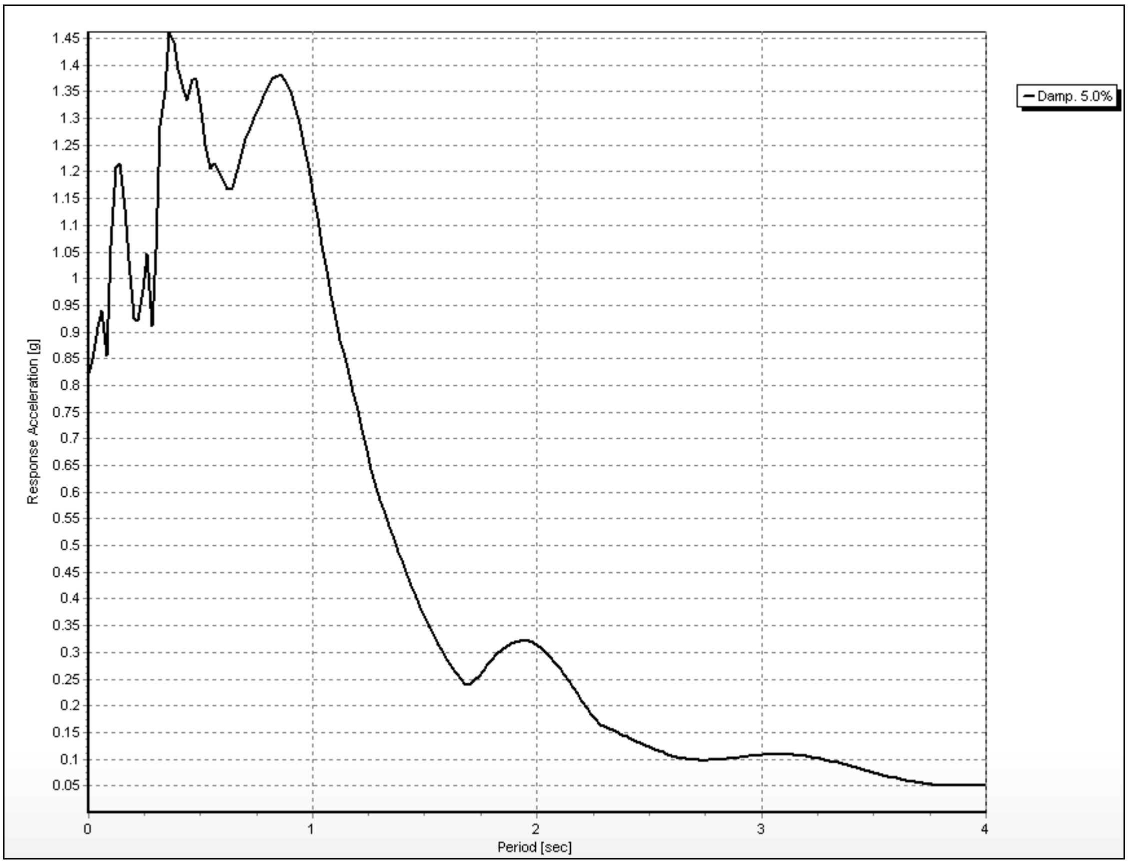

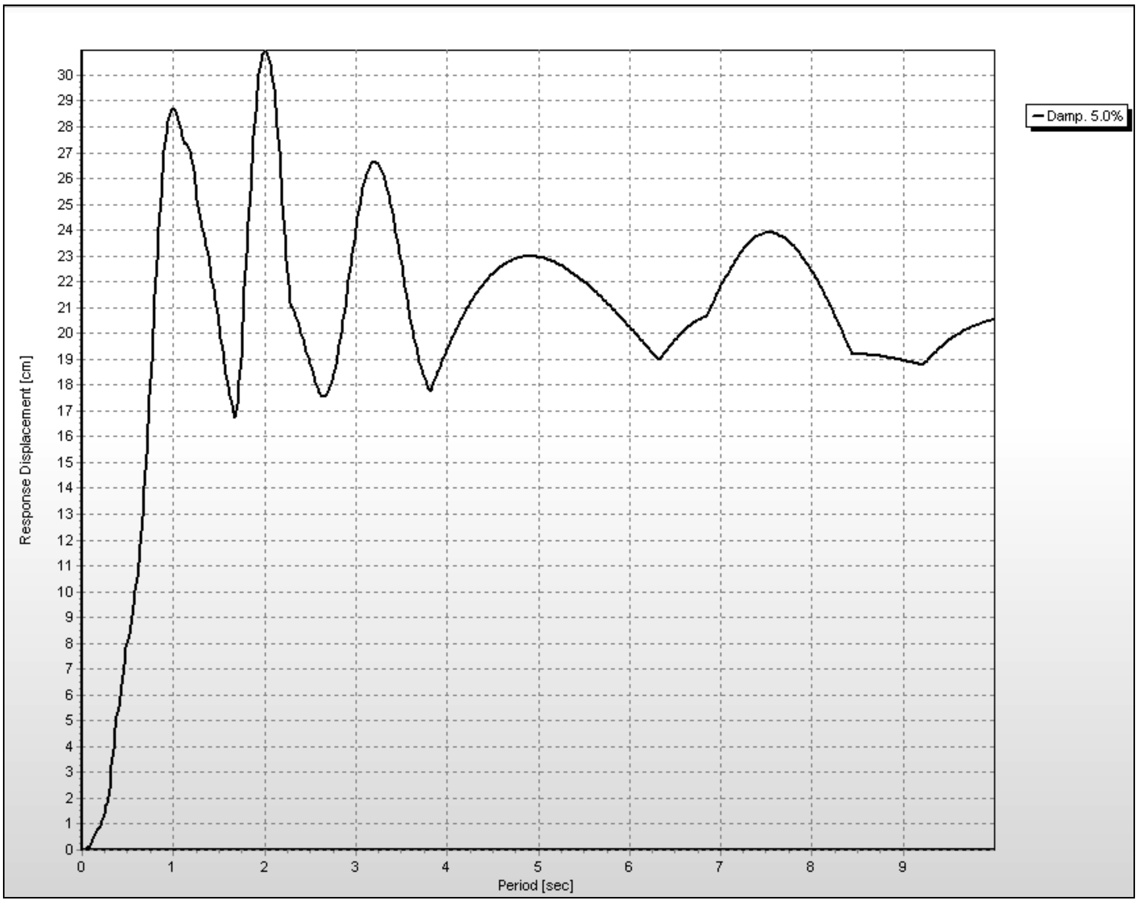

Figure 5.4 BOL090 record - response and displacement spectrum graphs

Duzce, Turkey 1999/11/12 DUZCE-DZC-U1	Station: Duzce DUZCE/DZC270

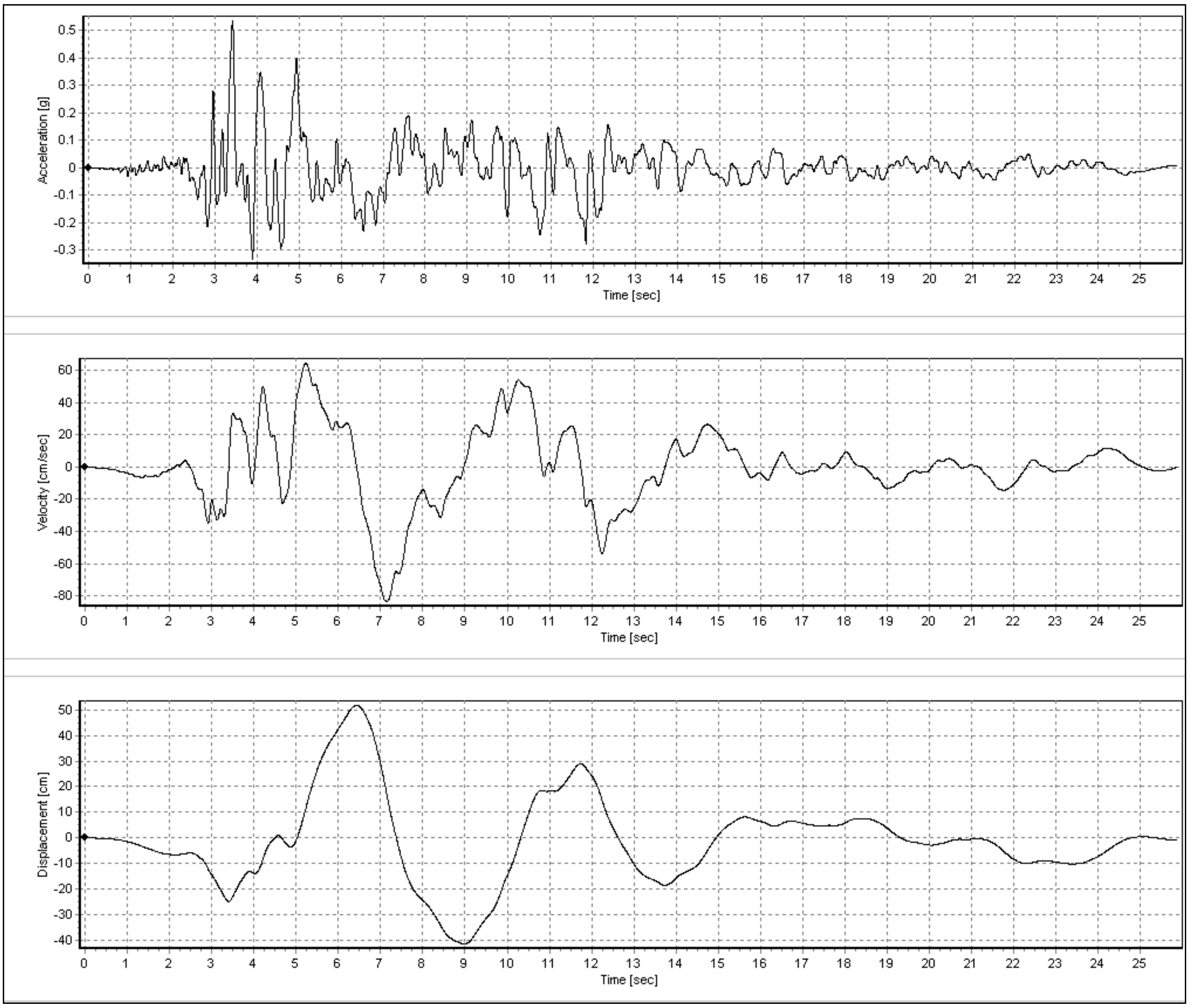

Figure 5.5 DZC270 record - acceleration, velocity and displacement time history graphs

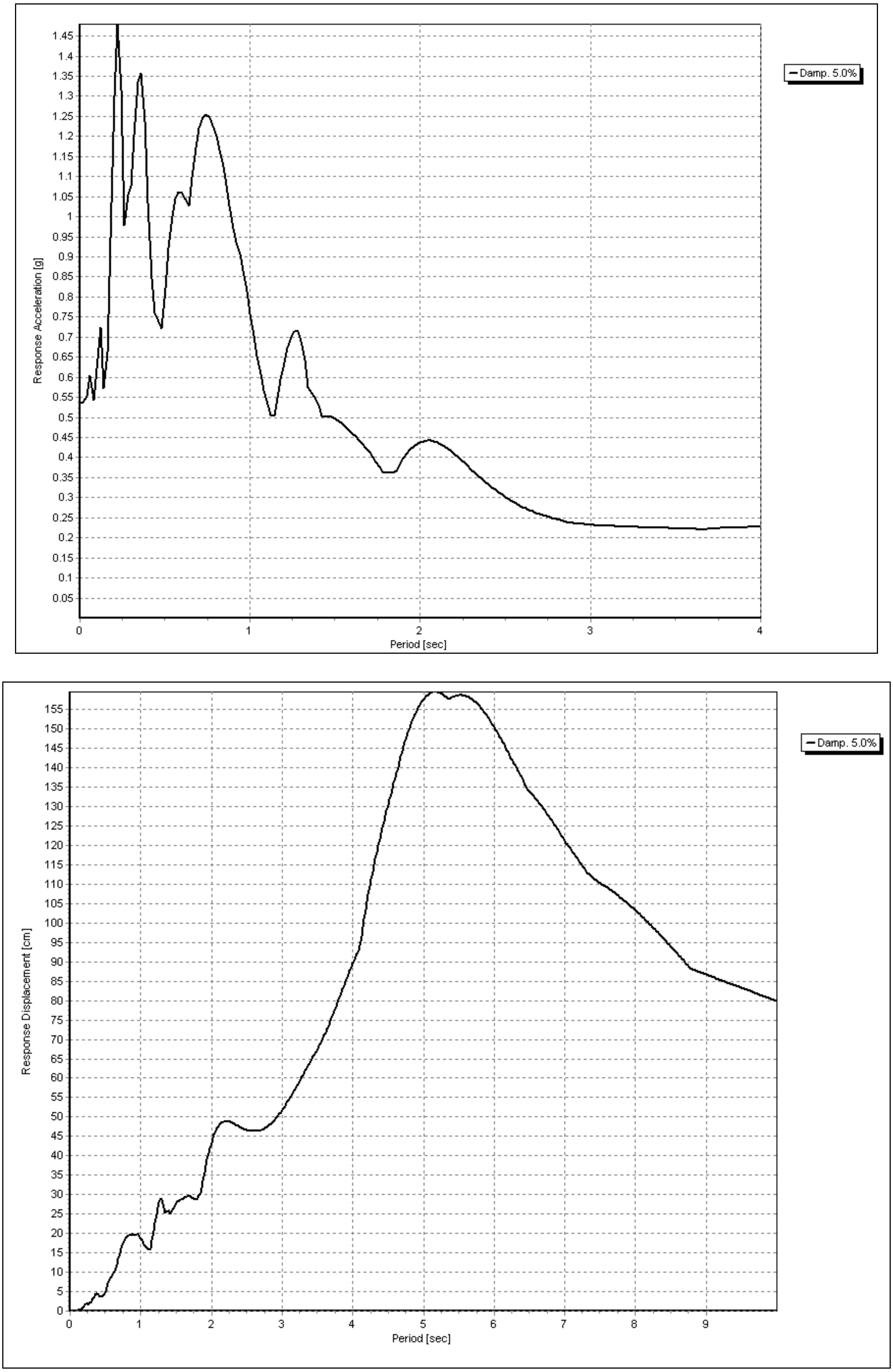

Figure 5.6 DZC270 record - response and displacement spectrum graphs

Kobe 1995/01/16 20:46	Station: 0 Takarazuka
KOBE-U2	KOBE/TAZ000

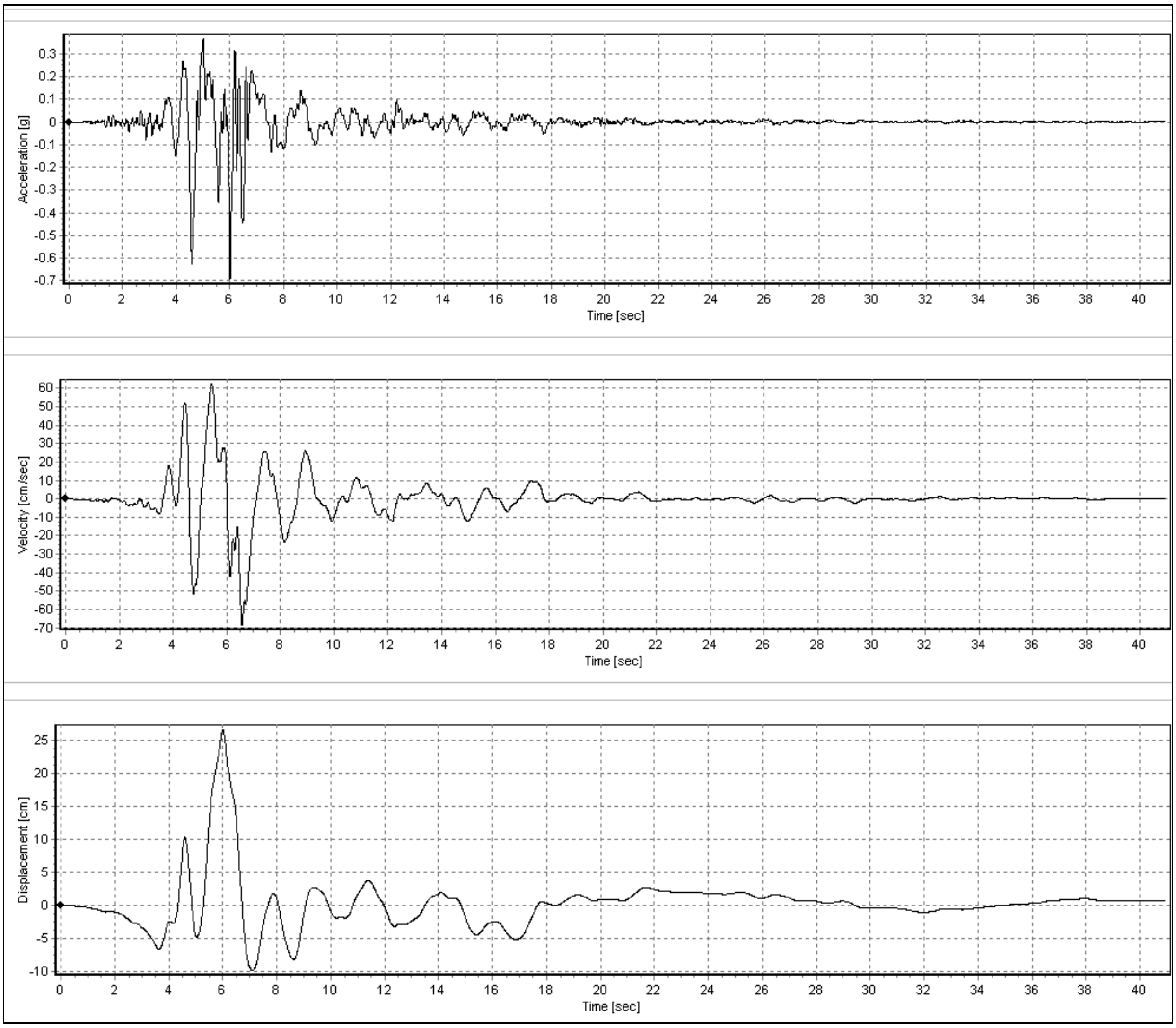

Figure 5.7 TAZ000 record - acceleration, velocity and displacement time history graphs

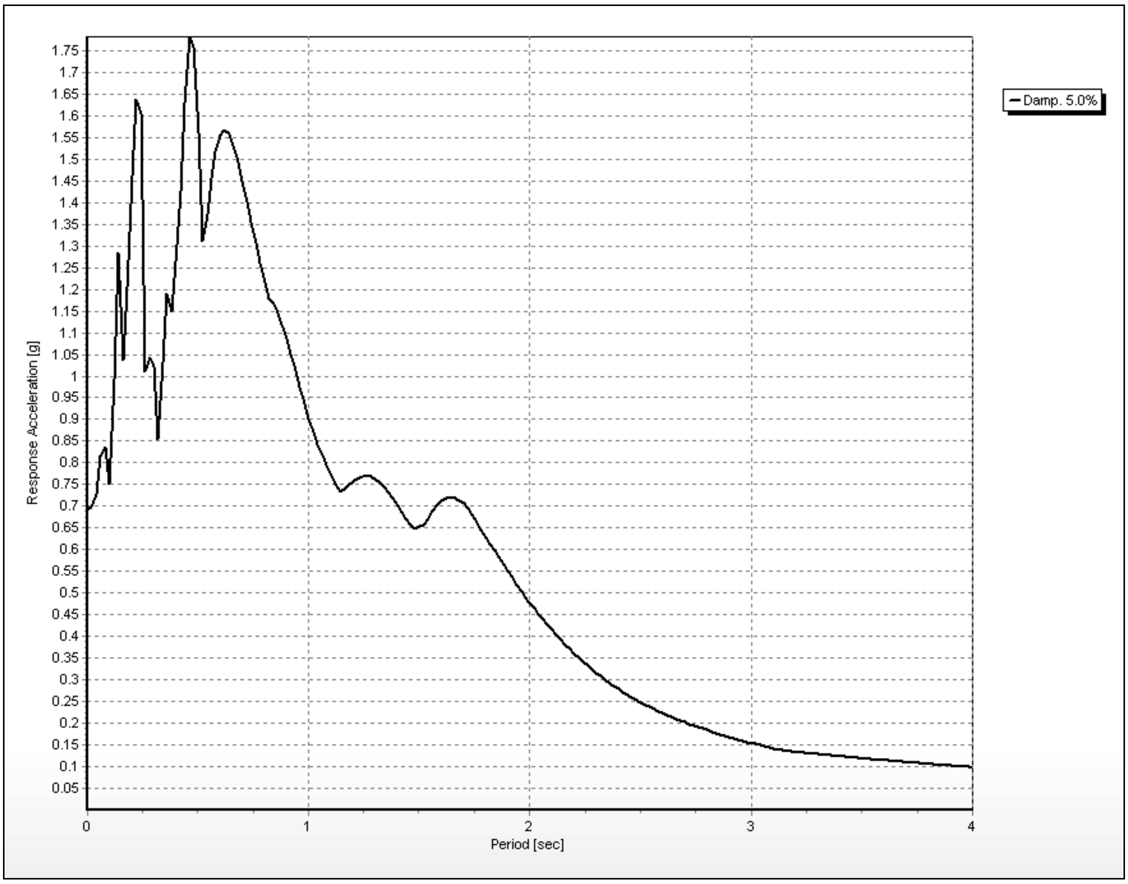

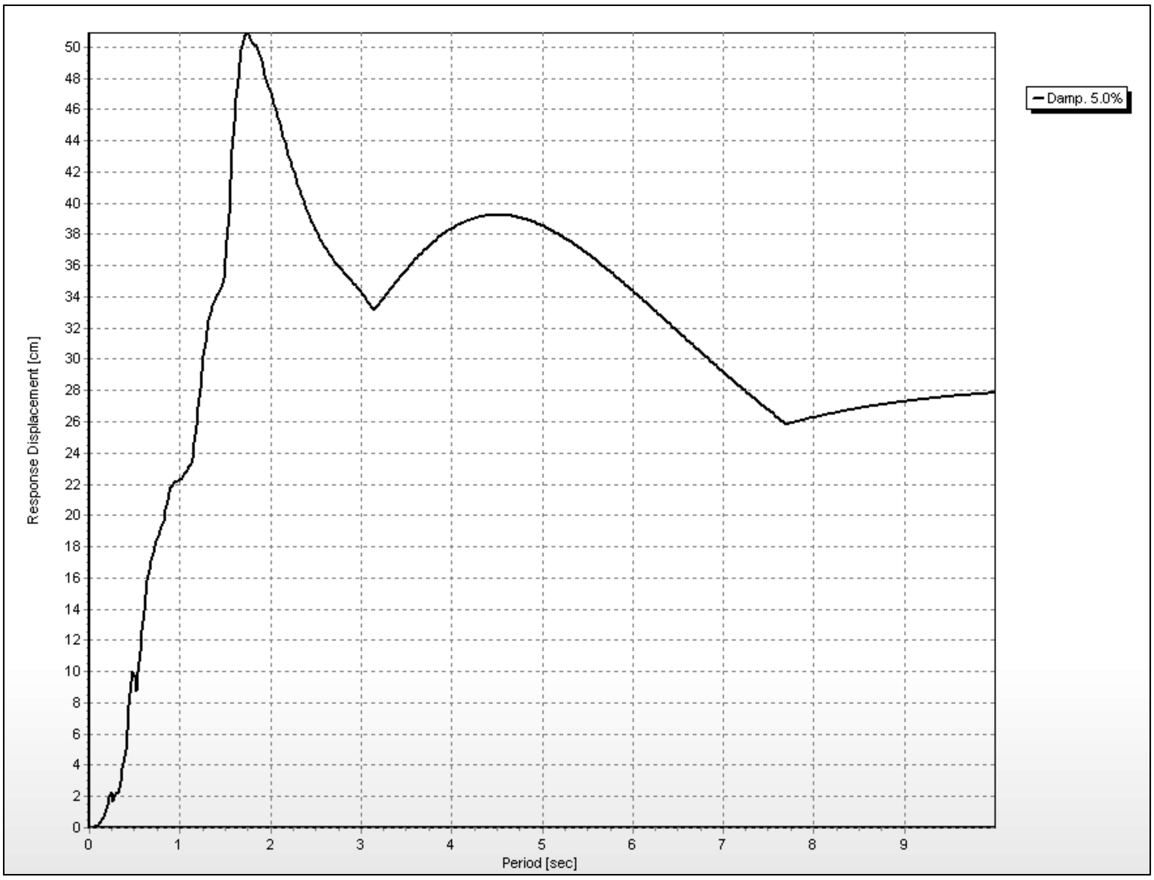

Figure 5.8 TAZ000 record - response and displacement spectrum graphs

Kobe 1995/01/16 20:46	Station: 0 Takarazuka
KOBE-U1	KOBE/TAZ090

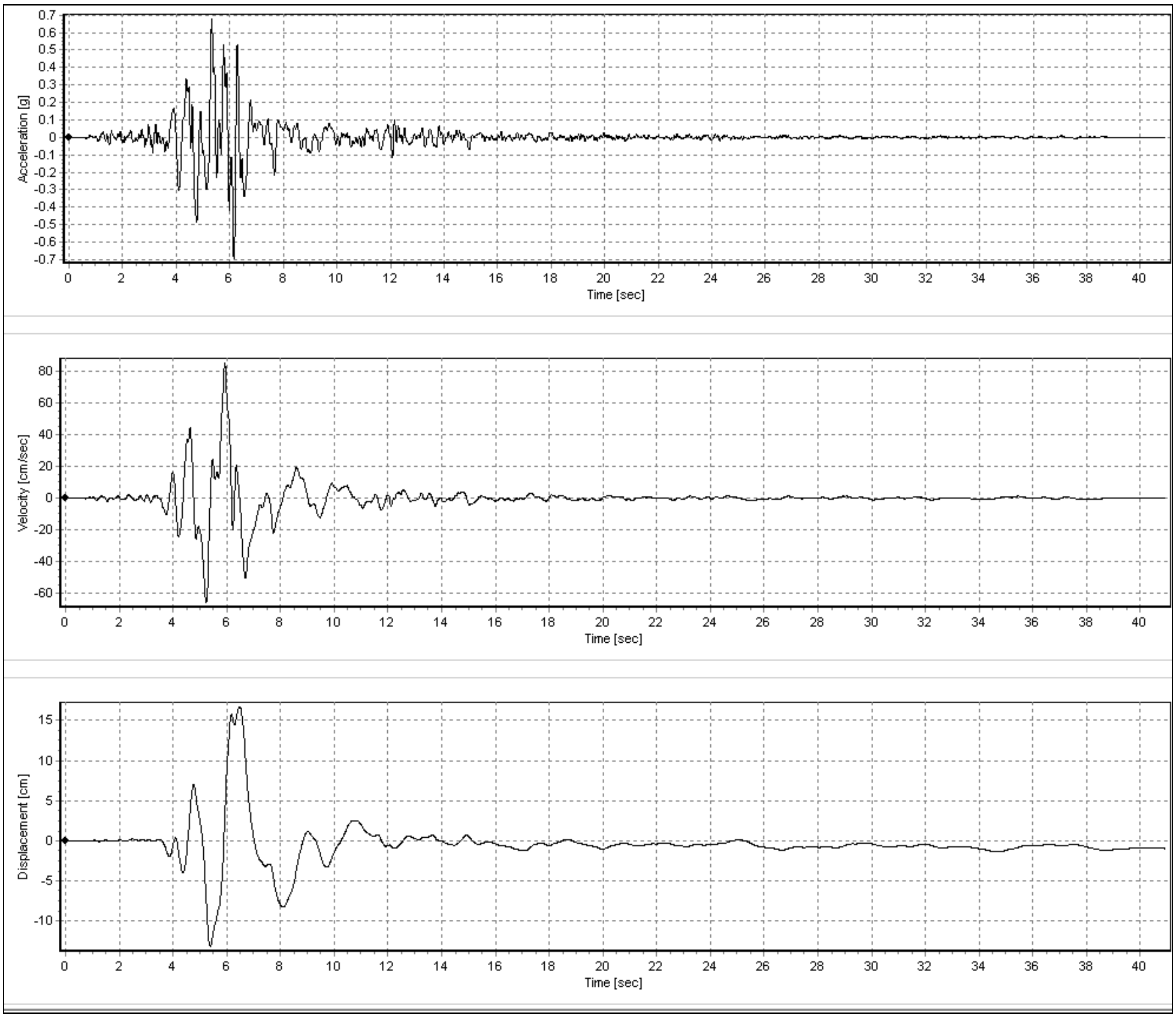

Figure 5.9 TAZ090 record - acceleration, velocity and displacement time history graphs

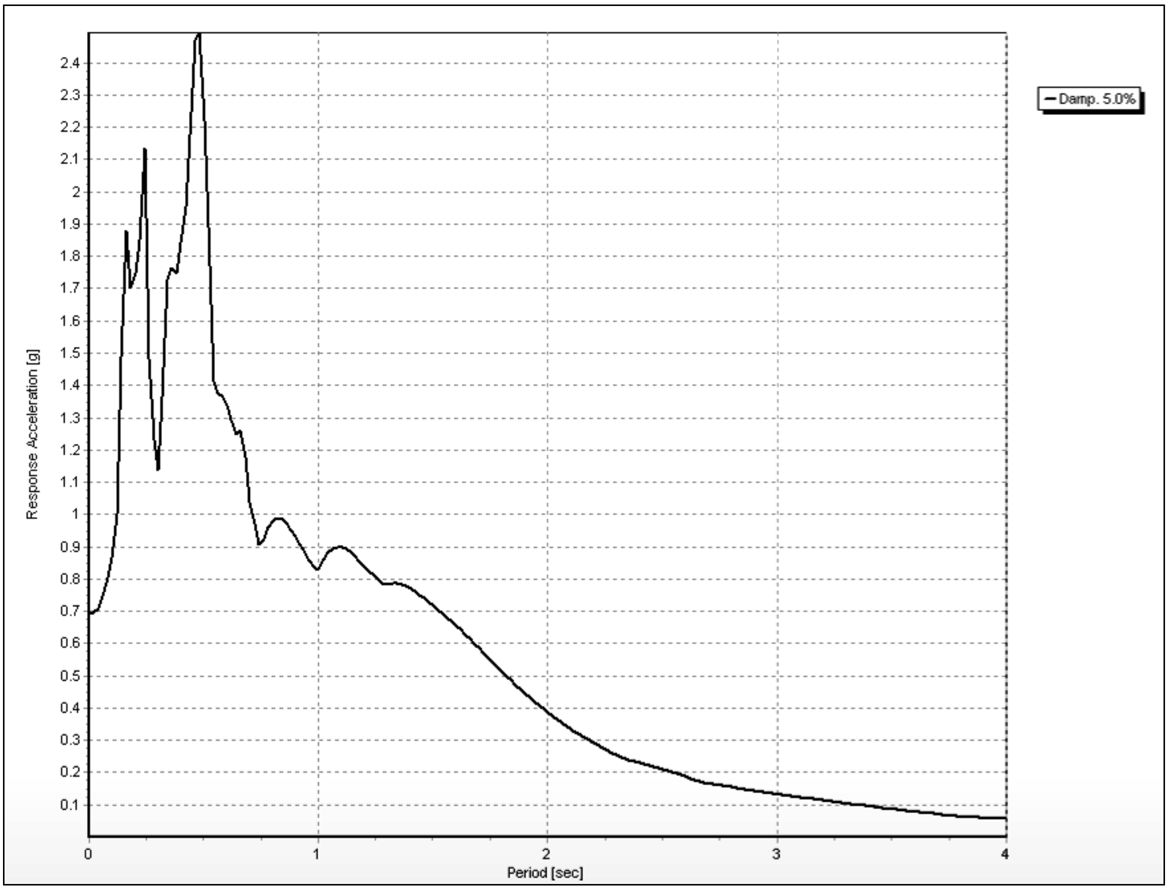

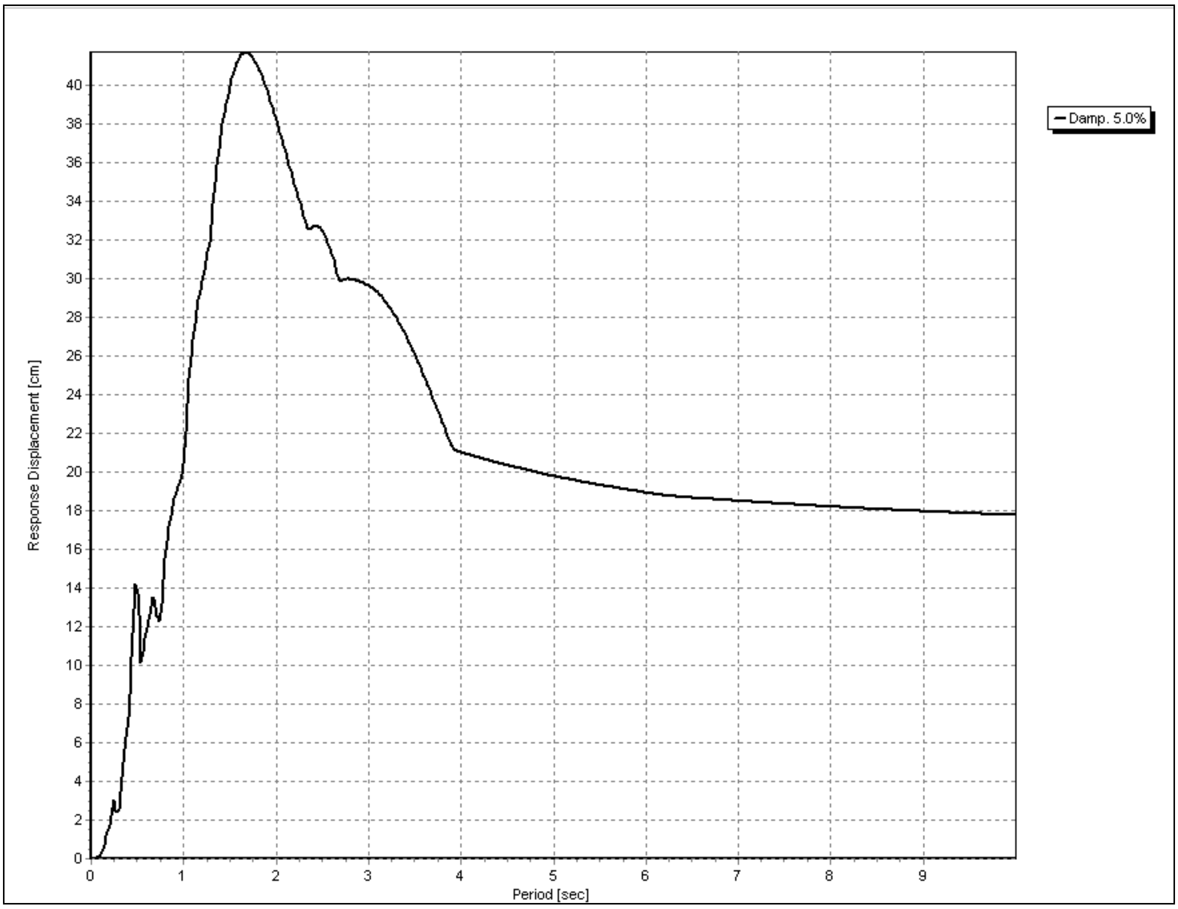

Figure 5.10 TAZ090 record - response and displacement spectrum graphs

Kocaeli, Turkey 1999/08/17	**Station: Yarimca**
KOCAELI-U2	KOCAELI/YPT060

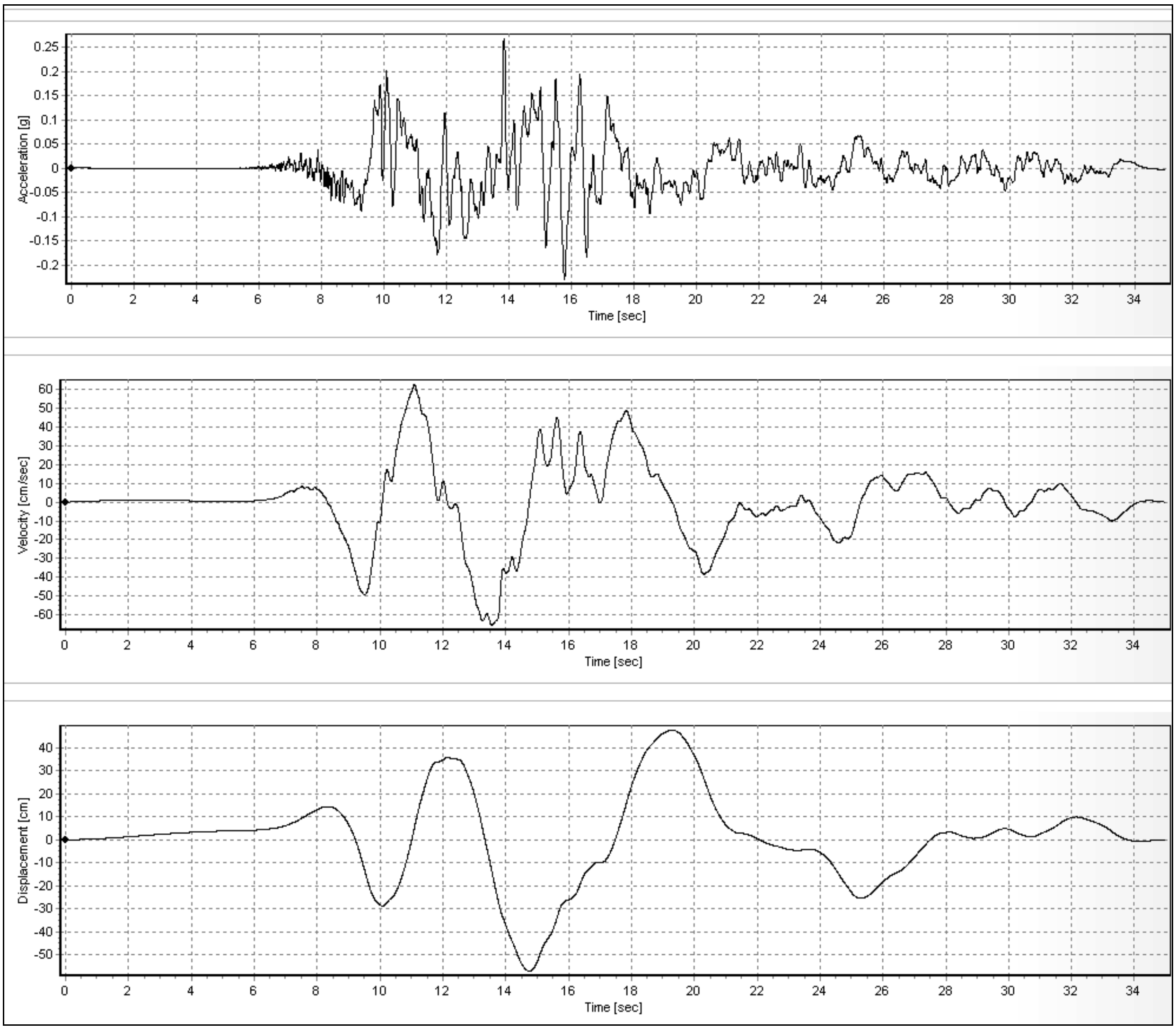

Figure 5.11 YPT060 record - acceleration, velocity and displacement time history graphs

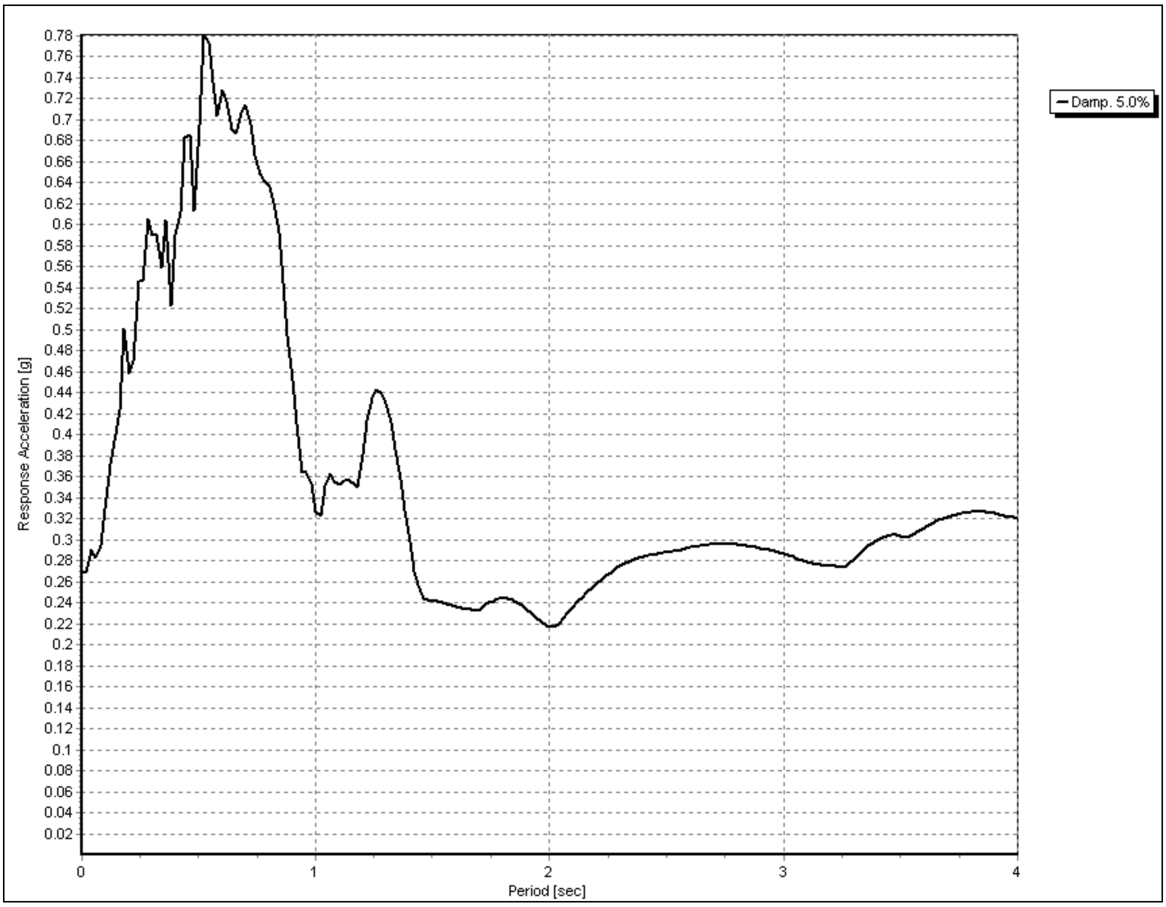

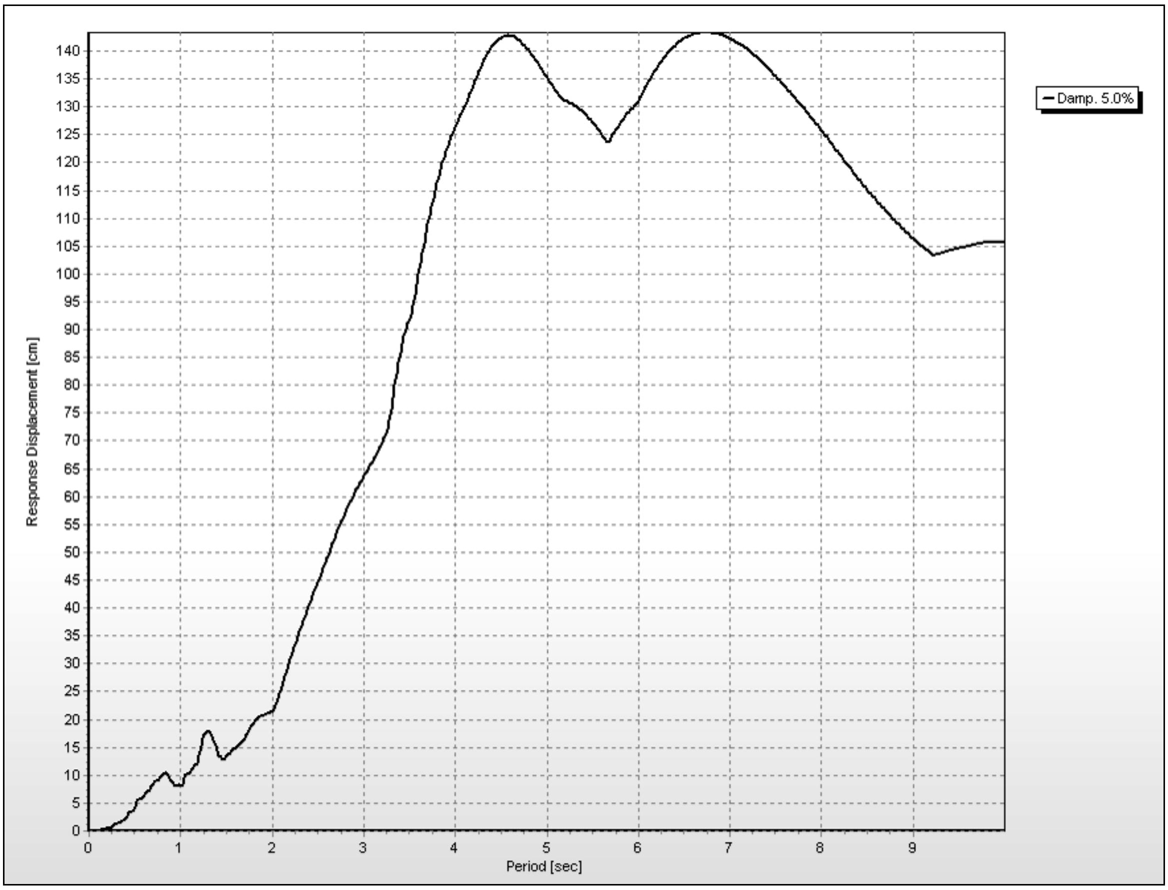

Figure 5.12 YPT060 record - response and displacement spectrum graphs

Kocaeli, Turkey 1999/08/17	Station: Yarımca
KOCAELI-U1	KOCAELI/YPT330

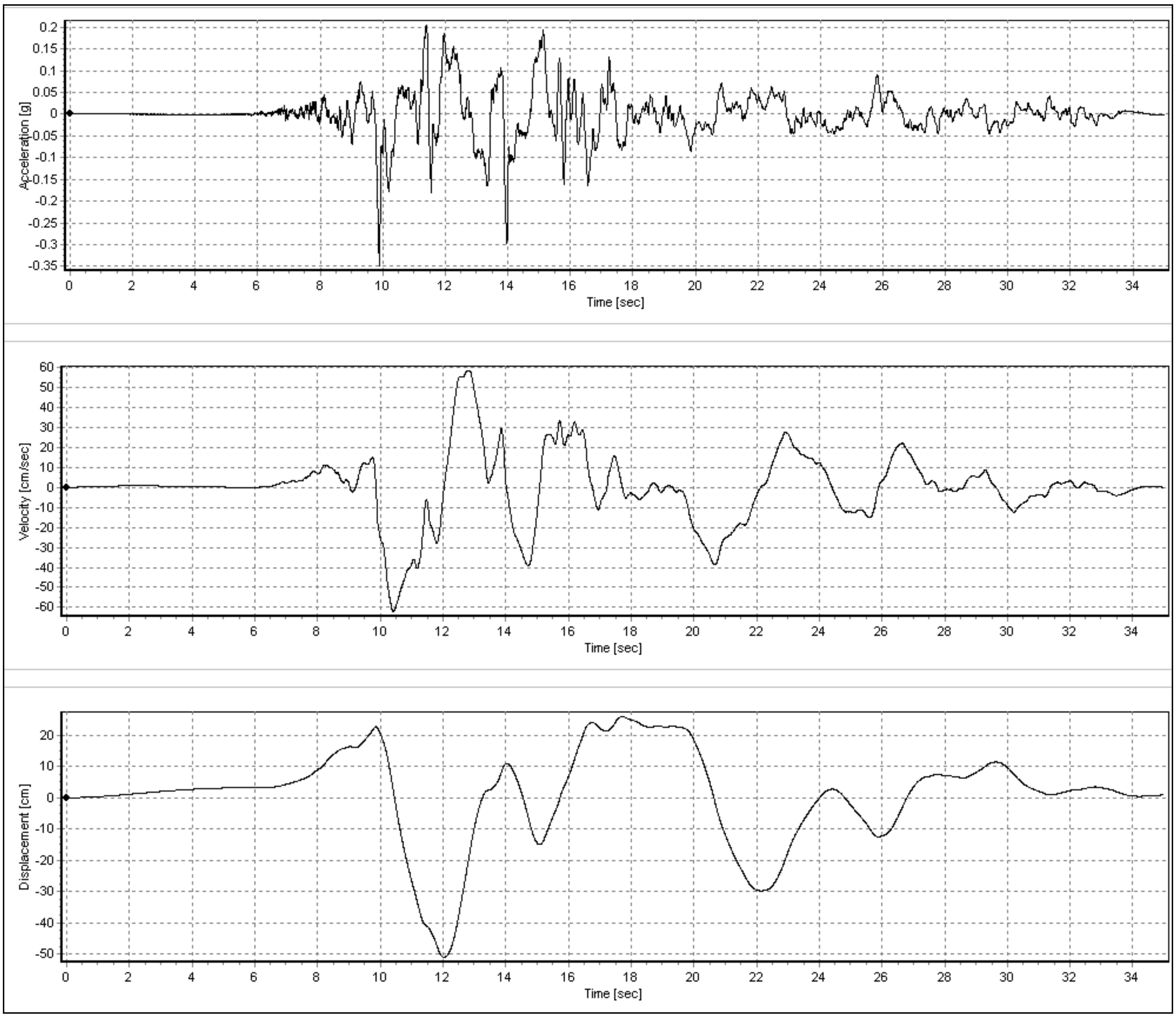

Figure 5.13 YPT330 record - acceleration, velocity and displacement time history graphs

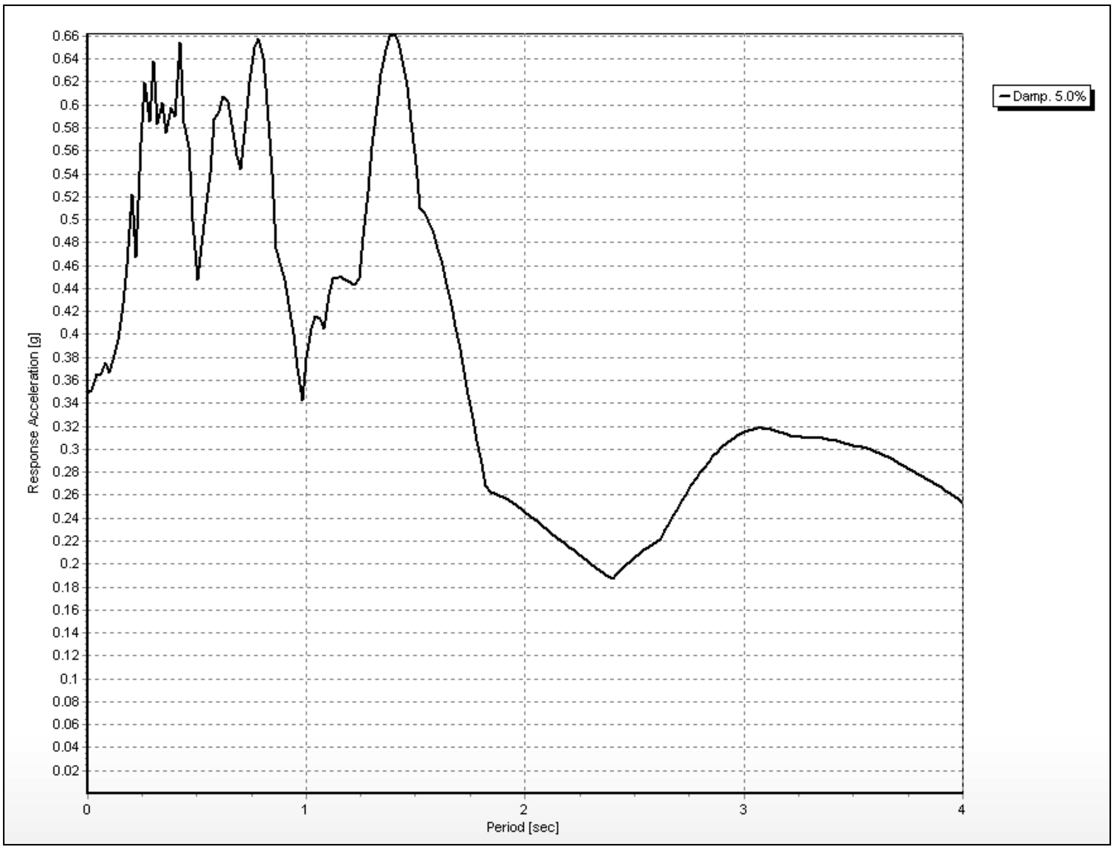

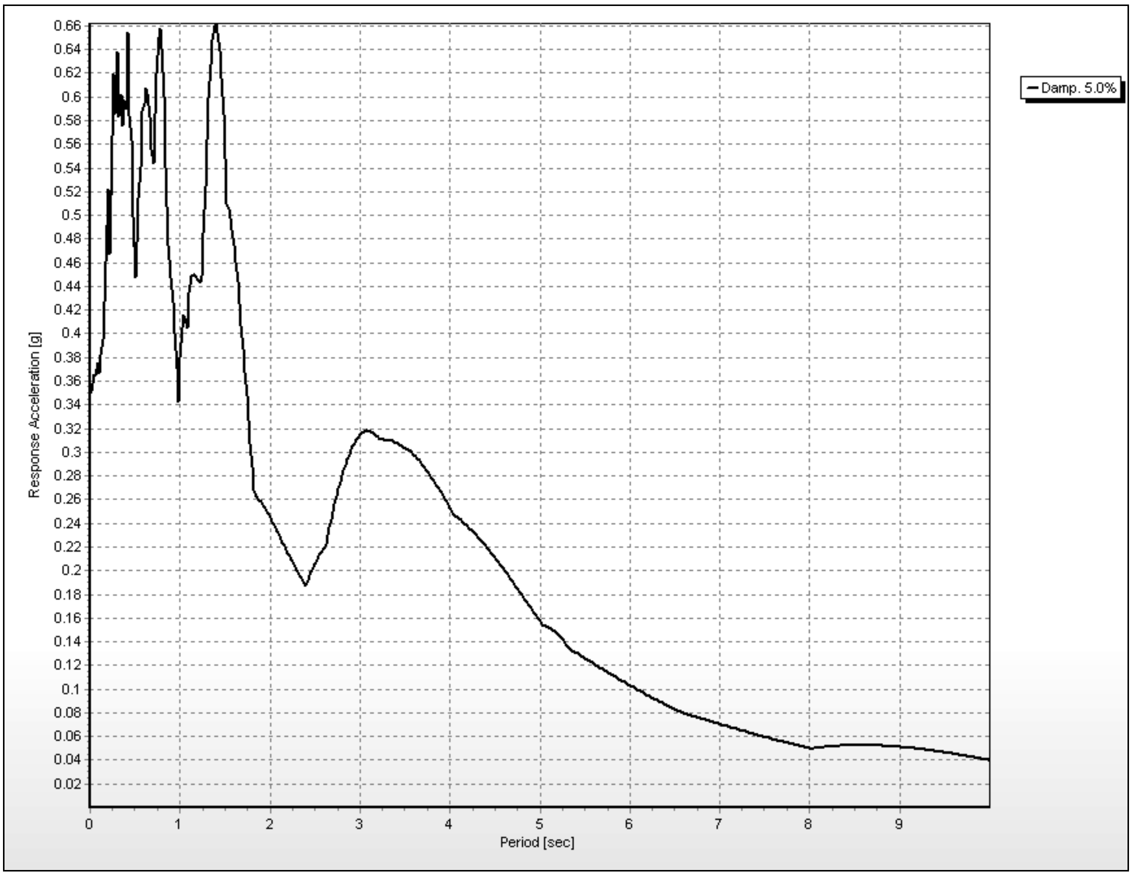

Figure 5.14 YPT330 record - response and displacement spectrum graphs

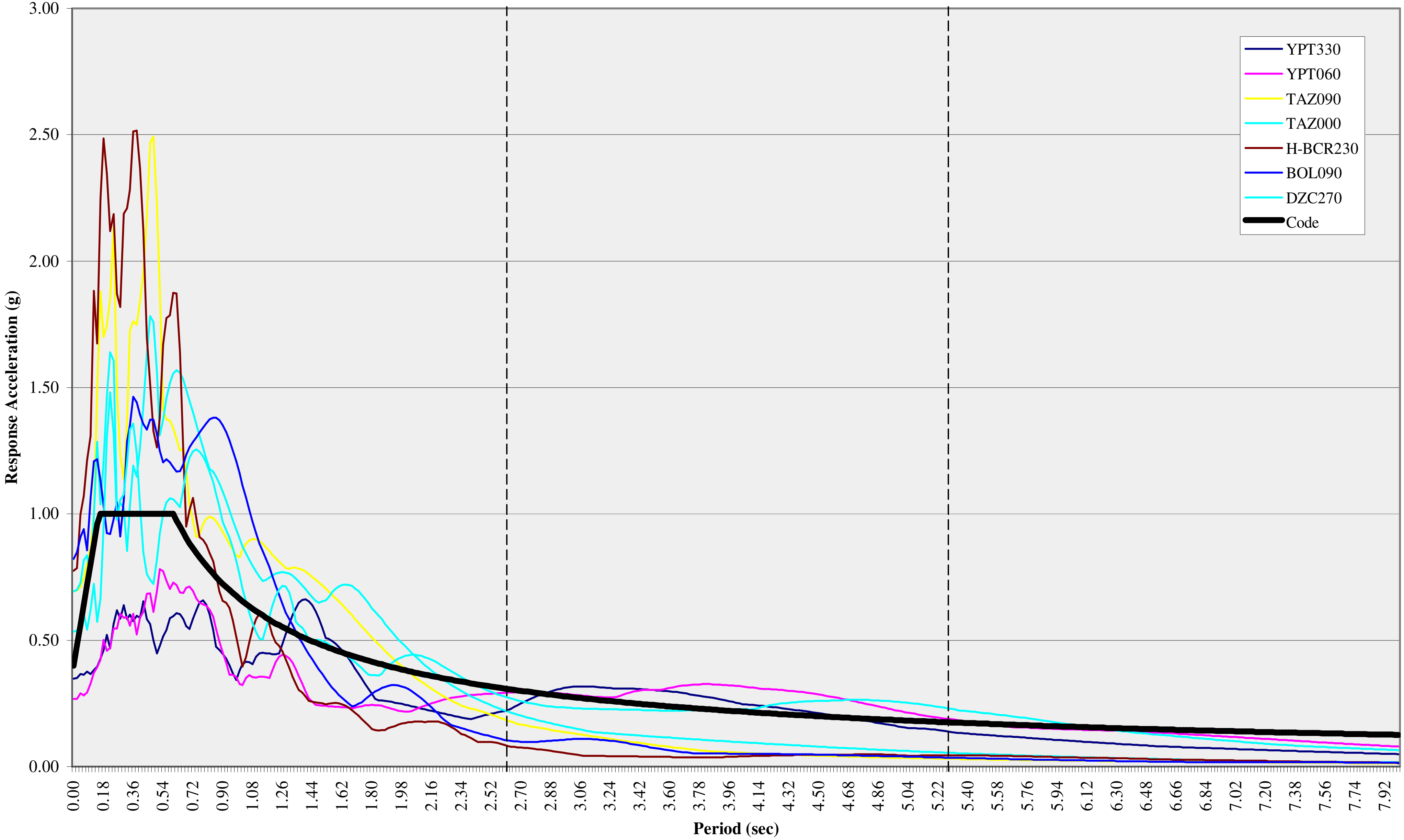

Figure 5.15 Acceleration response spectra

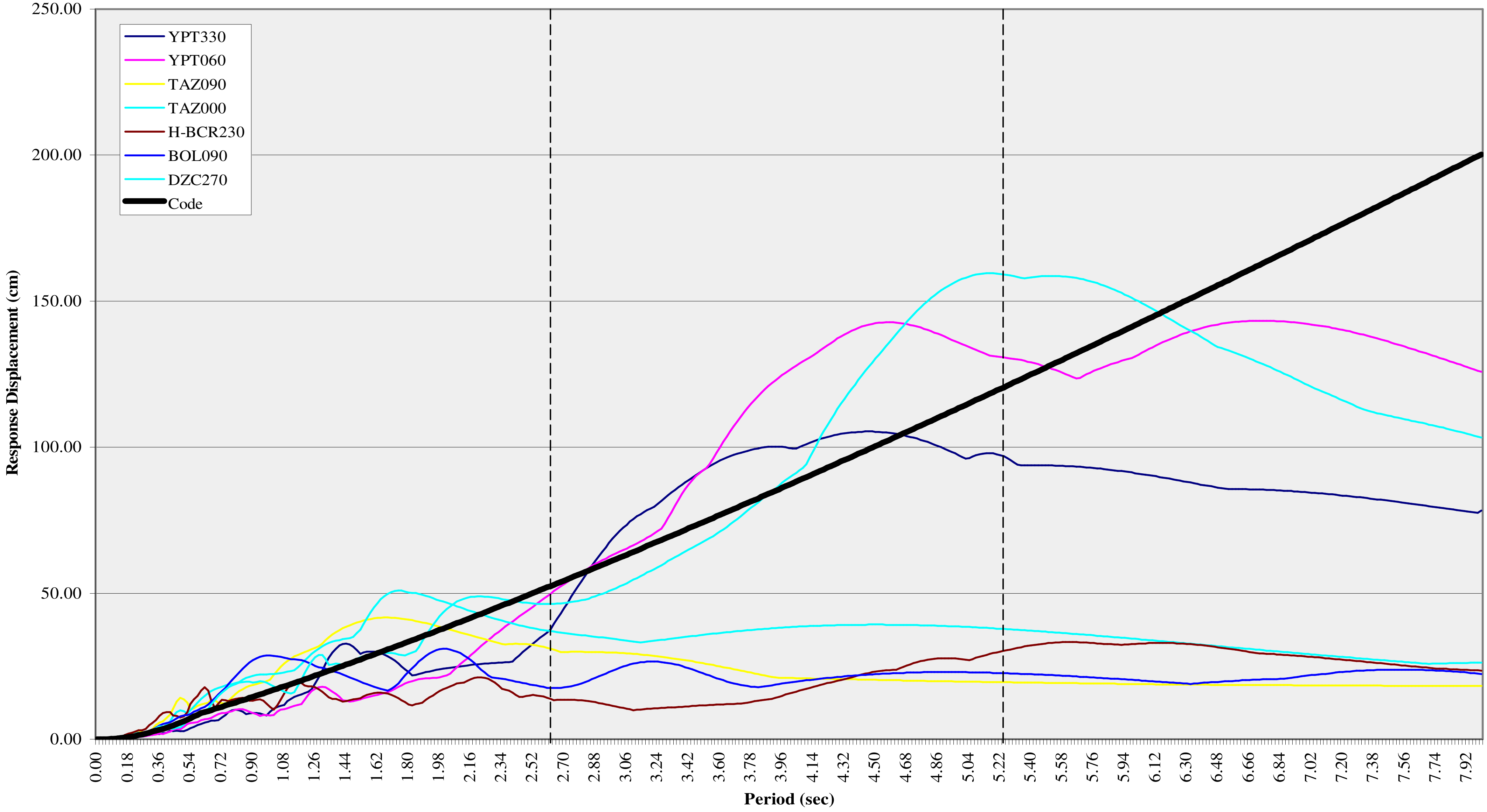

Figure 5.16 Displacement response spectra

5.2.4. Temperature Change Analysis

A temperature change analysis has been carried out in order to observe the influence of continuity on superstructure moments and the degree of the possible forces of eccentricity over the FPB devices.

22° of temperature change is applied in the sap model in two phases. In the first step, translational degrees of freedom for the FPB devices are set to Unisolated mode in SAP2000 program, locking translational movement of the FPB devices. A threshold shear force for sliding is calculated from the low friction coefficient of the FPB and the axial load over the FPB. After the first run of the analysis the results of the FPB devices are checked to see which ones have exceeded the threshold shear force for sliding. Before the second run of the analysis, the FPB's exceeding the threshold are set to their original stiffness properties in translational degrees of freedom. So, this two-step iterative approach gives closer results to a nonlinear analysis.

6. SUMMARY OF RESULTS

6.1.1. Preliminary Calculations

From known stiffness and mass values a preliminary hand calculation is undertaken to verify the results of the computer analysis and catch the characteristic parameters of the viaduct, for instance the period of a single pier.

• Stiffness of a single pier :

I_3 = 71.43 m^4

Cracked Section Coefficient = 0.257

E = 25,907,000 kN/m²

Pier Length = 49.10 m

K = $3EI/L^3$

= $(3*25{,}907{,}000*71.43*0.257)/49.10^3$

$K_{cracked}$ = 12,053 kN/m

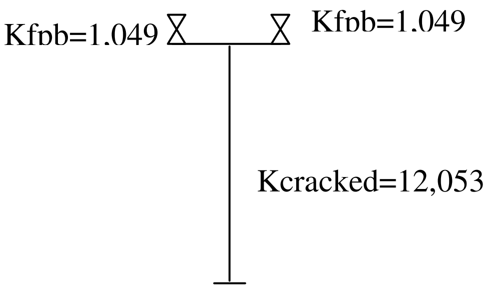

• Stiffness of FPB device :

R = 6.2 m

W = 6500 kN

K_{fpb} = W/R

= 1049 kN/m

• Period of a single isolated pier:

$1/k_{equivalent} = 1/k_{fpb} + 1/k_{pier}$

$= 1/(1{,}049*2) + 1/(12{,}053)$

$k_{equivalent}$ = 1,787 kN/m

Mass acting over the FPB's = 1,300 t

$T = 2\pi*(M/k)^{1/2}$

= **5.36 sec**

• Period of a single Unisolated pier:

M_{pier} = (14.316 m²*2.5 t/m³*49.10 m)/3 + 390 t + 1300 t

= 2276 t

$T = 2\pi*(M/k)^{1/2}$

= **2.80 sec**

6.1.2. Modal Analysis

6.1.2.1. Isolated System Model

The effective mode is painted in light blue.

- Longitudinal Direction

Mode	Period (Sec)	CircFreq (rad/sec)	Modal Participating Mass Ratios
1	5.24	1.20	0.4628
2	5.05	1.24	0.0012
3	4.81	1.31	0.0011
4	4.29	1.46	0.0003
5	3.11	2.02	0.0000
6	1.95	3.22	0.0000
7	1.57	4.01	0.0000
8	1.57	4.01	0.0604
9	1.52	4.13	0.0058
10	1.51	4.16	0.1411
11	1.47	4.28	0.0806
12	1.43	4.38	0.0001
13	1.43	4.40	0.0199
14	1.25	5.01	0.0000
15	1.17	5.39	0.0002
16	1.11	5.67	0.0023
17	1.08	5.81	0.0006
18	1.06	5.90	0.0012
19	0.87	7.23	0.0000
20	0.64	9.86	0.0000
21	0.46	13.64	0.0000
22	0.25	25.10	0.0684
23	0.23	26.76	0.0472
24	0.11	56.33	0.0123
25	0.07	95.37	0.0568
		Σ=	0.9624

Table 6.1 Modal frequencies and mass participations of the longitudinal analysis – Isolated System Model

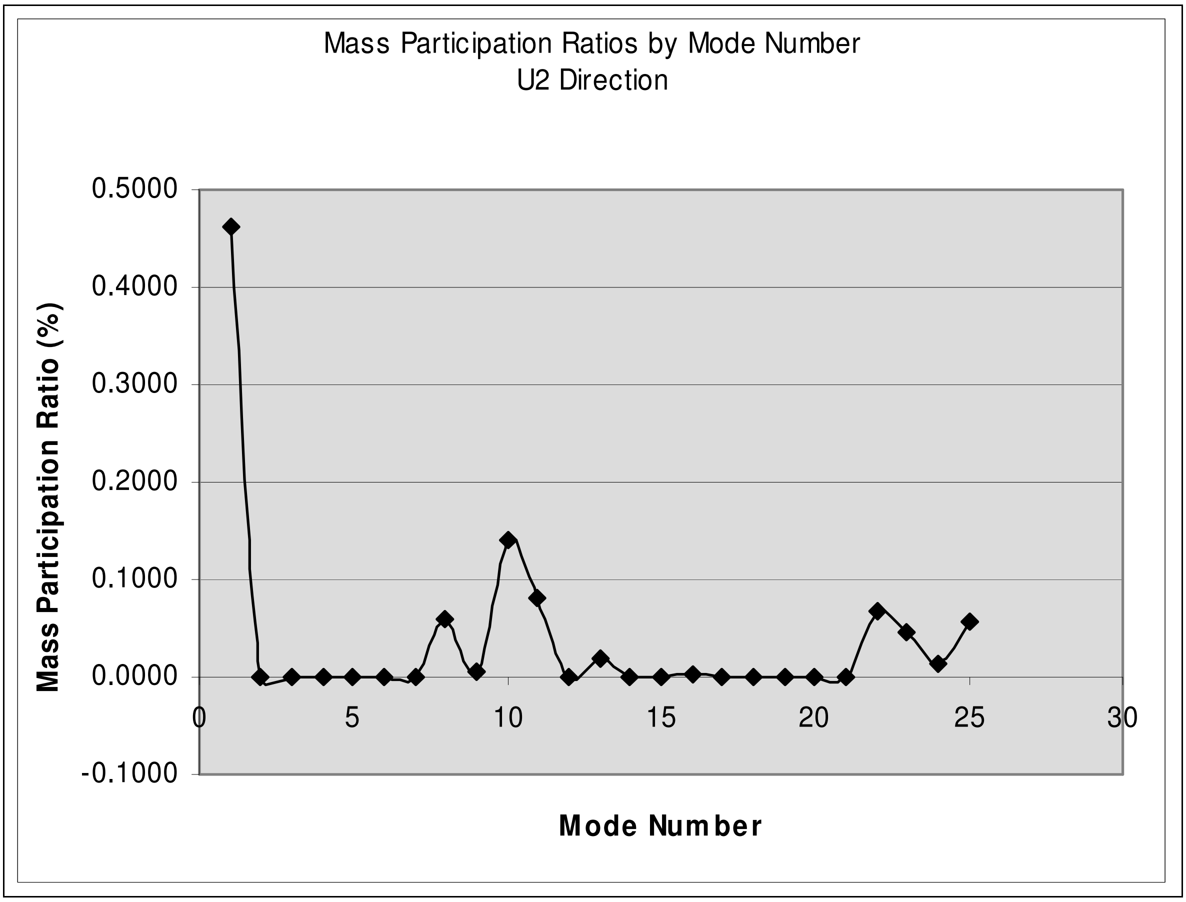

Figure 6.1 Mass participation ratios of the isolated system by mode number (Longitudinal Analysis)

- Transversal Direction

Mode	Period (Sec)	CircFreq (rad/sec)	Modal Participating Mass Ratios
1	5.24	1.20	0.0015
2	5.05	1.24	0.3841
3	4.81	1.31	0.0018
4	4.29	1.46	0.0255
5	3.11	2.02	0.0000
6	1.95	3.22	0.0002
7	1.57	4.01	0.0005
8	1.57	4.01	0.0012
9	1.52	4.13	0.0012
10	1.51	4.15	0.0006
11	1.47	4.28	0.0000
12	1.43	4.40	0.0000
13	1.27	4.93	0.0001
14	1.16	5.44	0.0014
15	1.11	5.68	0.1095
16	1.07	5.88	0.1742
17	1.03	6.08	0.0568
18	1.00	6.28	0.0165
19	0.87	7.23	0.0000
20	0.69	9.12	0.0000
21	0.49	12.87	0.0000
22	0.26	24.46	0.0009
23	0.20	31.74	0.0095
24	0.17	36.02	0.1072
25	0.06	103.67	0.0650
		Σ=	0.9578

Table 6.2 Modal frequencies and mass participations of the transversal analysis – Isolated System Model

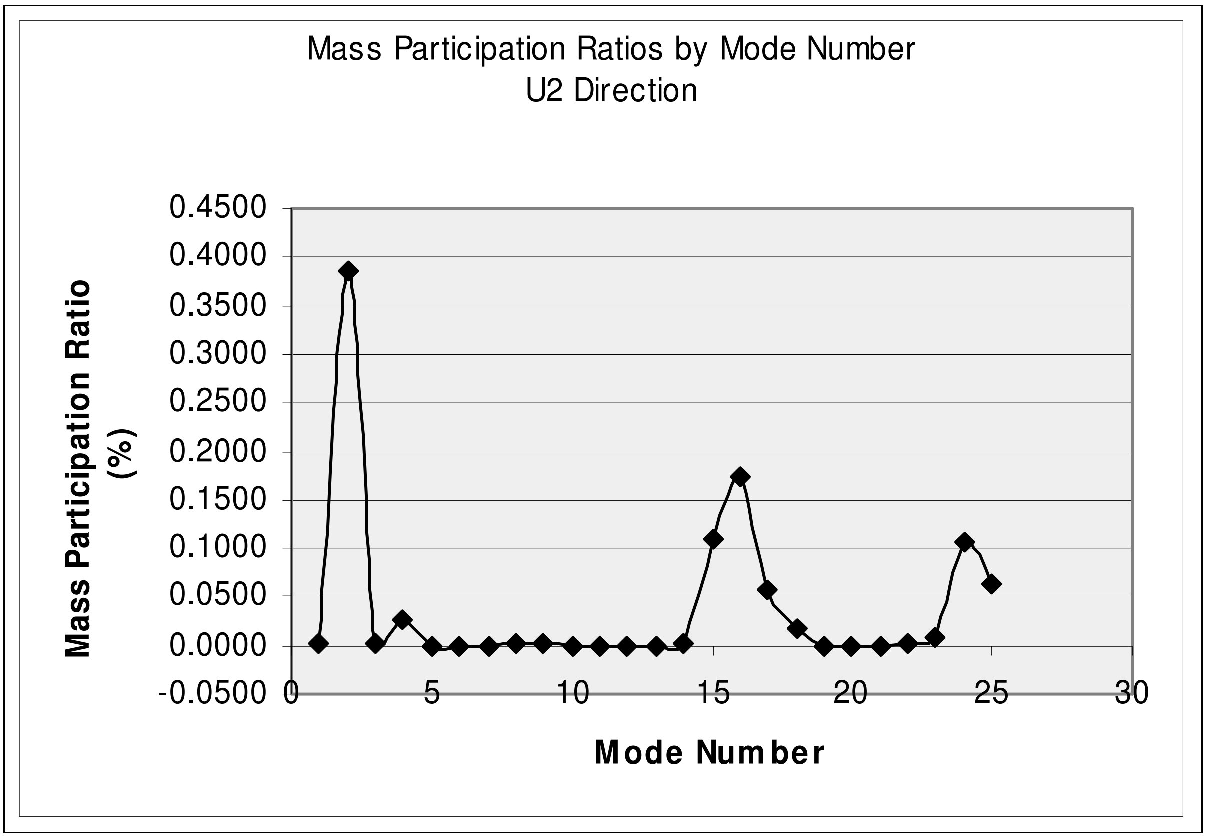

Figure 6.2 Mass participation ratios of the isolated system by mode number (Transversal Analysis)

- Mode Shapes

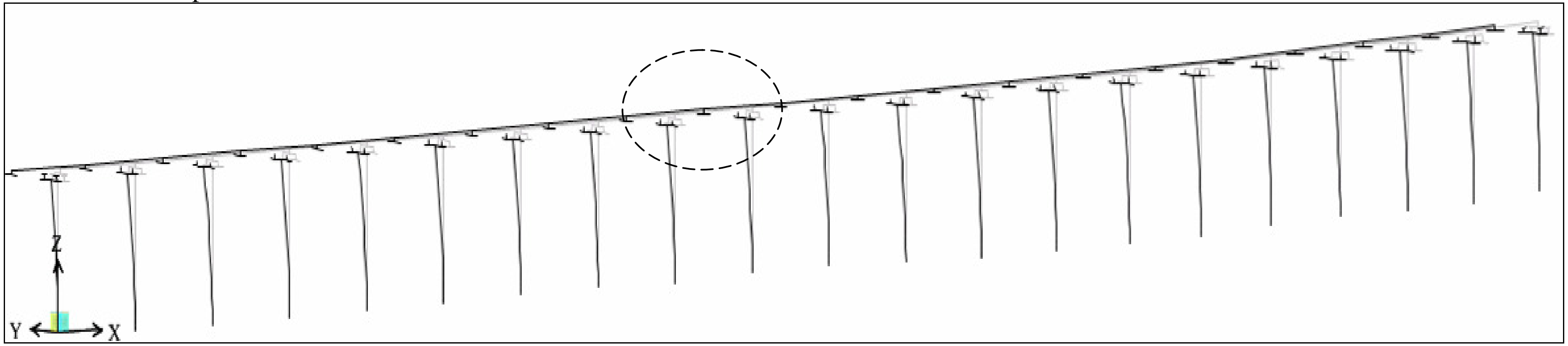

(a) A general view

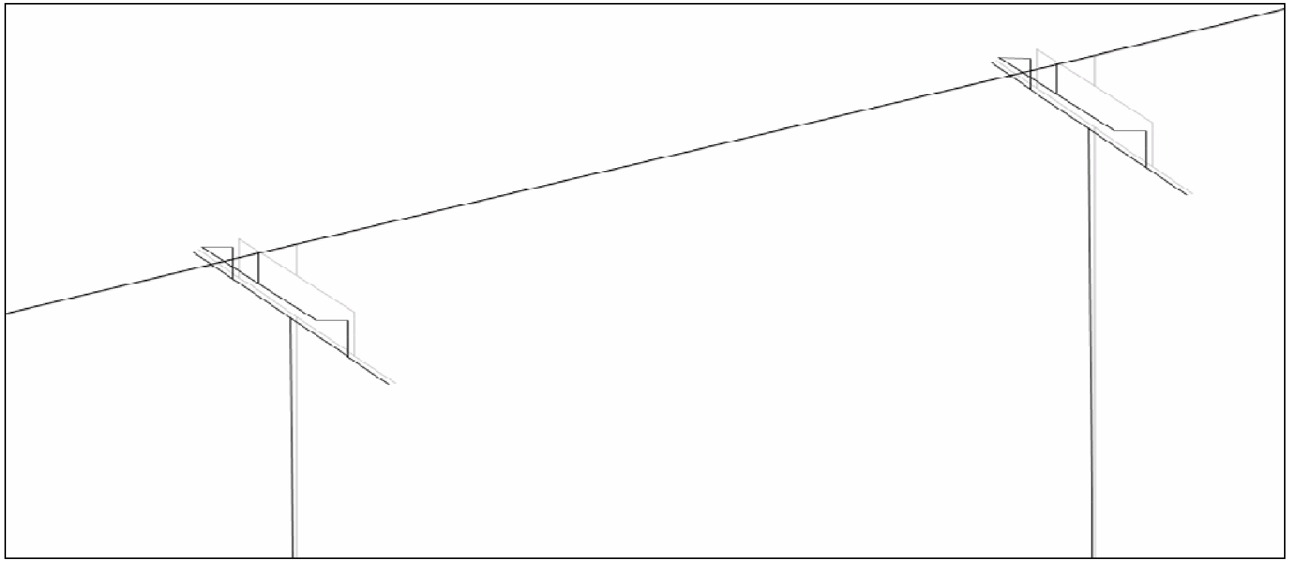

(b) A closer view

Figure 6.3 The first mode of the isolated system model is in U1 direction parallel to the bridge alignment with a period of 5.24 sec

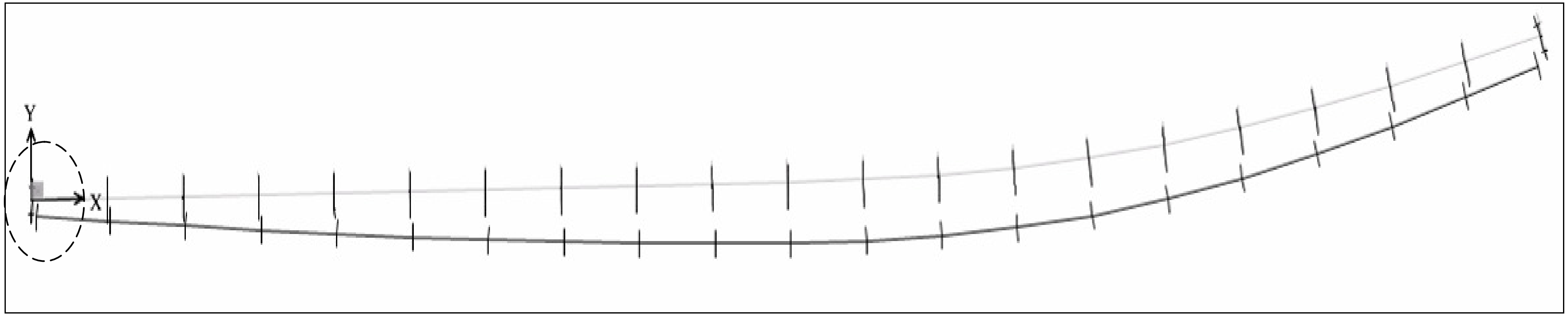

(a) A general view

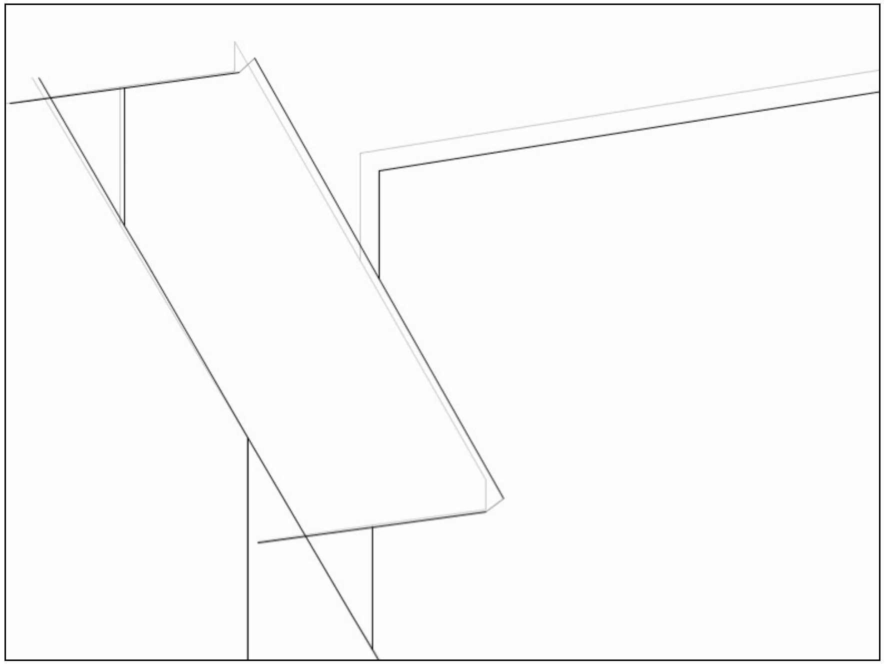

(b) A closer view

Figure 6.4 The second mode of the isolated system model is in U2 direction orthogonal to the bridge alignment with a period of 5.05 sec.

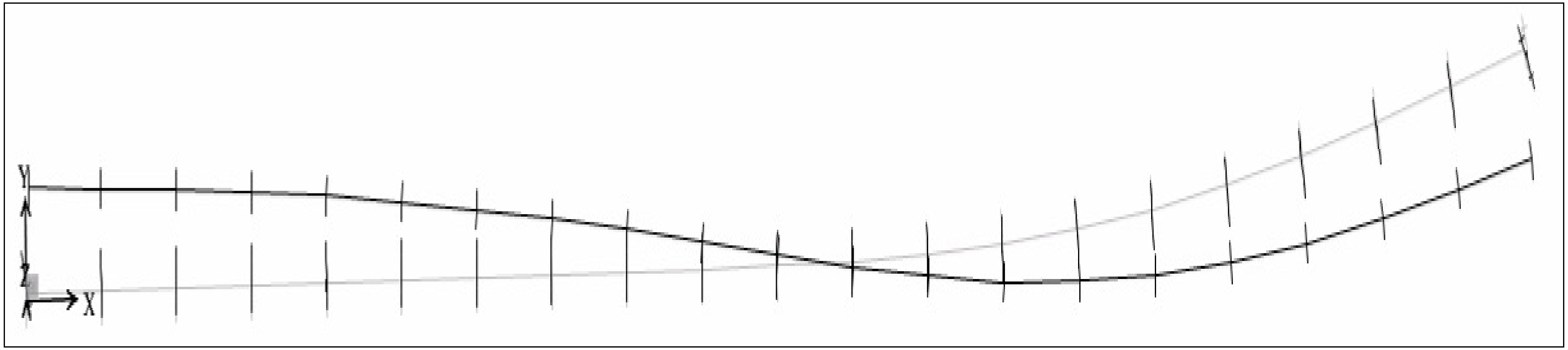

Figure 6.5 The third mode of the isolated system model is in U2 direction orthogonal to the bridge alignment with a period of 4.81 sec.

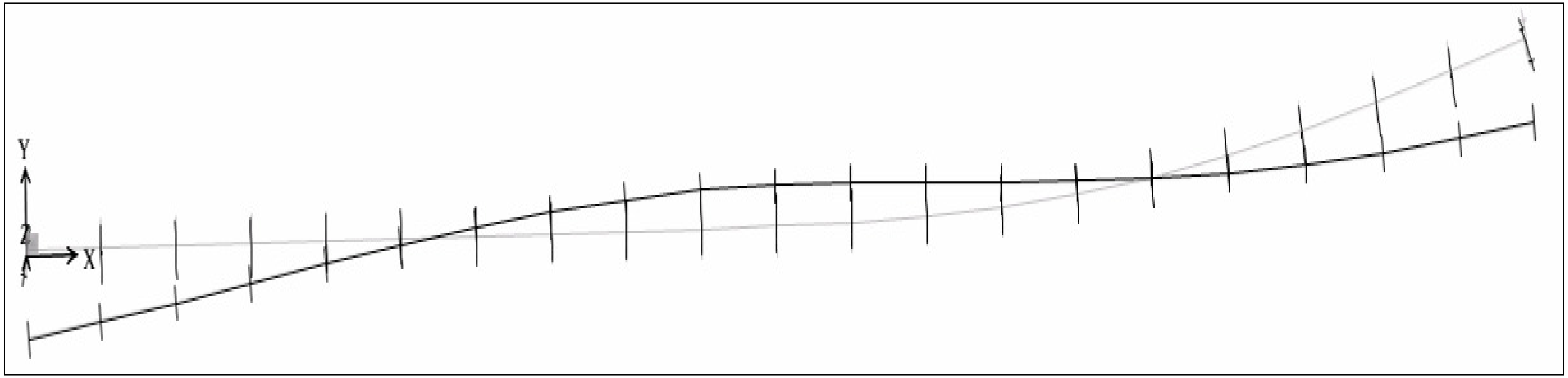

Figure 6.6 The fourth mode of the isolated system model is in U2 direction orthogonal to the bridge alignment with a period of 4.29 sec.

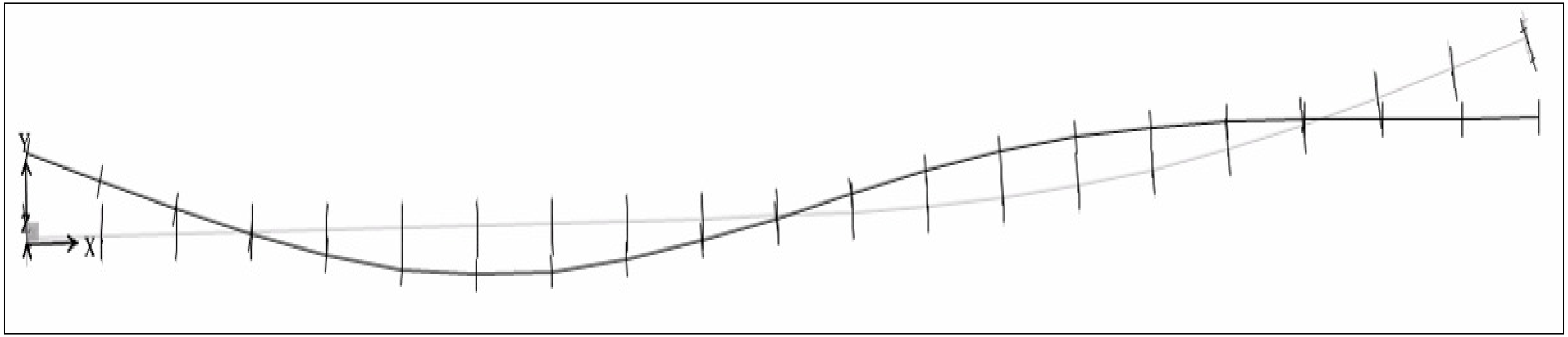

Figure 6.7 The fifth mode of the isolated system model is in U2 direction orthogonal to the bridge alignment with a period of 3.11 sec.

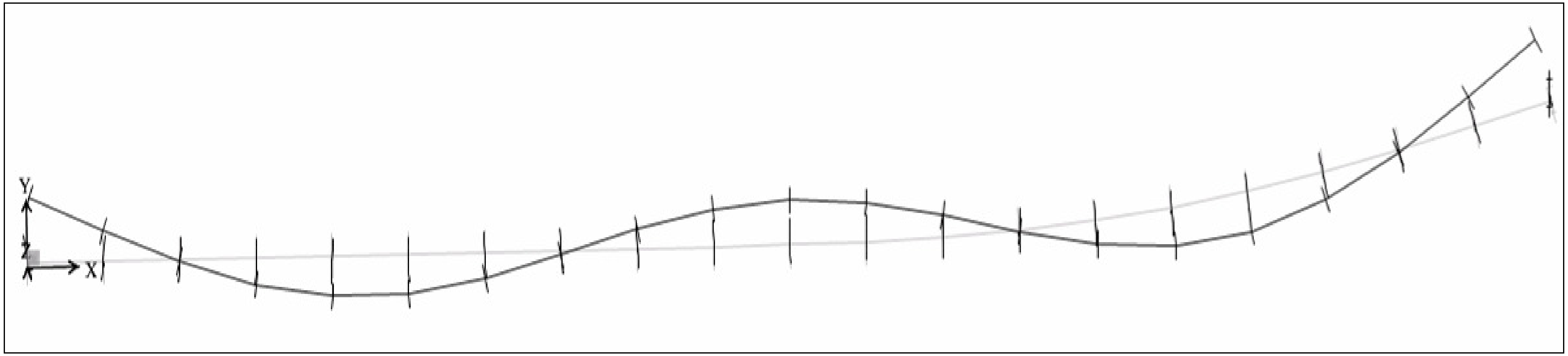

Figure 6.8 The sixth mode of the isolated system model is in U2 direction orthogonal to the bridge alignment with a period of 1.95 sec.

Others modes have single pier movements.

6.1.2.2. Unisolated System Model

The effective mode is painted in light blue.

- Longitudinal Direction

Mode	Period (Sec)	CircFreq (rad/sec)	Modal Participating Mass Ratios
1	2.68	2.34	0.7317
2	1.90	3.30	0.0122
3	1.84	3.42	0.0024
4	1.78	3.54	0.0048
5	1.66	3.79	0.0008
6	1.47	4.28	0.0001
7	1.21	5.18	0.0000
8	0.95	6.58	0.0000
9	0.76	8.32	0.0000
10	0.66	9.58	0.0000
11	0.61	10.34	0.0000
12	0.50	12.46	0.0000
13	0.43	14.51	0.0000
14	0.40	15.68	0.0001
15	0.37	17.12	0.0002
16	0.35	17.79	0.0012
17	0.32	19.38	0.0037
18	0.30	20.85	0.0852
19	0.28	22.74	0.0275
20	0.25	25.31	0.0058
21	0.22	27.99	0.0015
22	0.14	44.80	0.0182
23	0.12	52.81	0.0079
24	0.08	78.99	0.0337
25	0.04	176.87	0.0445
		Σ=	0.9818

Table 6.3 Modal frequencies and mass participations of the longitudinal analysis – Unisolated System Model

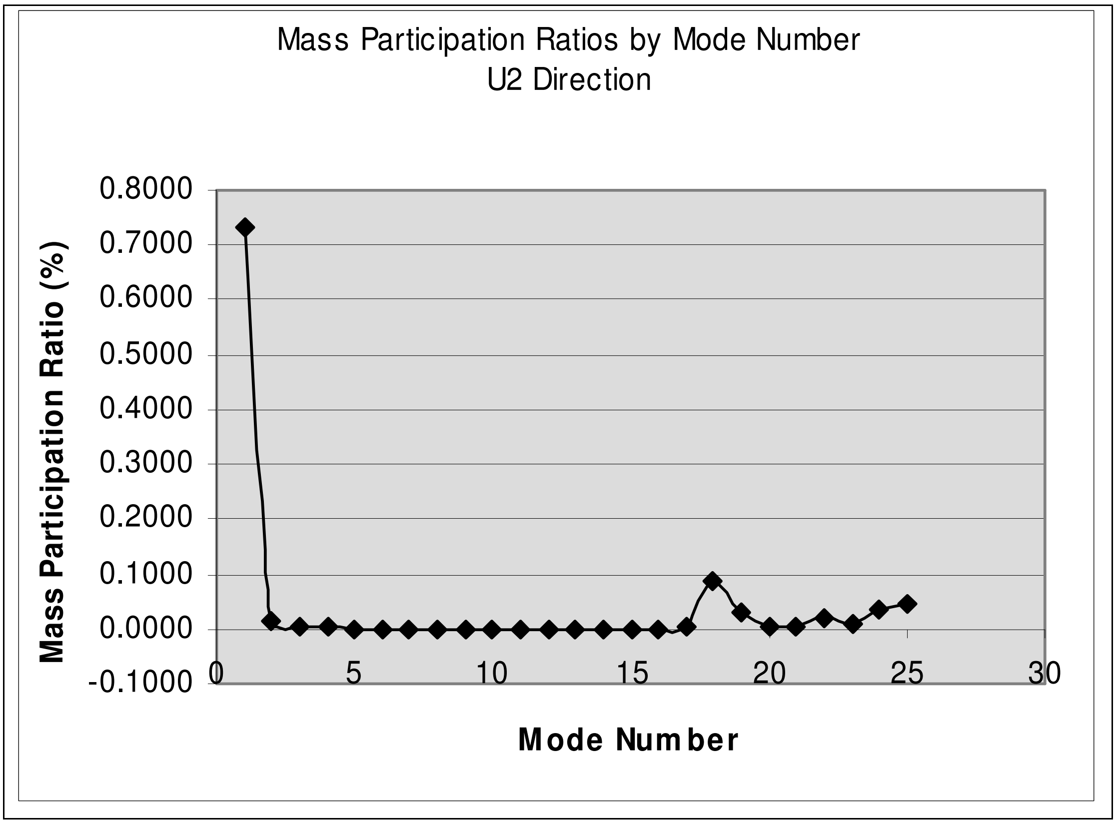

Figure 6.9 Mass participation ratios of the Unisolated system by mode number (Longitudinal Analysis)

- Transversal Direction

Mode	Period (Sec)	CircFreq (rad/sec)	Modal Participating Mass Ratios
1	2.68	2.34	0.0070
2	1.90	3.30	0.4366
3	1.84	3.42	0.1812
4	1.78	3.54	0.0999
5	1.66	3.79	0.0001
6	1.47	4.28	0.0135
7	1.21	5.18	0.0004
8	0.95	6.58	0.0008
9	0.76	8.32	0.0000
10	0.66	9.58	0.0006
11	0.61	10.34	0.0003
12	0.50	12.46	0.0000
13	0.43	14.51	0.0005
14	0.40	15.68	0.0007
15	0.37	16.82	0.0001
16	0.36	17.63	0.0005
17	0.34	18.69	0.0004
18	0.30	20.73	0.0042
19	0.26	24.03	0.0060
20	0.23	27.04	0.0636
21	0.22	28.56	0.0437
22	0.15	41.29	0.0074
23	0.11	57.35	0.0351
24	0.06	97.64	0.0289
25	0.03	188.50	0.0478
		Σ=	0.9792

Table 6.4 Modal frequencies and mass participations of the transversal analysis – Unisolated System Model

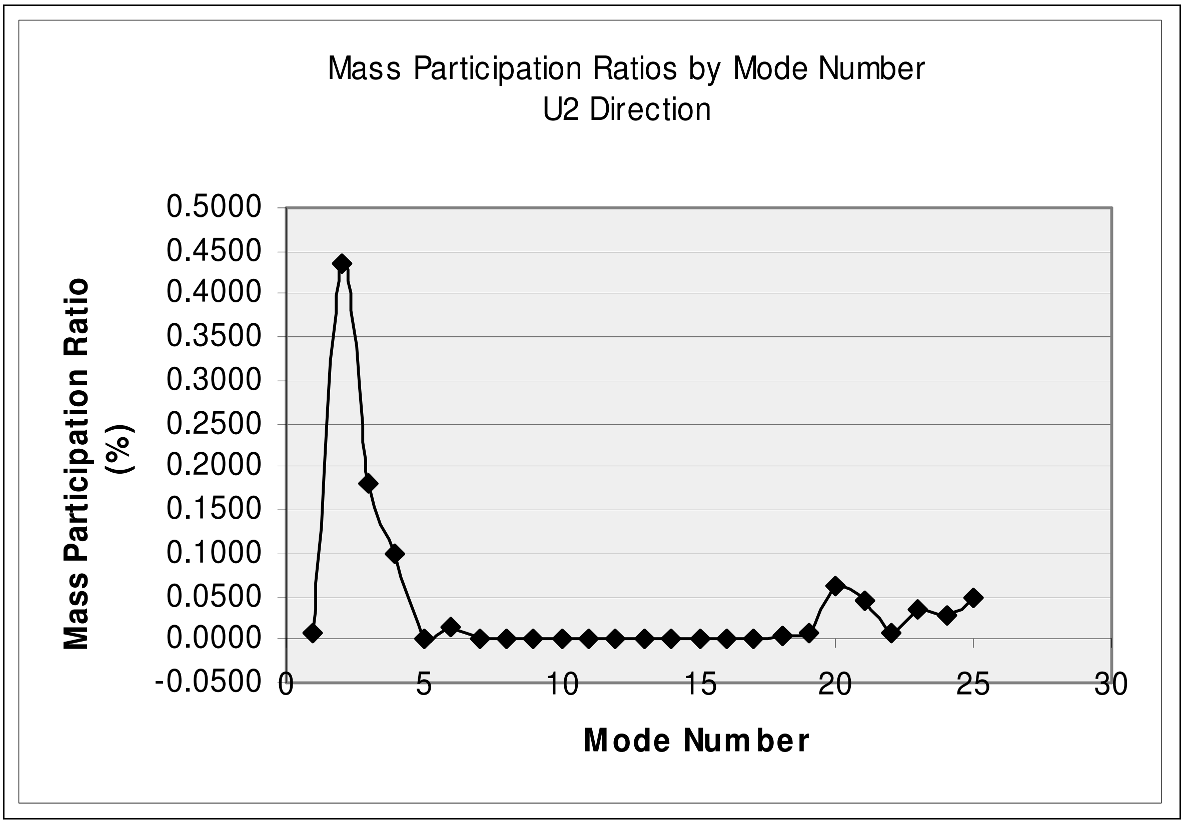

Figure 6.10 Mass participation ratios of the Unisolated system by mode number (Transversal Analysis)

- Mode Shapes

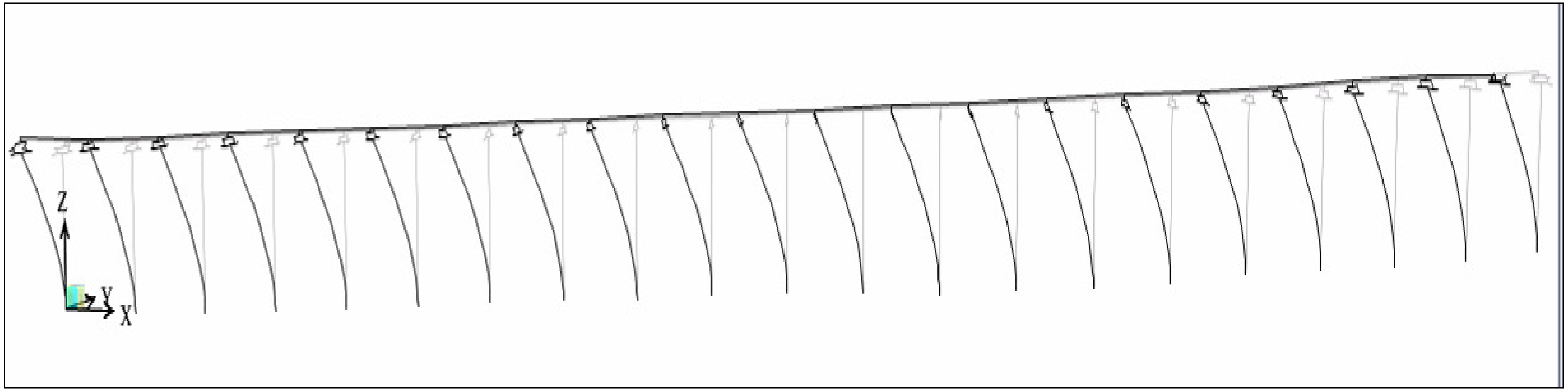

Figure 6.11 The first mode of the Unisolated system model is in U1 direction parallel to the bridge alignment with a period of 2.68 sec

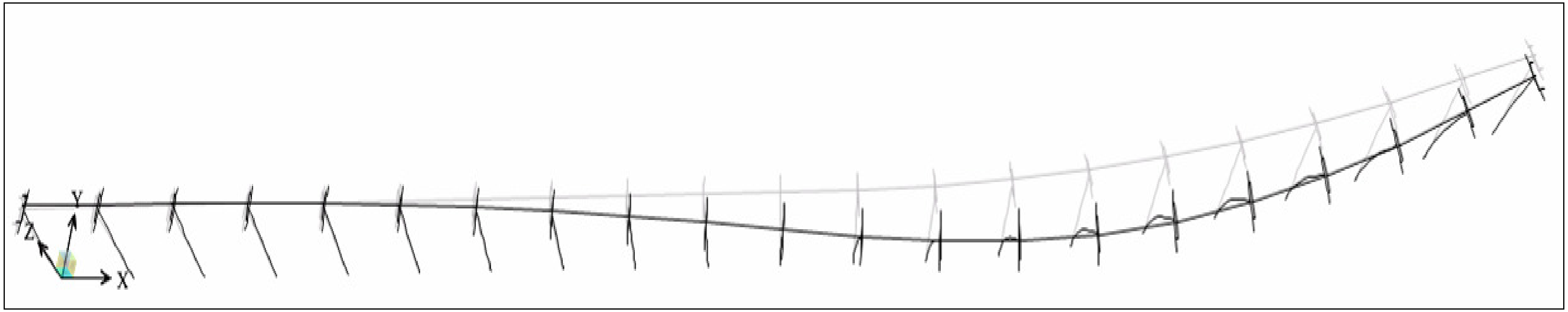

Figure 6.12 The second mode of the Unisolated system model is in U2 direction orthogonal to the bridge alignment with a period of 1.90 sec.

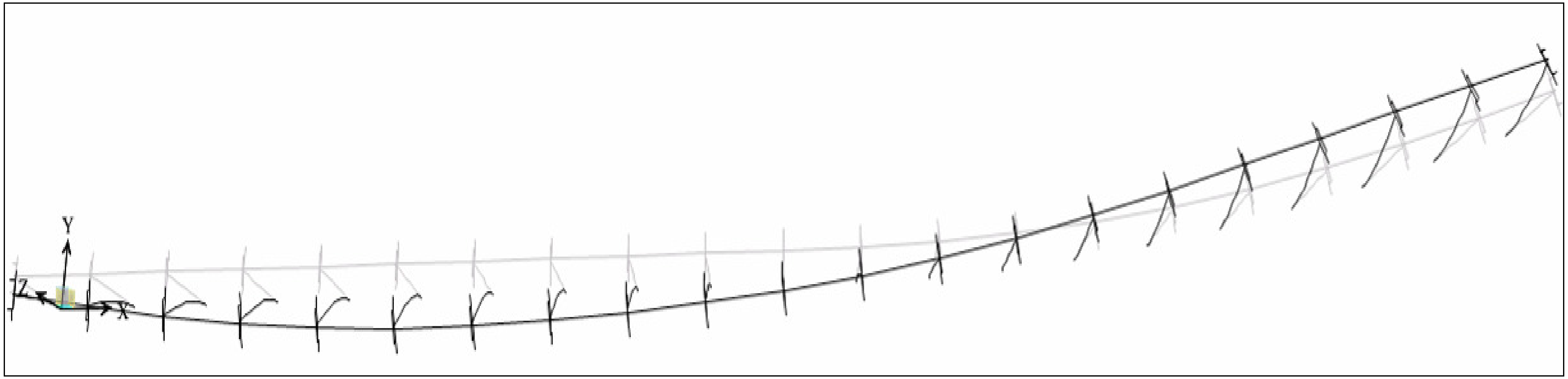

Figure 6.13 The third mode of the Unisolated system model is in U2 direction orthogonal to the bridge alignment with a period of 1.84 sec.

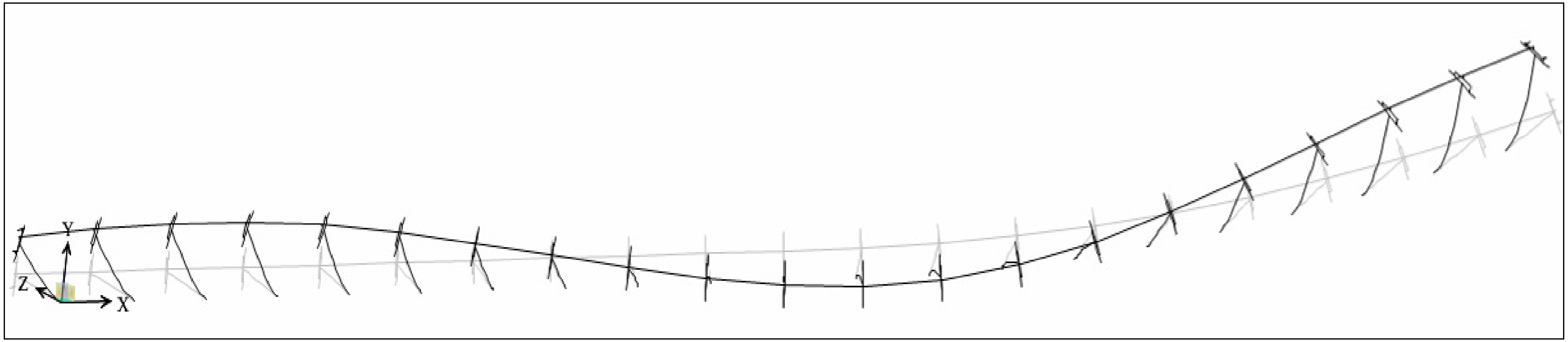

Figure 6.14 The fourth mode of the Unisolated system model is in U2 direction orthogonal to the bridge alignment with a period of 1.78 sec.

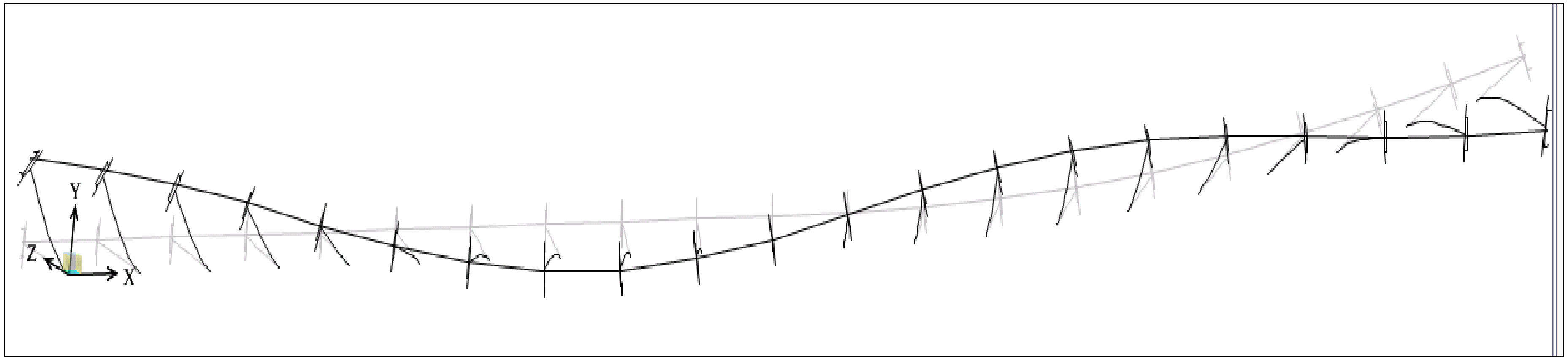

Figure 6.15 The fifth mode of the Unisolated system model is in U2 direction orthogonal to the bridge alignment with a period of 1.65 sec.

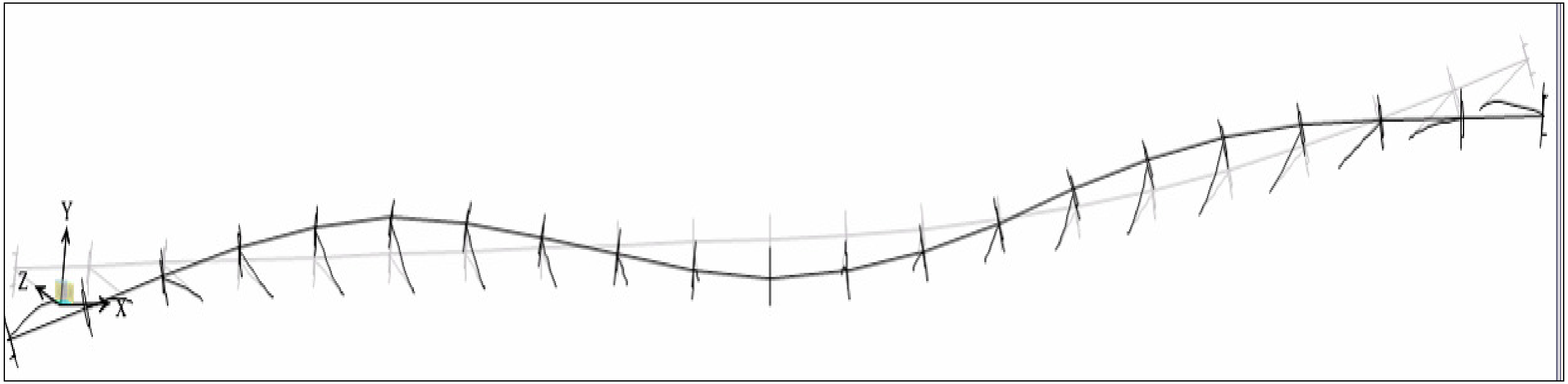

Figure 6.16 The sixth mode of the Unisolated system model is in U2 direction orthogonal to the bridge alignment with a period of 1.47 sec.

6.1.3. FPB Deformations of the Isolated System

In the records DZC270 and YPT060 the FPB's exceeded their capacity. When examined, these records have the largest displacement values, 150 cm and 130 cm respectively for periods around 5 sec.

FPB Deformations (Longitudinal Direction)

	EQ Applied in Longitudinal Direction														
Pier / Record	**01A H-CBR230 U1**		**02A BOL090 U1**		**03A DZC270 U1**		**04A TAZ000 U1**		**05A TAZ090 U1**		**06A YPT060 U1**		**07A YPT330 U1**		**Capacity**
(#)	*U2 (m)*		*U2 (m)*		*U2 (m)*		*U2 (m)*		*U2 (m)*		*U2 (m)*		*U2 (m)*		*U2 (m)*
20	0.17	0.18	0.29	0.29	0.97	0.97	0.84	0.82	0.66	0.64	1.07	1.06	0.80	0.79	0.90
21	0.07	0.07	0.17	0.17	0.82	0.81	0.55	0.54	0.37	0.37	0.84	0.84	0.61	0.60	0.70
22	0.09	0.09	0.19	0.19	0.82	0.82	0.59	0.59	0.40	0.40	0.87	0.87	0.64	0.63	0.70
23	0.08	0.08	0.18	0.18	0.82	0.81	0.58	0.58	0.39	0.39	0.86	0.86	0.63	0.63	0.70
24	0.08	0.08	0.18	0.18	0.82	0.81	0.58	0.58	0.40	0.40	0.86	0.86	0.63	0.63	0.70
25	0.08	0.08	0.18	0.18	0.82	0.81	0.58	0.58	0.40	0.40	0.86	0.86	0.63	0.63	0.70
26	0.09	0.09	0.19	0.19	0.82	0.82	0.59	0.58	0.41	0.41	0.90	0.90	0.67	0.67	0.70
27	0.09	0.09	0.19	0.19	0.82	0.82	0.59	0.58	0.41	0.41	0.90	0.90	0.67	0.67	0.70
28	0.08	0.08	0.18	0.18	0.82	0.81	0.58	0.58	0.40	0.40	0.86	0.86	0.63	0.63	0.70
29	0.09	0.09	0.19	0.19	0.82	0.82	0.58	0.59	0.41	0.41	0.90	0.90	0.67	0.67	0.70
30	0.09	0.09	0.19	0.20	0.82	0.82	0.58	0.59	0.41	0.42	0.90	0.90	0.67	0.67	0.70
31	0.08	0.08	0.18	0.19	0.81	0.83	0.57	0.59	0.39	0.40	0.86	0.86	0.62	0.63	0.70
32	0.07	0.08	0.17	0.18	0.83	0.86	0.56	0.58	0.37	0.38	0.83	0.84	0.59	0.60	0.70
33	0.07	0.08	0.16	0.18	0.83	0.86	0.56	0.58	0.37	0.38	0.83	0.84	0.58	0.60	0.70
34	0.07	0.08	0.16	0.17	0.83	0.86	0.55	0.57	0.36	0.38	0.83	0.84	0.58	0.59	0.70
35	0.07	0.08	0.16	0.17	0.84	0.86	0.55	0.57	0.36	0.38	0.82	0.84	0.58	0.59	0.70
36	0.08	0.08	0.17	0.18	0.82	0.85	0.56	0.58	0.37	0.39	0.85	0.87	0.61	0.62	0.70
37	0.08	0.08	0.17	0.18	0.83	0.86	0.55	0.57	0.36	0.38	0.84	0.86	0.60	0.61	0.70
38	0.08	0.08	0.16	0.17	0.85	0.87	0.55	0.56	0.35	0.36	0.83	0.84	0.57	0.58	0.70
39	0.07	0.07	0.14	0.15	0.82	0.85	0.50	0.51	0.32	0.32	0.80	0.81	0.55	0.56	0.70
40	0.16	0.14	0.27	0.26	0.93	0.95	0.78	0.88	0.55	0.68	0.97	1.03	0.71	0.74	0.90

Table 6.5 FPB Deformations of the Isolated System Model – Longitudinal Direction

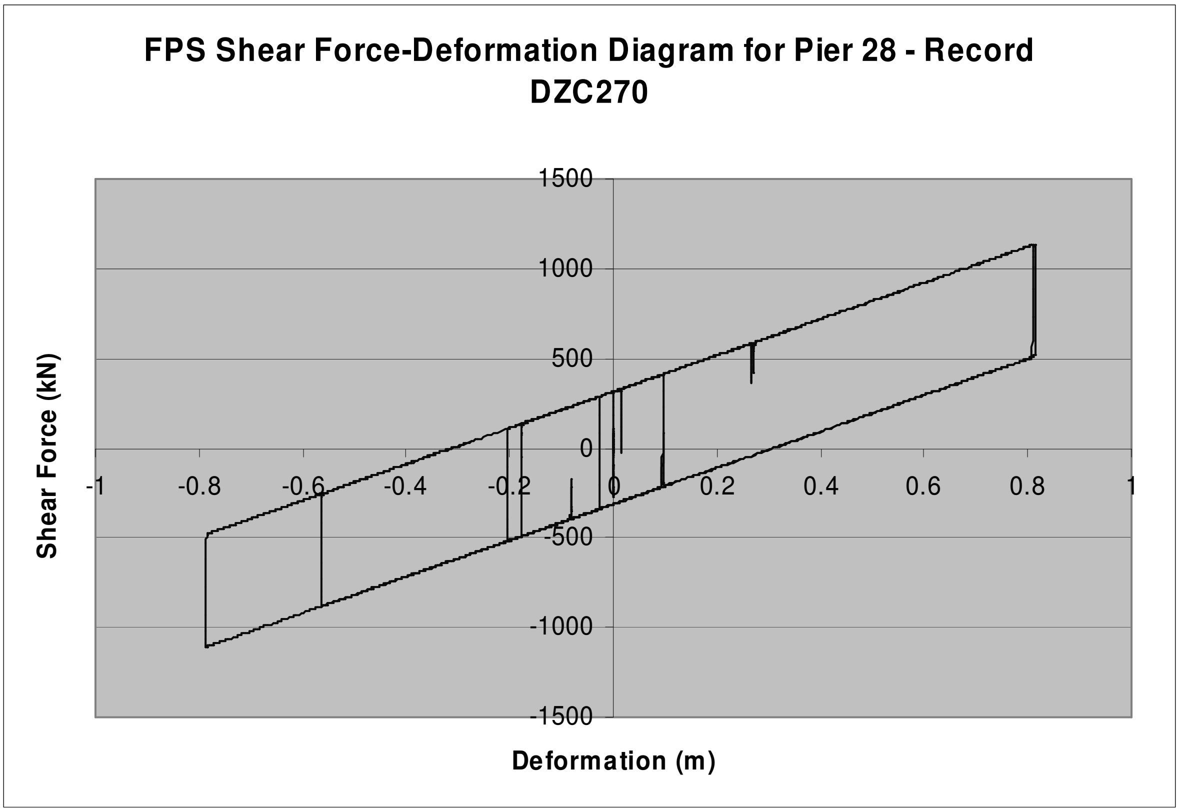

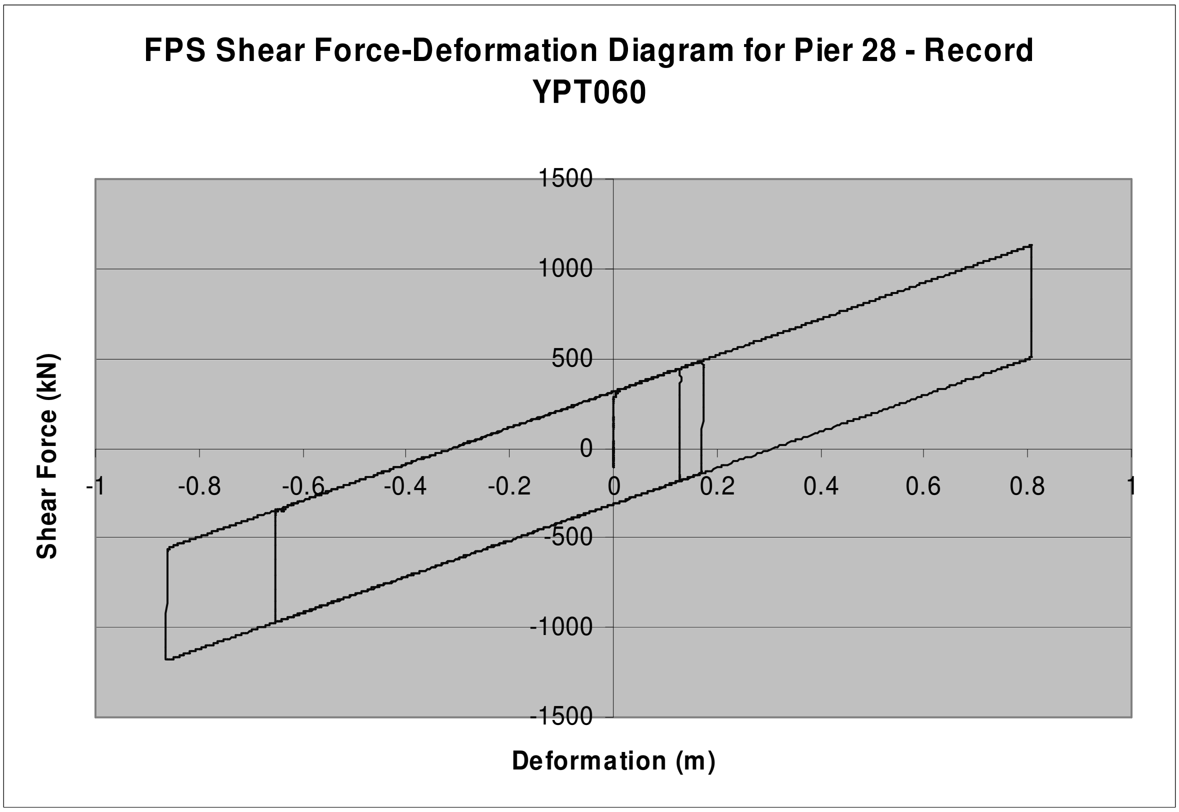

Figure 6.17 Shear Force-Deformation Graphs for Pier 28 -DZC270 and YPT060 longitudinal analyses

FPB Deformations (Transversal Direction)															
	EQ Applied in Transversal Direction														
Pier / Record	**01B H-CBR230 U2**		**02B BOL090 U2**		**03B DZC270 U2**		**04B TAZ000 U2**		**05B TAZ090 U2**		**06B YPT060 U2**		**07B YPT330 U2**		**Capacity**
(#)	*U3 (m)*		*U3 (m)*		*U3 (m)*		*U3 (m)*		*U3 (m)*		*U3 (m)*		*U3 (m)*		*U3 (m)*
20	0.29	0.29	0.50	0.50	1.01	1.01	0.46	0.46	0.54	0.54	0.88	0.89	0.52	0.52	0.90
21	0.20	0.20	0.33	0.33	0.90	0.90	0.33	0.33	0.46	0.46	0.85	0.85	0.45	0.45	0.70
22	0.21	0.21	0.35	0.35	0.92	0.92	0.34	0.35	0.48	0.48	0.87	0.87	0.46	0.46	0.70
23	0.20	0.20	0.34	0.34	0.91	0.91	0.34	0.34	0.48	0.48	0.86	0.86	0.47	0.46	0.70
24	0.20	0.20	0.34	0.34	0.91	0.91	0.34	0.34	0.48	0.48	0.86	0.86	0.47	0.47	0.70
25	0.20	0.19	0.34	0.34	0.91	0.91	0.34	0.34	0.48	0.48	0.85	0.86	0.47	0.47	0.70
26	0.20	0.20	0.36	0.35	0.89	0.89	0.35	0.35	0.46	0.46	0.85	0.85	0.47	0.47	0.70
27	0.19	0.19	0.35	0.35	0.89	0.89	0.35	0.35	0.46	0.46	0.85	0.85	0.47	0.47	0.70
28	0.19	0.19	0.33	0.33	0.90	0.90	0.34	0.34	0.47	0.47	0.86	0.86	0.47	0.47	0.70
29	0.19	0.19	0.35	0.35	0.88	0.88	0.35	0.35	0.46	0.46	0.85	0.85	0.46	0.46	0.70
30	0.19	0.19	0.35	0.35	0.88	0.88	0.35	0.35	0.47	0.46	0.85	0.85	0.46	0.46	0.70
31	0.19	0.19	0.33	0.33	0.90	0.90	0.35	0.35	0.48	0.48	0.86	0.86	0.46	0.46	0.70
32	0.19	0.19	0.31	0.31	0.92	0.92	0.36	0.36	0.49	0.49	0.87	0.87	0.47	0.47	0.70
33	0.19	0.19	0.31	0.31	0.92	0.92	0.36	0.36	0.49	0.49	0.87	0.87	0.47	0.47	0.70
34	0.19	0.18	0.31	0.31	0.92	0.92	0.36	0.36	0.48	0.48	0.87	0.87	0.48	0.48	0.70
35	0.18	0.18	0.30	0.30	0.92	0.92	0.36	0.36	0.48	0.48	0.86	0.86	0.48	0.48	0.70
36	0.18	0.18	0.32	0.32	0.90	0.90	0.34	0.34	0.48	0.48	0.85	0.85	0.47	0.47	0.70
37	0.18	0.18	0.31	0.31	0.89	0.89	0.33	0.33	0.47	0.47	0.83	0.83	0.47	0.47	0.70
38	0.18	0.18	0.30	0.30	0.90	0.90	0.35	0.35	0.47	0.47	0.82	0.82	0.48	0.48	0.70
39	0.17	0.17	0.27	0.27	0.87	0.87	0.32	0.32	0.45	0.45	0.80	0.80	0.46	0.46	0.70
40	0.30	0.30	0.44	0.44	0.94	0.95	0.44	0.44	0.58	0.58	0.89	0.89	0.52	0.52	0.90

Table 6.6 FPB Deformations of the Isolated System Model – Transversal Direction

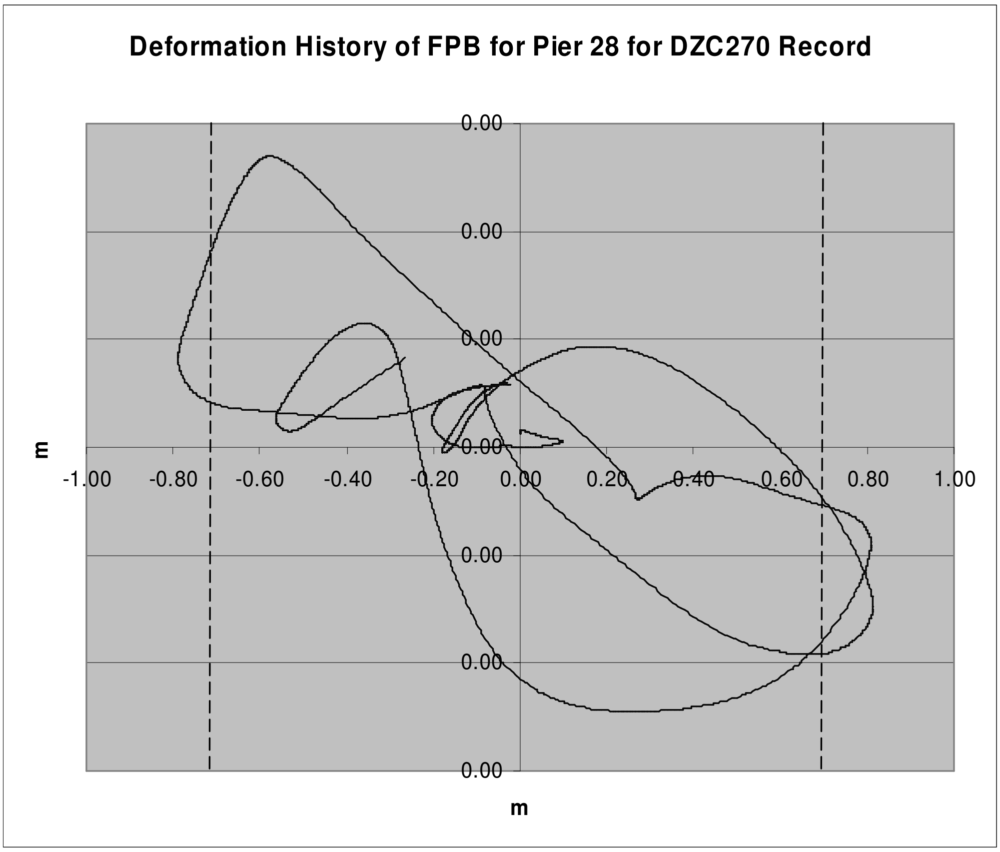

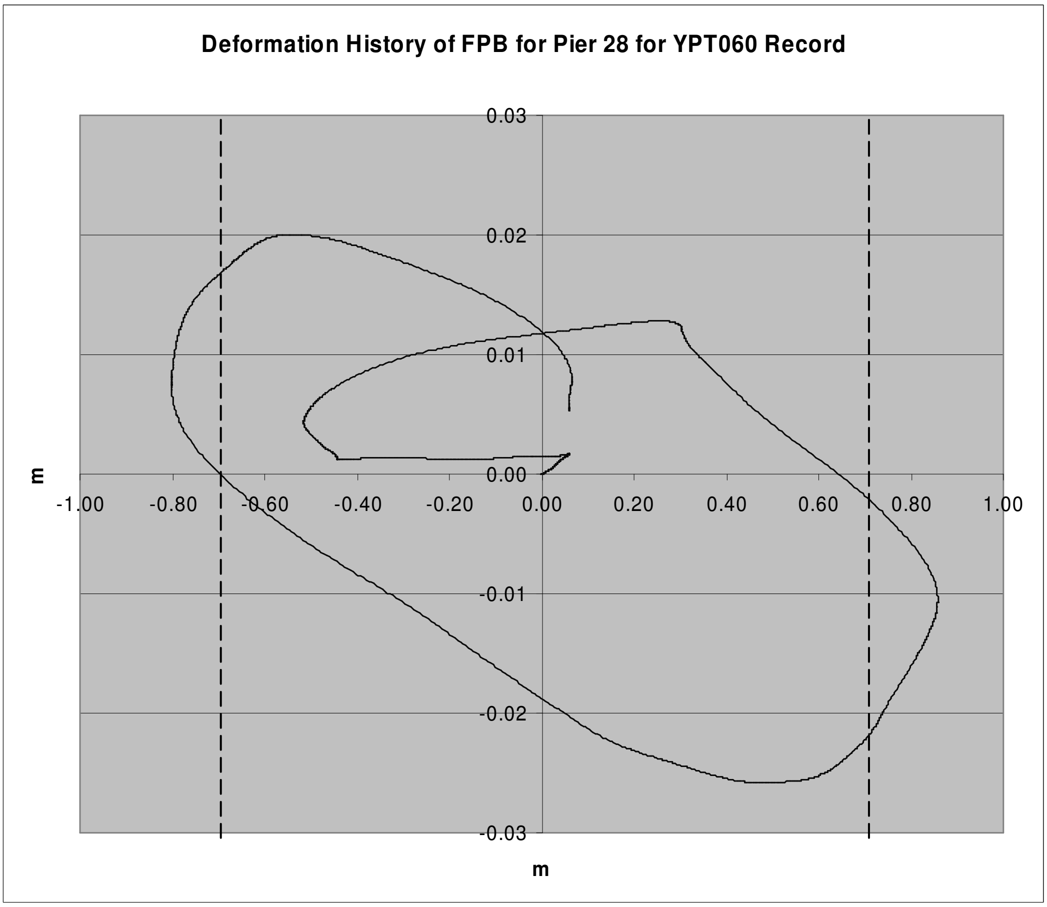

Figure 6.18 Deformation History Graphs for Pier 28 - DZC270 and YPT060 longitudinal analyses

6.1.4. Pier Frame Forces

6.1.4.1. Axial Forces

Axial forces remained as pressure forces during all analyses. No tension forces were observed.

- Isolated Model

Axial Forces ***(P)***

	EQ Applied in Longitudinal Direction							EQ Applied in Transversal Direction						
Pier / Record	**01A H-CBR230 U1**	**02A BOL090 U1**	**03A DZC270 U1**	**04A TAZ000 U1**	**05A TAZ090 U1**	**06A YPT060 U1**	**07A YPT330 U1**	**01B H-CBR230 U2**	**02B BOL090 U2**	**03B DZC270 U2**	**04B TAZ000 U2**	**05B TAZ090 U2**	**06B YPT060 U2**	**07B YPT330 U2**
(#)	*P (kN)*	*P (kN)*	*P (kN)*	*P (kN)*	*P (kN)*	*P (kN)*	*P (kN)*	*P (kN)*	*P (kN)*	*P (kN)*	*P (kN)*	*P (kN)*	*P (kN)*	*P (kN)*
20	32,619.78	32,357.96	32,306.59	32,569.86	32,991.85	32,070.41	32,139.99	31,871.12	31,859.24	31,887.79	31,868.02	31,871.70	31,904.79	31,887.53
21	35,718.23	35,747.48	35,772.39	35,839.95	35,784.87	35,697.51	35,759.16	35,659.74	35,649.84	35,673.47	35,660.18	35,649.24	35,665.49	35,658.31
22	33,993.36	34,009.03	34,012.05	34,060.26	34,064.74	33,986.95	34,024.13	33,976.02	33,957.71	33,971.77	33,967.07	33,961.42	33,965.86	33,961.52
23	34,384.41	34,391.45	34,396.28	34,413.30	34,401.96	34,386.32	34,392.61	34,396.39	34,380.98	34,381.24	34,384.39	34,380.81	34,376.28	34,373.94
24	34,275.00	34,281.46	34,288.52	34,302.93	34,290.93	34,273.21	34,284.15	34,289.74	34,271.53	34,274.20	34,273.54	34,275.84	34,273.01	34,268.59
25	34,292.89	34,298.86	34,299.07	34,312.39	34,306.86	34,292.38	34,306.42	34,316.05	34,299.20	34,295.53	34,298.42	34,309.37	34,298.54	34,290.18
26	33,957.20	33,974.08	33,967.77	34,042.78	34,009.54	33,961.96	33,995.41	33,952.35	33,939.70	33,958.40	33,946.87	33,943.16	33,955.97	33,944.14
27	33,949.23	33,955.10	33,965.95	33,980.81	33,970.55	33,950.19	33,964.17	33,957.72	33,941.10	33,954.43	33,945.16	33,944.15	33,944.88	33,943.92
28	34,303.33	34,308.01	34,307.21	34,329.37	34,321.42	34,301.31	34,309.45	34,309.58	34,294.64	34,292.40	34,296.95	34,303.72	34,297.46	34,292.11
29	33,976.42	33,991.63	33,982.61	34,040.74	34,017.98	33,980.72	33,995.24	33,975.84	33,956.65	33,961.06	33,957.32	33,958.59	33,953.12	33,952.72
30	33,951.98	33,961.40	33,958.34	33,995.22	33,986.08	33,953.67	33,958.90	33,981.04	33,967.92	33,951.60	33,958.97	33,967.83	33,951.09	33,945.19
31	34,368.99	34,377.45	34,394.63	34,406.46	34,391.05	34,378.41	34,401.65	34,418.40	34,380.59	34,370.07	34,372.15	34,375.93	34,363.22	34,353.60
32	34,736.28	34,737.82	34,768.65	34,786.03	34,765.07	34,745.50	34,769.70	34,782.54	34,737.18	34,734.57	34,742.98	34,740.86	34,719.99	34,716.18
33	34,728.56	34,730.76	34,734.70	34,747.52	34,738.62	34,731.72	34,731.21	34,799.16	34,755.83	34,748.91	34,762.95	34,756.56	34,754.03	34,731.67
34	34,768.44	34,775.33	34,787.18	34,799.91	34,786.60	34,776.57	34,783.20	34,830.07	34,785.98	34,782.61	34,795.03	34,789.78	34,784.39	34,768.63
35	34,810.70	34,812.62	34,820.78	34,831.49	34,822.33	34,816.58	34,827.86	34,886.69	34,830.59	34,836.02	34,840.69	34,844.43	34,835.99	34,821.31
36	34,505.59	34,511.35	34,530.40	34,554.33	34,526.37	34,520.51	34,523.06	34,556.86	34,514.97	34,500.60	34,521.48	34,524.43	34,497.72	34,490.75
37	34,664.35	34,674.21	34,674.13	34,692.11	34,681.09	34,670.04	34,682.31	34,731.14	34,688.54	34,703.50	34,696.09	34,699.64	34,691.30	34,681.09
38	34,670.75	34,667.97	34,723.03	34,877.00	34,754.85	34,685.41	34,723.93	34,694.24	34,653.54	34,669.34	34,680.44	34,662.27	34,660.07	34,647.91
39	36,486.74	36,537.31	36,527.52	36,588.40	36,579.64	36,495.40	36,500.60	36,511.35	36,486.73	36,516.76	36,470.66	36,495.24	36,536.19	36,481.78
40	33,617.15	33,108.16	33,257.05	33,227.59	33,398.94	33,022.23	32,881.13	32,919.28	32,811.91	32,842.17	32,828.41	32,795.80	32,822.39	32,734.78

Table 6.7 Axial Forces of the Isolated System Model

- Unisolated Model

Axial Forces *(P)*														
	EQ Applied in Longitudinal Direction							EQ Applied in Transversal Direction						
Pier / Record	**01A H-CBR230 U1**	**02A BOL090 U1**	**03A DZC270 U1**	**04A TAZ000 U1**	**05A TAZ090 U1**	**06A YPT060 U1**	**07A YPT330 U1**	**01B H-CBR230 U2**	**02B BOL090 U2**	**03B DZC270 U2**	**04B TAZ000 U2**	**05B TAZ090 U2**	**06B YPT060 U2**	**07B YPT330 U2**
(#)	*P (kN)*	*P (kN)*	*P (kN)*	*P (kN)*	*P (kN)*	*P (kN)*	*P (kN)*	*P (kN)*	*P (kN)*	*P (kN)*	*P (kN)*	*P (kN)*	*P (kN)*	*P (kN)*
20	32,523.74	32,176.00	32,271.66	32,281.68	32,531.28	32,235.62	32,215.33	31,924.52	31,872.59	31,890.97	31,883.82	31,916.59	31,863.00	31,860.05
21	35,959.51	35,839.90	35,969.26	36,054.90	35,956.74	36,056.19	36,032.97	35,674.38	35,660.16	35,673.64	35,682.50	35,672.37	35,663.28	35,662.37
22	34,030.88	34,019.03	34,105.49	34,079.63	34,048.19	34,078.56	34,084.98	33,966.19	33,949.02	33,956.34	33,952.56	33,968.87	33,949.70	33,949.38
23	34,426.50	34,398.51	34,408.51	34,427.68	34,414.77	34,426.40	34,420.83	34,391.90	34,377.12	34,380.95	34,382.72	34,396.03	34,374.85	34,373.50
24	34,322.90	34,272.65	34,276.12	34,286.89	34,280.10	34,278.18	34,272.53	34,293.13	34,265.47	34,271.18	34,271.35	34,285.48	34,262.99	34,263.99
25	34,335.58	34,302.65	34,303.78	34,300.03	34,304.25	34,293.92	34,295.85	34,330.66	34,296.07	34,303.78	34,310.15	34,315.37	34,286.47	34,289.39
26	34,021.64	33,948.21	33,968.68	33,952.59	33,955.26	33,963.04	33,951.71	33,957.08	33,932.41	33,941.45	33,948.82	33,959.82	33,933.40	33,934.20
27	34,012.45	33,951.55	33,952.45	33,951.86	33,948.01	33,950.89	33,945.30	33,972.66	33,938.70	33,952.78	33,949.03	33,960.78	33,934.48	33,935.01
28	34,338.57	34,308.46	34,306.54	34,302.06	34,301.91	34,296.77	34,295.34	34,331.78	34,291.04	34,309.92	34,312.49	34,319.45	34,286.98	34,284.99
29	34,108.55	33,982.63	33,992.98	34,013.64	33,985.73	33,996.56	33,971.14	33,969.06	33,947.47	33,950.45	33,969.52	33,957.53	33,942.84	33,942.71
30	33,987.25	33,953.53	33,951.44	33,946.91	33,956.10	33,945.68	33,943.94	33,976.69	33,961.26	33,970.07	33,983.84	33,983.21	33,959.94	33,956.47
31	34,458.18	34,375.25	34,375.31	34,379.75	34,386.10	34,375.17	34,374.99	34,411.95	34,296.07	34,370.22	34,381.75	34,384.42	34,349.08	34,347.95
32	34,818.04	34,741.03	34,746.25	34,735.30	34,745.09	34,737.04	34,731.23	34,784.99	34,733.24	34,745.39	34,743.15	34,756.49	34,714.65	34,711.11
33	34,756.13	34,732.58	34,732.16	34,733.62	34,736.42	34,724.67	34,726.49	34,794.88	34,753.43	34,764.56	34,766.48	34,778.55	34,733.21	34,739.73
34	34,821.19	34,770.36	34,779.61	34,785.54	34,788.04	34,780.34	34,773.41	34,828.12	34,785.31	34,792.88	34,790.21	34,805.67	34,761.11	34,761.92
35	34,843.94	34,818.55	34,813.54	34,813.24	34,814.62	34,808.01	34,806.93	34,895.00	34,833.12	34,843.89	34,864.31	34,859.52	34,812.00	34,817.40
36	34,594.25	34,513.72	34,512.17	34,513.45	34,510.75	34,507.79	34,499.56	34,553.37	34,508.92	34,506.59	34,507.78	34,526.17	34,485.16	34,487.76
37	34,686.85	34,670.76	34,674.97	34,672.78	34,676.09	34,670.59	34,669.51	34,729.27	34,683.90	34,690.78	34,710.49	34,708.12	34,666.12	34,666.01
38	34,760.72	34,690.40	34,763.74	34,752.45	34,742.73	34,840.58	34,787.86	34,692.88	34,647.96	34,663.75	34,718.80	34,709.04	34,643.88	34,649.66
39	36,701.35	36,555.17	36,730.70	36,668.59	36,682.68	36,684.85	36,670.19	36,509.07	36,462.15	36,477.66	36,475.52	36,491.78	36,447.89	36,452.80
40	33,461.28	33,069.55	33,050.49	33,245.89	33,139.37	32,955.96	32,952.44	32,897.78	32,786.00	32,770.94	32,828.41	32,805.99	32,703.89	32,734.93

Table 6.8 Axial Forces of the Unisolated System Model

6.1.4.2. Shear Forces

The shear capacity of the piers greatly exceeds the earthquke demand.

- Isolated Model

Shear Forces ***(Longitudinal Direction)***								
	EQ Applied in Longitudinal Direction							
Pier / Record	**01A H-CBR230 U1**	**02A BOL090 U1**	**03A DZC270 U1**	**04A TAZ000 U1**	**05A TAZ090 U1**	**06A YPT060 U1**	**07A YPT330 U1**	**Shear Capacity**
(#)	*V2 (kN)*	*V2 (kN)*	*V2 (kN)*	*V2 (kN)*	*V2 (kN)*	*V2 (kN)*	*V2 (kN)*	*V2 (kN)*
20	7,312.36	4,557.08	5,849.27	10,501.19	10,834.43	4,451.64	5,813.57	30,000.00
21	7,604.30	4,190.15	5,876.26	7,990.19	6,918.41	5,111.01	4,445.87	30,000.00
22	7,741.08	4,184.73	5,374.81	8,372.89	7,266.46	5,012.47	4,540.61	30,000.00
23	7,710.25	4,186.95	5,499.06	8,270.59	7,181.27	5,031.25	4,518.49	30,000.00
24	7,727.08	4,184.97	5,466.78	8,299.14	7,203.03	5,020.90	4,524.16	30,000.00
25	7,733.40	4,185.06	5,472.72	8,293.62	7,196.97	5,017.47	4,521.94	30,000.00
26	7,410.27	3,969.33	5,080.13	8,508.26	7,481.47	4,774.47	4,693.91	30,000.00
27	7,411.98	3,964.95	5,068.61	8,507.58	7,476.22	4,774.65	4,693.52	30,000.00
28	7,744.77	4,176.22	5,473.23	8,294.74	7,187.57	5,015.66	4,519.78	30,000.00
29	7,411.00	3,963.22	5,040.93	8,507.77	7,462.09	4,780.42	4,690.05	30,000.00
30	7,405.36	3,960.70	5,029.65	8,508.87	7,456.81	4,784.05	4,690.17	30,000.00
31	7,450.84	3,889.47	5,467.45	8,180.74	7,091.50	4,997.63	4,484.48	30,000.00
32	7,934.53	4,431.03	5,967.71	7,849.88	6,897.99	5,185.46	4,205.37	30,000.00
33	7,908.50	4,416.44	5,988.69	7,832.71	6,864.25	5,193.74	4,192.91	30,000.00
34	7,861.30	4,392.75	6,019.31	7,773.15	6,773.33	5,195.02	4,146.42	30,000.00
35	7,857.30	4,392.64	6,023.96	7,770.12	6,755.66	5,200.11	4,145.01	30,000.00
36	7,589.76	4,100.72	5,849.92	8,149.69	6,879.59	5,069.65	4,379.09	30,000.00
37	7,522.61	4,071.38	6,011.77	8,050.98	6,695.53	5,075.01	4,297.12	30,000.00
38	7,721.01	4,306.41	5,891.82	7,659.22	6,447.32	5,175.18	3,988.97	30,000.00
39	7,589.76	4,368.16	5,834.68	7,240.66	6,035.94	5,241.81	3,906.23	30,000.00
40	8,105.45	4,068.82	5,573.53	9,714.23	8,166.44	4,461.85	4,605.21	30,000.00

Table 6.9 Shear Forces of the Isolated System Model – Longitudinal Direction

Shear Forces *(Transversal Direction)*								
	EQ Applied in Transversal Direction							
Pier / Record	**01B H-CBR230 U2**	**02B BOL090 U2**	**03B DZC270 U2**	**04B TAZ000 U2**	**05B TAZ090 U2**	**06B YPT060 U2**	**07B YPT330 U2**	**Shear Capacity**
(#)	*V3 (kN)*	*V3 (kN)*	*V3 (kN)*	*V3 (kN)*	*V3 (kN)*	*V3 (kN)*	*V3 (kN)*	*V3 (kN)*
20	8,631.38	15,104.40	10,311.12	13,514.02	16,010.04	5,672.69	5,766.77	42,000.00
21	7,830.24	9,304.44	9,004.33	11,829.15	12,334.90	7,027.67	5,134.41	42,000.00
22	7,714.51	10,455.34	9,052.53	12,452.98	12,710.57	6,928.79	4,921.74	42,000.00
23	7,765.88	10,258.48	9,057.97	12,258.75	12,566.23	6,965.00	4,974.48	42,000.00
24	7,697.89	10,323.17	8,965.64	12,289.38	12,625.08	6,901.23	4,963.86	42,000.00
25	7,698.23	10,339.31	8,942.77	12,295.92	12,695.03	6,865.83	4,997.11	42,000.00
26	7,408.58	10,382.35	8,467.94	11,666.81	12,032.40	6,751.47	5,104.73	42,000.00
27	7,480.47	10,334.01	8,476.09	11,699.90	12,031.03	6,799.87	5,092.78	42,000.00
28	7,772.92	10,277.34	8,989.04	12,391.34	12,742.98	6,957.67	4,983.19	42,000.00
29	7,472.48	10,219.85	8,451.78	11,770.84	12,017.98	6,972.56	5,114.85	42,000.00
30	7,462.25	10,186.11	8,580.63	11,750.11	12,008.18	6,939.97	5,147.99	42,000.00
31	7,638.76	10,027.89	9,095.48	12,133.62	12,636.01	6,949.47	5,009.17	42,000.00
32	7,927.74	9,795.81	9,590.82	12,947.33	13,462.02	6,926.57	5,213.07	42,000.00
33	8,002.87	9,763.39	9,534.97	12,857.06	13,408.22	7,045.30	5,098.10	42,000.00
34	7,941.12	9,709.87	9,378.57	12,762.66	13,355.63	7,059.91	5,027.07	42,000.00
35	7,917.16	9,736.66	9,311.29	12,820.05	13,405.35	6,946.77	5,047.23	42,000.00
36	7,925.55	9,926.19	8,993.89	12,015.10	12,407.84	6,976.15	4,808.19	42,000.00
37	7,872.93	9,684.41	8,978.64	11,840.43	12,212.39	6,914.23	4,793.24	42,000.00
38	7,692.45	9,501.87	9,268.21	12,607.78	13,092.47	7,081.71	5,059.03	42,000.00
39	7,521.27	8,127.09	9,365.76	11,661.88	12,474.03	7,200.95	5,259.75	42,000.00
40	9,085.71	14,192.63	8,581.12	14,990.29	15,499.93	6,604.67	6,232.36	42,000.00

Table 6.10 Shear Forces of the Isolated System Model – Transversal Direction

- Unisolated Model

Shear Forces

	EQ Applied in Longitudinal Direction							
Pier / Record	**01A H-CBR230 U1**	**02A BOL090 U1**	**03A DZC270 U1**	**04A TAZ000 U1**	**05A TAZ090 U1**	**06A YPT060 U1**	**07A YPT330 U1**	**Shear Capacity**
(#)	*V2 (kN)*	*V2 (kN)*	*V2 (kN)*	*V2 (kN)*	*V2 (kN)*	*V2 (kN)*	*V2 (kN)*	*V2 (kN)*
20	8,891.38	4,688.10	7,765.32	7,219.10	7,673.16	9,247.94	8,226.85	30,000.00
21	8,436.27	4,862.45	7,516.25	5,549.28	7,084.81	8,912.12	7,768.98	30,000.00
22	8,493.24	4,931.00	7,553.51	5,518.92	7,082.06	8,895.48	7,766.46	30,000.00
23	8,529.00	5,013.64	7,563.49	5,583.45	7,085.47	8,894.52	7,802.08	30,000.00
24	8,797.93	5,111.00	7,634.89	5,512.95	7,038.59	8,925.35	7,840.27	30,000.00
25	9,123.57	5,205.17	7,724.34	5,396.91	6,966.28	8,973.42	7,884.24	30,000.00
26	9,198.04	5,003.80	7,922.19	6,104.30	7,236.08	9,240.69	8,077.70	30,000.00
27	9,494.14	5,020.89	8,032.36	5,928.10	7,153.90	9,291.46	8,088.96	30,000.00
28	10,003.79	5,342.95	7,968.03	5,059.73	6,740.01	9,136.28	7,974.40	30,000.00
29	9,732.37	5,065.39	8,180.58	5,767.11	7,067.48	9,316.56	8,053.14	30,000.00
30	9,601.20	5,097.99	8,210.93	5,883.58	7,094.10	9,271.80	7,999.65	30,000.00
31	9,721.77	5,198.54	7,907.76	4,859.57	6,768.12	9,036.79	7,772.19	30,000.00
32	9,504.86	5,619.15	7,967.02	4,550.92	6,883.54	8,520.11	7,502.97	30,000.00
33	9,364.64	5,493.13	7,938.29	4,680.24	6,861.59	8,544.91	7,488.42	30,000.00
34	9,265.86	5,348.72	7,867.78	4,756.00	6,789.91	8,569.57	7,465.16	30,000.00
35	9,264.64	5,238.86	7,822.94	4,799.92	6,731.52	8,597.41	7,461.92	30,000.00
36	9,453.51	5,072.38	8,222.75	5,263.81	6,687.46	9,092.84	7,649.15	30,000.00
37	9,411.44	5,036.88	8,291.03	5,250.20	6,580.71	9,080.64	7,591.65	30,000.00
38	9,175.17	5,003.50	7,734.11	4,687.82	6,449.70	8,549.65	7,302.50	30,000.00
39	9,179.86	4,967.91	7,772.88	4,686.79	6,428.47	8,523.03	7,251.49	30,000.00
40	9,194.36	4,961.26	8,335.48	5,028.02	6,359.41	9,055.58	7,542.65	30,000.00

Table 6.11 Shear Forces of the Unisolated System Model – Longitudinal Direction

Shear Forces								
	EQ Applied in Transversal Direction							
Pier / Record	**01B H-CBR230 U2**	**02B BOL090 U2**	**03B DZC270 U2**	**04B TAZ000 U2**	**05B TAZ090 U2**	**06B YPT060 U2**	**07B YPT330 U2**	**Shear Capacity**
(#)	*V3 (kN)*	*V3 (kN)*	*V3 (kN)*	*V3 (kN)*	*V3 (kN)*	*V3 (kN)*	*V3 (kN)*	*V3 (kN)*
20	9,936.46	5,854.19	7,839.01	15,158.09	13,986.00	6,267.25	6,485.22	42,000.00
21	10,692.75	6,867.80	9,271.21	17,475.04	15,361.65	6,514.62	6,815.87	42,000.00
22	10,886.49	7,276.23	10,553.75	18,379.05	16,083.55	6,608.23	7,500.82	42,000.00
23	9,726.44	8,074.58	11,055.88	18,671.47	15,615.68	6,605.71	8,142.09	42,000.00
24	11,078.81	8,490.54	11,763.99	18,904.60	16,087.91	6,838.20	8,358.77	42,000.00
25	11,505.68	8,579.60	12,001.55	18,012.76	15,199.68	6,920.07	8,414.81	42,000.00
26	10,868.23	8,889.11	12,040.62	17,344.71	14,273.18	6,944.10	8,225.35	42,000.00
27	11,125.62	8,748.26	11,111.45	17,095.75	13,838.69	6,718.80	7,858.21	42,000.00
28	11,556.48	8,223.85	10,620.28	16,671.33	13,538.77	6,475.64	7,242.46	42,000.00
29	11,023.01	8,502.27	11,439.04	17,060.81	14,081.64	6,661.32	7,443.18	42,000.00
30	10,175.45	8,631.95	11,907.57	16,848.42	13,287.49	6,773.44	7,446.98	42,000.00
31	10,367.20	8,579.60	12,026.49	16,875.27	14,141.83	6,721.88	7,105.96	42,000.00
32	11,093.39	8,856.78	12,121.83	17,151.11	14,483.18	6,701.55	6,993.68	42,000.00
33	10,249.55	9,256.64	12,214.97	17,017.66	14,336.24	6,782.25	7,124.92	42,000.00
34	10,407.29	9,369.55	12,159.53	16,808.18	14,319.80	7,051.25	7,240.99	42,000.00
35	11,354.02	9,167.01	12,197.54	16,705.09	14,214.37	7,231.21	7,328.07	42,000.00
36	11,040.17	9,054.14	12,140.59	17,117.89	14,161.86	7,337.89	7,743.42	42,000.00
37	9,959.48	8,443.11	11,312.14	17,143.26	13,769.15	6,871.55	7,632.44	42,000.00
38	10,151.92	7,419.43	10,298.75	17,064.88	14,693.23	6,417.97	6,883.03	42,000.00
39	10,194.97	6,606.07	9,739.63	17,476.40	15,083.30	6,405.73	6,627.17	42,000.00
40	9,356.44	5,838.54	7,683.55	15,911.81	12,949.67	6,006.83	6,694.29	42,000.00

Table 6.12 Shear Forces of the Unisolated System Model – Transversal Direction

6.1.4.3. Moment Forces

In the isolated model the effective yield moment capacities of the piers exceeded the demand of the earthquakes letting the system behave linearly. In the Unisolated model Kobe Earthquake Taz000 record plastic hinges formed at four piers, but with strain values within the limits of the code.

- Isolated Model

Moment Forces ***(Transversal)***

	EQ Applied in Transversal Direction							
Pier / Record	**01B H-CBR230 U2**	**02B BOL090 U2**	**03B DZC270 U2**	**04B TAZ000 U2**	**05B TAZ090 U2**	**06B YPT060 U2**	**07B YPT330 U2**	**Effective Yield Moment**
(#)	*M2 (kNm)*	*M2 (kNm)*	*M2 (kNm)*	*M2 (kNm)*	*M2 (kNm)*	*M2 (kNm)*	*M2 (kNm)*	*M2 (kNm)*
20	227,578.71	561,634.96	362,350.90	465,108.70	433,528.09	223,144.16	198,982.29	766,300.00
21	171,380.63	314,059.76	318,329.92	335,057.27	355,714.40	278,423.29	203,179.64	766,300.00
22	171,678.06	351,768.68	321,096.39	351,728.06	373,031.40	276,457.72	196,869.21	766,300.00
23	164,719.60	344,271.82	323,339.29	345,855.67	367,414.83	277,112.97	199,070.61	766,300.00
24	162,264.70	347,115.19	321,126.72	345,716.70	369,302.88	275,031.80	198,741.72	766,300.00
25	161,345.88	347,398.64	319,592.36	345,078.99	371,064.54	271,770.36	199,143.00	766,300.00
26	168,532.29	372,122.89	308,590.48	347,222.98	341,186.93	273,393.40	195,099.79	766,300.00
27	171,671.77	370,085.58	308,011.99	348,007.12	340,777.89	275,051.60	194,529.22	766,300.00
28	168,803.10	344,188.98	318,081.40	347,328.48	372,540.29	274,836.85	197,736.51	766,300.00
29	173,938.50	365,645.96	305,844.18	351,180.73	341,039.77	279,854.58	194,505.88	766,300.00
30	173,701.34	365,166.49	309,850.20	350,752.68	339,847.15	279,707.60	195,699.99	766,300.00
31	164,784.80	337,290.15	324,576.53	348,218.91	371,166.65	273,085.47	199,152.77	766,300.00
32	155,557.05	312,888.25	344,661.48	358,418.10	390,293.93	277,961.95	199,763.31	766,300.00
33	155,007.69	312,374.45	343,441.12	355,560.13	388,407.18	281,358.40	198,016.13	766,300.00
34	155,189.36	310,684.01	338,026.25	351,894.13	385,984.89	282,316.20	196,774.52	766,300.00
35	158,011.75	311,931.79	335,497.07	352,157.25	386,330.11	278,302.19	196,863.56	766,300.00
36	163,532.55	332,285.82	318,246.63	337,993.63	362,003.92	276,413.06	193,712.48	766,300.00
37	161,410.91	323,110.83	317,251.87	333,834.12	355,779.14	274,314.64	193,036.51	766,300.00
38	155,637.02	303,706.24	332,460.49	346,351.65	377,553.61	286,667.82	191,562.19	766,300.00
39	145,901.78	259,533.92	335,052.60	314,872.36	350,026.37	293,335.25	201,241.98	766,300.00
40	242,042.62	489,692.79	296,269.43	444,661.53	486,705.99	259,575.52	216,854.44	766,300.00

Table 6.13 Moment Forces of the Isolated System Model – Transversal Direction

Moment Forces *(Longitudinal)*

	EQ Applied in Longitudinal Direction							
Pier / Record	**01A H-CBR230 U1**	**02A BOL090 U1**	**03A DZC270 U1**	**04A TAZ000 U1**	**05A TAZ090 U1**	**06A YPT060 U1**	**07A YPT330 U1**	**Effective Yield Moment**
(#)	*M3 (kNm)*	*M3 (kNm)*	*M3 (kNm)*	*M3 (kNm)*	*M3 (kNm)*	*M3 (kNm)*	*M3 (kNm)*	*M3 (kNm)*
20	99,782.25	167,660.37	207,114.45	316,140.55	336,307.51	124,015.10	207,709.62	479,500.00
21	87,096.71	98,981.60	224,117.88	189,463.36	167,921.78	194,524.38	178,430.83	479,500.00
22	87,844.24	103,765.98	218,578.13	201,939.59	190,068.18	181,600.37	180,830.54	479,500.00
23	87,820.07	102,587.42	219,827.96	198,509.20	184,098.71	185,170.92	180,268.22	479,500.00
24	87,882.05	102,962.08	219,440.07	199,477.49	185,597.27	184,289.56	180,410.09	479,500.00
25	87,824.92	103,000.36	219,357.99	199,241.03	185,299.53	184,496.13	180,336.30	479,500.00
26	84,854.14	105,478.02	217,949.78	193,599.19	196,310.26	186,142.46	193,454.92	479,500.00
27	84,651.06	105,576.68	217,797.95	193,577.17	196,290.07	185,897.34	193,541.43	479,500.00
28	87,218.48	103,273.83	218,958.32	199,226.61	185,478.79	184,302.61	180,238.24	479,500.00
29	84,142.00	105,716.85	217,402.40	193,724.06	196,122.53	185,157.41	193,308.08	479,500.00
30	83,892.39	105,690.05	217,348.76	193,780.11	196,068.72	184,873.89	193,206.76	479,500.00
31	86,770.78	103,108.57	218,345.75	199,924.09	184,064.62	184,333.12	179,566.47	479,500.00
32	90,173.59	100,425.06	219,325.61	200,070.17	171,417.21	183,153.41	169,679.03	479,500.00
33	90,174.82	99,974.00	218,993.01	199,696.56	170,229.31	183,215.46	169,227.63	479,500.00
34	89,931.40	98,943.06	218,684.05	198,146.73	167,087.56	183,231.06	167,462.46	479,500.00
35	89,836.55	98,872.38	218,414.11	198,038.28	166,503.15	183,847.47	167,433.95	479,500.00
36	85,892.06	100,132.27	215,878.19	196,839.20	174,823.84	183,959.04	175,226.03	479,500.00
37	85,312.48	98,252.54	215,315.37	194,491.23	167,965.87	184,662.59	172,346.34	479,500.00
38	88,039.58	95,916.92	216,467.74	195,945.05	161,727.23	181,137.73	161,269.64	479,500.00
39	87,769.31	91,052.40	222,488.01	183,074.91	149,518.44	192,441.69	159,545.60	479,500.00
40	88,974.82	147,633.75	187,305.51	345,500.08	287,787.01	132,782.91	171,412.60	479,500.00

Table 6.14 Moment Forces of the Isolated System Model – Longitudinal Direction

- Unisolated Model

Moment Forces *(Transversal)*								
	EQ Applied in Transversal Direction							
Pier / Record	**01B H-CBR230 U2**	**02B BOL090 U2**	**03B DZC270 U2**	**04B TAZ000 U2**	**05B TAZ090 U2**	**06B YPT060 U2**	**07B YPT330 U2**	**Effective Yield Moment**
(#)	*M2 (kNm)*	*M2 (kNm)*	*M2 (kNm)*	*M2 (kNm)*	*M2 (kNm)*	*M2 (kNm)*	*M2 (kNm)*	*M2 (kNm)*
20	153,512.91	240,780.21	346,612.92	506,259.47	520,132.38	219,269.52	283,822.58	766,300.00
21	169,289.78	266,593.57	348,821.01	571,181.95	573,025.11	240,190.43	294,946.19	766,300.00
22	176,310.35	313,874.33	395,975.79	677,598.16	627,512.42	272,391.73	319,461.78	766,300.00
23	185,226.89	353,864.76	461,607.69	757,098.94	640,898.56	291,589.20	332,138.42	766,300.00
24	206,619.81	374,528.65	502,819.14	807,966.17	641,916.51	299,919.95	346,036.16	766,300.00
25	209,550.39	377,167.03	514,990.72	803,987.81	612,147.65	291,644.68	340,956.13	766,300.00
26	203,264.97	384,964.37	507,850.57	780,682.07	584,021.74	287,691.62	333,174.21	766,300.00
27	198,246.45	377,273.83	463,315.30	711,885.53	561,792.28	275,907.12	314,823.50	766,300.00
28	179,977.93	359,630.47	447,660.98	622,760.68	540,353.11	260,155.64	291,010.17	766,300.00
29	186,575.29	371,627.58	486,921.47	608,805.63	558,447.30	268,685.79	291,808.39	766,300.00
30	196,811.90	382,995.51	516,077.06	589,285.33	551,837.73	276,624.77	298,726.48	766,300.00
31	200,051.86	377,167.03	523,063.26	595,812.31	555,391.96	276,649.82	301,824.40	766,300.00
32	201,868.27	403,370.52	524,553.49	614,892.67	555,652.86	279,885.50	295,075.12	766,300.00
33	202,564.45	420,329.01	529,500.97	657,093.02	558,772.07	290,737.02	307,024.85	766,300.00
34	196,539.52	425,045.18	525,549.48	717,580.59	558,805.11	298,637.84	317,190.66	766,300.00
35	199,418.06	416,146.22	515,274.61	749,990.48	554,952.42	302,520.46	323,411.66	766,300.00
36	198,982.23	405,870.44	509,852.58	770,782.49	561,909.64	303,509.76	330,301.29	766,300.00
37	180,296.04	374,562.98	479,839.77	725,954.31	563,952.98	286,416.74	317,429.07	766,300.00
38	168,335.00	326,665.23	423,996.61	642,086.02	567,613.91	259,183.56	287,704.91	766,300.00
39	165,392.34	283,937.41	362,668.91	570,769.20	564,534.35	242,540.97	265,122.31	766,300.00
40	146,385.55	244,668.88	329,872.10	519,716.70	530,037.36	224,495.40	274,360.65	766,300.00

Table 6.15 Moment Forces of the Unisolated System Model – Transversal Direction

Moment Forces *(Longitudinal)*

	EQ Applied in Longitudinal Direction							
Pier / Record	**01A H-CBR230 U1**	**02A BOL090 U1**	**03A DZC270 U1**	**04A TAZ000 U1**	**05A TAZ090 U1**	**06A YPT060 U1**	**07A YPT330 U1**	**Effective Yield Moment**
(#)	*M3 (kNm)*	*M3 (kNm)*	*M3 (kNm)*	*M3 (kNm)*	*M3 (kNm)*	*M3 (kNm)*	*M3 (kNm)*	*M3 (kNm)*
20	167,898.67	120,272.09	324,498.68	257,047.55	207,026.50	364,301.33	304,161.39	479,500.00
21	128,425.22	116,938.26	298,304.73	233,197.76	188,335.33	349,274.39	283,648.57	479,500.00
22	127,374.98	118,432.29	299,133.16	233,573.45	189,521.16	348,480.38	282,704.74	479,500.00
23	125,227.31	119,450.79	299,267.49	233,556.41	190,362.93	349,026.08	283,231.63	479,500.00
24	122,866.88	120,786.19	300,255.98	233,540.59	191,285.70	349,682.32	283,182.15	479,500.00
25	121,195.07	122,043.78	301,472.13	233,444.71	192,066.78	350,624.99	283,135.85	479,500.00
26	149,395.80	121,125.67	311,866.38	244,715.75	197,037.62	360,026.25	296,360.91	479,500.00
27	151,222.58	121,483.85	313,402.47	244,433.20	196,765.56	360,627.74	296,598.14	479,500.00
28	125,851.39	124,027.87	305,098.06	233,221.92	193,114.86	352,933.86	283,248.46	479,500.00
29	157,258.32	121,070.60	315,613.69	243,426.54	197,651.00	360,565.41	297,274.45	479,500.00
30	161,506.71	120,300.19	316,421.67	243,036.08	198,939.50	359,790.19	297,922.06	479,500.00
31	132,901.27	122,550.40	304,607.01	231,379.56	189,633.00	350,743.70	283,702.48	479,500.00
32	112,867.37	125,515.39	291,400.10	219,483.17	187,020.36	337,906.58	274,774.62	479,500.00
33	113,442.75	123,704.78	291,942.81	219,464.82	185,512.84	337,898.14	274,855.59	479,500.00
34	114,521.36	121,683.84	293,377.04	218,629.71	184,456.12	337,981.14	274,436.45	479,500.00
35	117,417.34	120,342.78	294,409.47	218,922.40	183,827.45	338,346.91	274,004.45	479,500.00
36	152,483.96	114,353.50	310,070.23	228,412.70	191,186.55	349,747.51	283,977.29	479,500.00
37	153,309.41	112,830.80	311,567.36	227,331.74	192,918.73	349,322.68	283,036.50	479,500.00
38	118,890.82	116,111.97	297,910.70	216,374.39	184,927.68	337,602.46	271,784.20	479,500.00
39	120,289.72	116,121.95	299,469.97	217,322.47	186,036.89	336,809.94	270,968.34	479,500.00
40	144,151.47	110,006.09	311,295.99	225,085.91	195,256.44	351,964.98	283,818.90	479,500.00

Table 6.16 Moment Forces of the Unisolated System Model – Longitudinal Direction

As seen on the Table 6.15 plastic hinges are formed at Kobe Earthquake Taz000 record at piers 24, 25, 26 and 36 with moment values 807,966.17 kN-m, 803,987.81 kN-m, 780,682.07 kN-m, 770,782.49 kN-m respectively; while the effective yield moment is 766,300.00.

Strain Values (04B TAZ000 U2 Record)

Pier	**Effective Yield Moment**	**Moment**	**Rotation** *(plastic)*	**Plastic Hinge Length**	**Curvature** *(plastic)*	**Curvature** *(elastic)*	**Curvature** *(total)*	**Reinforcement Strain** *(total)*	**Confined Concrete Strain** *(total)*	**Unconfined Concrete Strain** *(total)*
(#)	*M2 (kNm)*	*M2 (kNm)*	*R1 (radians)*	*Lp (m)*	*K1 (1/m)*	*K1 (1/m)*	*K1 (1/m)*			
24	766,300.00	807,966.17	0.001618	4.20	3.8524E-04	7.1480E-04	1.1000E-03	0.006480	0.002179	0.002242
25	766,300.00	803,987.81	0.001610	4.20	3.8333E-04	7.1480E-04	1.0981E-03	0.006467	0.002177	0.002239
26	766,300.00	780,682.07	0.001527	4.10	3.7244E-04	7.1480E-04	1.0872E-03	0.006395	0.002161	0.002223
36	766,300.00	770,782.49	0.001546	4.20	3.6810E-04	7.1480E-04	1.0829E-03	0.006369	0.002156	0.002216

Table 6.17 Strain values for piers 24, 25, 26 and 36

Seismic demand on plastic hinges is evaluated by assessing material strains. In the serviceability performance level, the structure should remain operational and no damage should occur. To satisfy these objectives, limit strains for serviceability are conservatively defined as the concrete strain at the beginning of concrete spalling and the steel strain resulting in crack widths equal to 1.0 mm. Serviceability limit corresponds to a concrete strain, $\varepsilon_c = 0.004$ and a steel strain, $\varepsilon_s = 0.015$, whichever occurs first. Beyond these limits, the structure might be damaged and repairs might be needed. In the damage control performance level, the structure is again required to remain operational whereas repairable damage is accepted. Corresponding limit strains are conservatively defined as the damage control strains of a confined and properly detailed section. Damage control limit corresponds to a concrete strain, $\varepsilon_c = 0.018$ and a steel strain, $\varepsilon_s = 0.060$, whichever occurs first. Strain limits are

Strain limits for concrete and steel			
Performance level	Strain limits for cover concrete, εc	Strain limits for confined concrete, εc	Strain limits for steel, εs
Serviceability, S1	0.004000		0.015000
Damage Control, S2		0.018000	0.060000

Table 6.18 Strain limits for concrete and steel

Hence the strain values of the reinforcement fiber, confined concrete and unconfined concrete are within serviceability limits there isn't a critical situation for the piers.

6.1.5. Pier Top Displacements (Drifts)

- Isolated Model –Longitudinal Analyses

Pier Top Displacements *(Longitudinal)*									
	EQ Applied in Longitudinal Direction								
Pier / Record	**01A H-CBR230 U1**	**02A BOL090 U1**	**03A DZC270 U1**	**04A TAZ000 U1**	**05A TAZ090 U1**	**06A YPT060 U1**	**07A YPT330 U1**	**Pier Length**	**Max Drift**
(#)	*U1 (m)*	*U1 (m)*	*U1 (m)*	*U1 (m)*	*U1 (m)*	*U1 (m)*	*U1 (m)*	*(m)*	*(m/m)*
20	0.14	0.25	0.30	0.45	0.47	0.19	0.31	46.00	0.0102
21	0.11	0.19	0.38	0.25	0.26	0.32	0.30	48.00	0.0079
22	0.12	0.20	0.37	0.29	0.29	0.30	0.30	48.00	0.0077
23	0.12	0.20	0.37	0.28	0.29	0.30	0.30	48.00	0.0077
24	0.12	0.20	0.37	0.28	0.29	0.30	0.30	48.00	0.0077
25	0.12	0.20	0.37	0.28	0.29	0.30	0.30	48.00	0.0077
26	0.11	0.20	0.36	0.25	0.29	0.30	0.31	47.00	0.0076
27	0.11	0.20	0.35	0.25	0.29	0.30	0.31	47.00	0.0075
28	0.12	0.20	0.37	0.28	0.29	0.30	0.30	48.00	0.0077
29	0.11	0.20	0.35	0.25	0.29	0.30	0.31	47.00	0.0075
30	0.11	0.20	0.35	0.25	0.29	0.30	0.31	47.00	0.0075
31	0.12	0.20	0.37	0.28	0.29	0.30	0.30	48.00	0.0077
32	0.12	0.20	0.38	0.31	0.29	0.31	0.28	49.00	0.0078
33	0.12	0.20	0.38	0.31	0.28	0.31	0.28	49.00	0.0078
34	0.11	0.20	0.38	0.30	0.28	0.31	0.28	49.00	0.0078
35	0.11	0.20	0.38	0.30	0.28	0.31	0.28	49.00	0.0078
36	0.11	0.20	0.36	0.27	0.28	0.30	0.28	48.00	0.0076
37	0.11	0.20	0.37	0.27	0.28	0.30	0.28	48.00	0.0076
38	0.11	0.20	0.38	0.30	0.28	0.31	0.27	49.00	0.0077
39	0.11	0.19	0.39	0.28	0.26	0.32	0.26	49.00	0.0079
40	0.13	0.23	0.30	0.54	0.46	0.21	0.28	48.00	0.0113

Table 6.19 Pier displacements of the isolated system model – longitudinal direction

- Isolated Model –Transversal Analyses

Pier Top Displacements ***(Transversal)***

	EQ Applied in Transversal Direction								
Pier / Record	**01B H-CBR230 U2**	**02B BOL090 U2**	**03B DZC270 U2**	**04B TAZ000 U2**	**05B TAZ090 U2**	**06B YPT060 U2**	**07B YPT330 U2**	**Pier Length**	**Max Drift**
(#)	*U2 (m)*	*U2 (m)*	*U2 (m)*	*U2 (m)*	*U2 (m)*	*U2 (m)*	*U2 (m)*	*(m)*	*(m/m)*
20	0.16	0.37	0.23	0.31	0.30	0.15	0.13	46.00	0.0081
21	0.13	0.23	0.22	0.23	0.23	0.20	0.14	48.00	0.0049
22	0.13	0.25	0.22	0.25	0.25	0.20	0.14	48.00	0.0052
23	0.13	0.24	0.22	0.24	0.25	0.20	0.14	48.00	0.0051
24	0.13	0.24	0.22	0.24	0.25	0.20	0.14	48.00	0.0051
25	0.13	0.24	0.22	0.24	0.25	0.20	0.14	48.00	0.0052
26	0.13	0.25	0.21	0.23	0.23	0.19	0.13	47.00	0.0054
27	0.13	0.25	0.21	0.24	0.23	0.19	0.13	47.00	0.0054
28	0.13	0.24	0.22	0.24	0.25	0.20	0.14	48.00	0.0052
29	0.13	0.25	0.21	0.24	0.23	0.20	0.13	47.00	0.0053
30	0.13	0.25	0.21	0.24	0.23	0.20	0.13	47.00	0.0053
31	0.13	0.24	0.23	0.24	0.25	0.20	0.14	48.00	0.0051
32	0.13	0.23	0.25	0.25	0.25	0.21	0.15	49.00	0.0051
33	0.13	0.23	0.25	0.25	0.25	0.21	0.15	49.00	0.0051
34	0.12	0.23	0.24	0.24	0.25	0.22	0.15	49.00	0.0050
35	0.13	0.23	0.24	0.24	0.25	0.22	0.15	49.00	0.0050
36	0.13	0.23	0.23	0.23	0.23	0.21	0.14	48.00	0.0049
37	0.13	0.23	0.23	0.23	0.23	0.21	0.14	48.00	0.0048
38	0.13	0.22	0.25	0.24	0.23	0.23	0.15	49.00	0.0051
39	0.12	0.20	0.25	0.22	0.21	0.24	0.16	49.00	0.0052
40	0.18	0.32	0.23	0.29	0.32	0.19	0.15	48.00	0.0067

Table 6.20 Pier displacements of the isolated system model – transversal direction

- Unisolated Model – Longitudinal Analyses

Pier Top Displacements ***(Longitudinal)***									
	EQ Applied in Longitudinal Direction								
Pier / Record	**01A H-CBR230 U1**	**02A BOL090 U1**	**03A DZC270 U1**	**04A TAZ000 U1**	**05A TAZ090 U1**	**06A YPT060 U1**	**07A YPT330 U1**	**Pier Length**	**Max Drift**
(#)	*U1 (m)*	*U1 (m)*	*U1 (m)*	*U1 (m)*	*U1 (m)*	*U1 (m)*	*U1 (m)*	*(m)*	*(m/m)*
20	0.15	0.19	0.50	0.40	0.32	0.55	0.45	46.00	0.0120
21	0.15	0.18	0.50	0.39	0.32	0.56	0.46	48.00	0.0117
22	0.15	0.18	0.50	0.40	0.32	0.56	0.45	48.00	0.0116
23	0.15	0.18	0.50	0.40	0.32	0.56	0.45	48.00	0.0117
24	0.15	0.18	0.50	0.40	0.32	0.56	0.45	48.00	0.0117
25	0.15	0.18	0.50	0.40	0.32	0.56	0.45	48.00	0.0117
26	0.15	0.18	0.50	0.40	0.32	0.56	0.45	47.00	0.0119
27	0.15	0.18	0.50	0.40	0.32	0.56	0.45	47.00	0.0119
28	0.15	0.18	0.50	0.40	0.32	0.56	0.45	48.00	0.0117
29	0.15	0.18	0.50	0.40	0.32	0.56	0.45	47.00	0.0119
30	0.15	0.18	0.50	0.40	0.32	0.56	0.45	47.00	0.0119
31	0.15	0.18	0.50	0.39	0.32	0.56	0.45	48.00	0.0117
32	0.15	0.18	0.50	0.40	0.32	0.56	0.45	49.00	0.0114
33	0.15	0.18	0.50	0.40	0.32	0.56	0.45	49.00	0.0114
34	0.15	0.18	0.50	0.40	0.32	0.56	0.45	49.00	0.0114
35	0.15	0.18	0.50	0.39	0.32	0.56	0.45	49.00	0.0114
36	0.15	0.18	0.49	0.39	0.32	0.55	0.45	48.00	0.0115
37	0.15	0.18	0.49	0.39	0.32	0.55	0.45	48.00	0.0115
38	0.15	0.18	0.49	0.39	0.32	0.55	0.45	49.00	0.0112
39	0.15	0.18	0.49	0.38	0.31	0.55	0.44	49.00	0.0112
40	0.14	0.17	0.48	0.37	0.32	0.55	0.45	48.00	0.0115

Table 6.21 Pier displacements of the unisolated system model – longitudinal direction

- unisolated Model – Transversal Analyses

Pier Top Displacements *(Transversal)*									
	EQ Applied in Transversal Direction								
Pier / Record	**01B H-CBR230 U2**	**02B BOL090 U2**	**03B DZC270 U2**	**04B TAZ000 U2**	**05B TAZ090 U2**	**06B YPT060 U2**	**07B YPT330 U2**	**Pier Length**	**Max Drift**
(#)	*U2 (m)*	*U2 (m)*	*U2 (m)*	*U2 (m)*	*U2 (m)*	*U2 (m)*	*U2 (m)*	*(m)*	*(m/m)*
20	0.11	0.18	0.24	0.36	0.36	0.16	0.20	46.00	0.0079
21	0.12	0.20	0.27	0.43	0.41	0.19	0.22	48.00	0.0090
22	0.13	0.24	0.30	0.52	0.44	0.21	0.24	48.00	0.0109
23	0.14	0.27	0.34	0.59	0.47	0.23	0.26	48.00	0.0123
24	0.15	0.28	0.38	0.63	0.47	0.23	0.27	48.00	0.0130
25	0.15	0.29	0.38	0.62	0.46	0.23	0.26	48.00	0.0130
26	0.14	0.28	0.37	0.58	0.43	0.22	0.25	47.00	0.0123
27	0.12	0.27	0.34	0.52	0.41	0.21	0.23	47.00	0.0112
28	0.13	0.27	0.33	0.48	0.39	0.20	0.22	48.00	0.0099
29	0.14	0.27	0.36	0.44	0.39	0.20	0.21	47.00	0.0094
30	0.14	0.28	0.38	0.43	0.39	0.20	0.22	47.00	0.0092
31	0.15	0.30	0.40	0.45	0.40	0.21	0.23	48.00	0.0093
32	0.16	0.32	0.42	0.47	0.41	0.22	0.23	49.00	0.0096
33	0.16	0.33	0.42	0.51	0.42	0.23	0.25	49.00	0.0105
34	0.16	0.34	0.41	0.56	0.43	0.23	0.26	49.00	0.0115
35	0.15	0.33	0.40	0.59	0.43	0.23	0.27	49.00	0.0121
36	0.14	0.31	0.38	0.59	0.43	0.23	0.26	48.00	0.0123
37	0.13	0.29	0.36	0.56	0.43	0.22	0.25	48.00	0.0116
38	0.13	0.26	0.33	0.50	0.42	0.21	0.23	49.00	0.0103
39	0.12	0.23	0.29	0.45	0.41	0.19	0.21	49.00	0.0092
40	0.11	0.19	0.25	0.41	0.40	0.18	0.22	48.00	0.0085

Table 6.22 Pier displacements of the unisolated system model – transversal direction

6.1.6. Temperature Change Analysis

Pier	FPB Deformations		Pier Base Moments
(#)	*U2 (m)*		*M3 (kN-m)*
20	0.07	0.07	8,875.10
21	0.06	0.06	6,498.46
22	0.05	0.06	5,861.76
23	0.05	0.05	5,066.50
24	0.00	0.00	26,365.05
25	0.00	0.00	21,918.11
26	0.00	0.00	18,077.58
27	0.00	0.00	13,429.05
28	0.00	0.00	8,448.28
29	0.00	0.00	4,152.50
30	0.00	0.00	460.06
31	0.00	0.00	4,856.97
32	0.00	0.00	8,927.93
33	0.00	0.00	13,193.42
34	0.00	0.00	17,459.90
35	0.00	0.00	21,827.49
36	0.00	0.00	27,126.78
37	0.05	0.05	5,261.27
38	0.06	0.06	6,134.72
39	0.06	0.06	6,792.69
40	0.07	0.07	9,128.46

Table 6.23 Temperature change analysis results for the isolated system model

7. RESULTS AND CONCLUSIONS

The preliminary hand calculations matched the computer analysis results, verifying the model. In the hand calculation the period of a pier was estimated 5.36 seconds, and matched the computer analysis with the result 5.24 seconds. For the “unisolated” system model, the result of the preliminary hand calculation was 2.80 seconds, again matching the computer analysis result 2.68 seconds.

In the modal analyses, for the isolated system, first six modes are FPB sliding modes; the rest are single pier movements.

The FPB deformations of the isolated system was within the capacity of the devices except two strong ground motion data : Duzce270 and YTP060 records; which have the largest spectral displacement values for periods about 5 seconds as seen on Figure 5.16 Displacement response spectra. The largest deformation value is 91 cm versus the capacity 70 cm.

For the isolated system model; the largest shear forces are 10 MN in longitudinal direction and 16 MN in transversal direction versus the capacities 30 MN and 42 MN respectively. For the unisolated system model; the largest shear forces are 10 MN in longitudinal direction and 19 MN in transversal direction versus the capacities 30 MN and 42 MN respectively. The results show that in both system shear failure is not a matter.

For the isolated system model; the largest moment forces are 346 MN-m in longitudinal direction and 562 MN-m in transversal direction versus the effective yield moment capacities 480 MN-m and 766 MN respectively; resulting in a linear behavior of the piers.

For the unisolated system model; the largest moment forces are 364 MN-m in longitudinal direction and 808 MN-m in transversal direction versus the effective yield moment capacities 480 MN-m and 766 MN respectively; resulting in formation of plastic hinge zones in piers 24, 25, 26 and 36 for the TAZ000 record of the Kobe earthquake. The resulting strain values of the confined concrete, unconfined concrete and the reinforcement fiber are within the serviceability limits for *ACI 318 code* **[Ref. 1]**

The results of the temperature change analysis show that the largest moment value at the base of the piers is 27 MN-m showing minimal charge to piers.

For the isolated system model, the largest drift value of the top of the pier is 0.011 in longitudinal direction. For the unisolated system model, the largest drift value of the top of the pier is 0.013 in transversal direction.

In the scope of these results,

- The FPS isolation lets the bridge behave almost linearly for design earthquakes (except for 4 hinges).
- The bridge would be within serviceability limits with continuous deck and without FPS isolation for design earthquakes.

BIBLIOGRAPHY

Ref. 1 American Concrete Institute (ACI) Committee 318. *Building Code Requirements for Structural Concrete (ACI 318-95) and Commentary (ACI 318R-95)*, 1995.

Ref. 2 A.K. Chopra. *Dynamics of Structures: Theory and Applications to Earthquake Engineering*. Prentice-Hall, New Jersey, 1995.

Ref. 3 Priestley M.J.N. Mander, J.B. and Park R. *Theoretical stress-strain model for confined concrete*. Journal of Structural Engineering, 114(8):1804–1826, August 1988.

Ref. 4 T. Paulay and M.J.N. Priestley. *Seismic Design of Concrete and Masonry Structures*. John Wiley & Sons Inc., New York, 1993.

Ref. 5 M.J.N. Priestley, F. Seible, and G.M. Calvi. *Seismic Design and Retrofit of Bridges*. John Wiley & Sons Inc., New York, 1996.

Ref. 6 Computers and Structures, Inc. *Analysis Reference Manual For SAP2000*, 1995.

Ref. 7 Farzad Naeim, James M. Kelly. *Design of Seismic Isolated Structures, From Theory to Practice*, John Wiley & Sons Inc., New York, 1999

Ref. 8 G. Michele Calvi and M. J. Nigel Priestley. *Preliminary Report on Repair and Retrofit of Viaduct 1*, 2001

Ref. 9 M. J. N. Priestley and G. M. Calvi. *Strategies for Repair and Seismic Upgrading of Bolu Viaduct 1, Turkey*, Journal of Earthquake Engineering, Vol. 6, Special Issue 1, 2002

Ref. 10 Panayiotis C. Roussis, Michael C. Constantinou, Mustafa Erdik, Eser Durukal, Murat Dicleli. *Assessment of Performance of Seismic Isolation System of Bolu Viaduct*

Ref. 11 S. W. Park, H. Ghasemi, J. Shen, P.G. Somerville, W.P. Yen and M. Yashinsky. *Simulation of the seismic performance of the Bolu Viaduct subjected to near-fault ground motions*, Earthquake Engineering and Structural Dynamics, 2004

Ref. 12 A. S. Mokha, M. C. Constantinou and A. M. Reinhorn. *Experimental Study and Analytical Prediction of Earthquake Response of a Sliding Isolation System with a Spherical Surface*, Technical Report NCEER-90-0020, 1990

Ref. 13 General Directorate of Highways, Several brochures about Gümüşova-Gerede Motorway

Ref. 14 Astaldi SPA, Miscellaneous documents and diagrams related to Bolu Viaduct

LIST OF SYMBOLS

A0	= Effective area for torsion
Al	= Area of longitudinal reinforcement for torsion
Ash	= Area of shear-friction reinforcement
At	= Area of transverse reinforcement for torsion
Av	= Area of transverse reinforcement in the direction of shear force applied
bw	= Width of section
d	= Effective section depth
f'_c	= Compressive strength of concrete
fy	= Yield strength of reinforcement
H	= Column height
Mn	= Nominal flexural strength
Mo	= Over-strength moment capacity of plastic hinge
ph	= Perimeter of the area within transverse torsion reinforcement
s	= Spacing of transverse reinforcement
Td	= Design torsion force
Tn	= Nominal torsional strength
Vc	= Contribution of concrete to shear capacity
Vd	= Design shear force
Vn	= Nominal shear strength
Vs	= Contribution of shear reinforcement to shear capacity
Vsf	= Shear-friction capacity
φ	= Strength reduction factor
φo	= Over-strength factor for plastic hinges
μ	= Friction coefficient